1968

Studies Of The Physical Forces Required To Explain The Equilibrium Of The Membrane Of The Red Cell

Brij Bhushan Shrivastav

STUDIES OF THE PHYSICAL FORCES REQUIRED TO EXPLAIN THE EQUILIBRIUM OF THE MEMBRANE OF THE RED CELL

by

Brij Bhushan Shrivastav, B. Sc., M. Sc.
Department of Biophysics

Submitted in partial fulfillment
of the requirements for the degree of
Doctor of Philosophy

Faculty of Graduate Studies
The University of Western Ontario
London, Canada
August, 1968

In the memory of my late father,
Gajanand Prashad Shrivastav,
and to my mother, Mrs. Kaushalya
Devi Shrivastav.

This work was supported by a grant from the Life Insurance Medical Research Fund. The author wishes to express his indebtedness to this organization.

ACKNOWLEDGEMENTS

With immense pleasure I express my deepest thanks to Professor Alan C. Burton for his able guidance, encouragement and generous advice.

My sincere thanks are also due to: Dr. R. I. Duncan for editing, Dr. A. C. Groom and Dr. S. P. Ahuja for reading the rough draft of this thesis, and to Mrs. Dorothy Elston and Mr. George Flett for technical help. Professor G. H. Reavely and Dr. W. R. Church of the Geology Department provided facilities for polarization microscopy. I am indebted to them for their kind assistance.

I am grateful to Mrs. Vera Jordan who took great care in typing the thesis and to Miss Catherine Appleford who retyped some sections.

Last, but not least, I am thankful to all my colleagues for their cooperation and help from time to time.

August, 1968.

CONTENTS

LIST OF TABLES

LIST OF ILLUSTRATIONS

ABSTRACT

The biconcave discoidal shape of the red cell seems to demand the existence of a force of attraction between the opposite parts of its membrane. A normally acting force p^1 due to the presence of long chain molecules linking the two membranes at the dimple region of a red cell has been proposed.

Considering the membrane of a red cell as a soap-film, this force p^1 has been calculated at its various singular points to be a maximum (2.82 mm of H_2O) at the dimple center, and a minimum (0.66 mm of H_2O) at the periphery of the red cell.

The force of attraction between charged plates of a parallel plate capacitor with nylon fiber 'bridges' between them first increases with the distance between the plates, then after attaining a maximum, falls, following the classical laws of electrostatics. Similarly, when a red cell is swelled in hypotonic solution of decreasing tonicity, the proposed force p^1 first increases, attains a maximum and then falls as the cell is further swelled.

Polarization microscopy of the different interior regions of the normal and swelled red cells suggests that the

interior of the red cell at the dimple region is birefringent, while its rim interior is isotropic. Quantitative measurements show that the relative intensity of the polarized light passing along the major diameter of the red cell and through its dimple interior is a periodic function of the cell orientation between the crossed polarizer and analyzer.

Reduction in interfacial tension of the membrane of red cells by suspending them in buffered Ringer solution with low concentration of Tween 80, a surfactant, changes their normal biconcave shape. The least thickness of these cells decreases by 43.4% of the normal value.

The increase and decrease of the force of attraction as the red cell is swelled, the birefringent properties of the dimple interior region, and the decrease in the least thickness by decreasing interfacial tension of the cell membrane suggest bridges of the long chain molecules linking the two surfaces.

I. INTRODUCTION

The vital role of the red blood cells is well recognized. In man, the red cells are non-nucleated and biconcave discoid in shape. Normal human red cells are formed in the red marrow of some bones. The adult erythrocytes, after having lost their nuclei and sub-nuclear particles (mitochondria, RNA granules, etc.) retain many enzymes, proteins, carbohydrates, lipids, anions and cations, and finally become simple cells structurally. It is the hemoglobin in the red cells which has a strong affinity for the oxygen it carries from the lungs to the body tissues. On the way back, it carries carbon dioxide, a waste product of the body cells. This respiratory pigment, hemoglobin, is in very high concentration in the red cells, so that it is nearly in the crystalline state (Ponder, 1955).

After the first report that the red cell is flat by Leeuwenhock in 1673, (Baker, 1948), the simple biconcave discoidal shape of the normal adult erythrocyte has been the subject of much comment and speculation, but very little has been written from the point of view of the biophysicists. In the basal state, an average individual absorbs about 250 ml. of oxygen per minute. For this amount of oxygen turnover, a

rapid and complete oxygenation of the red cells is needed in the lungs. The hemoglobin content is about 15 grams per 100 ml. of whole human blood. Had there been hemoglobin in the form of a solution in the blood, 15 grams of it per 100 ml. would have produced a fluid too viscous for effective circulation and the osmotic pressure of the plasma would have increased considerably (Harris, 1965, p.198). Therefore, hemoglobin in the form of red cells is necessary, in the body, for its normal physiological function of transporting oxygen from the lungs to the other tissues. Teleologically also, not only the hemoglobin in packets in blood, but the biconcave discoidal shape of the red cells is supposed to be best for effective diffusion of gases uniformly to all regions of its interior for reaction with hemoglobin with maximal speed (Hartridge, 1919). However, other considerations such as maximum diameter must also be added, as a thinner disc would have served this purpose even better. In comparison to a sphere of the same volume, a red cell has a larger surface area facilitating gaseous exchange.

In the circulation, the red cells pass through the capillaries of diameter less than their own diameters, in single file, with surrounding plasma trapped between them (Krogh, 1929). During their passage through such capillaries, where the main diffusion of the gases takes place, the red cells offer very little, practically negligible,resistance to distortion in shape in passing through, mixing the plasma thoroughly, and thus greatly enhancing the capacity of

hemoglobin to take on and give up oxygen (Prothero and Burton, 1961). The mixing motion and the contact of the red cells with the vessel walls do not apparently increase the resistance to blood flow (Prothero and Burton 1962a, 1962b). On the other hand, the biconcave discoidal shape of a red cell is one which would permit moderate shape change without stretching the cell membrane, a feature which would be of obvious advantage to a cell which is constantly squeezing through narrow passages.

Thus, it would be better to emphasize teleologically the importance of non-sphericity of the red cell to allow it to be deformed without stretching of the membrane, which results in hemolysis (Rand and Burton, 1963). The shape, as well as the size, of the red cells determine the size of quasi-cylindrical channels through which they could pass without hemolysis (Burton, 1966). This fact may, in future, explain the reason for the 120 day life cycle of the red cells. As the red cells grow older, they become more sphericitic, making them less competent for deformation without stretch in the membrane while passing through narrow vessels (Canham and Burton, 1968).

When a red cell is transferred into a hypotonic environment, its membrane acquires a new equilibrium position. This new equilibrium of the red cell membrane depends on the tonicity of the hypotonic solution to which it is transferred. Therefore, besides the equilibrium of the normal shape of the red cell membrane in plasma, it may also acquire various

equilibrium positions in the hypotonic solutions of different tonicities.

Since the turn of this century, a great amount of work has been done on red blood cells, and the literature concerning red blood cells is increasing rapidly. Yet the physical equilibria of a red blood cell in plasma and of a swelling red cell in hypotonic solutions are still mysteries. The present work was, therefore, undertaken to throw some light on how a normal red cell and its different configurations in hypotonic solutions, from a biconcave discoidal shape to a sphere, can represent physical equilibria under the various forces that may act.

II. HISTORICAL REVIEW

1. Introduction

Classically, a red blood cell was thought to be composed of two main parts; a membrane, and a highly concentrated solution of hemoglobin. In a very broad way, a red cell can still be divided into these two components. The membrane can be regarded to a greater extent, both functionally and structurally in the intact red cell, as a separate entity. The rest of the constituents of the red cell which are enveloped by the membrane can be regarded as the second component. The oxygen consumption of a suspension of the red cells is very low. However, the oxygen consumption of the membrane alone of the red cells is comparable to the oxygen consumption of the membranes of other living cells. The respiration of reticulocytes (which are non-nucleated and immediate precursor of the red cells) is nearly fifty times greater than that of the mature red cells. This shows that only the membrane of a mature erythrocyte is alive (Ponder, 1948, p. 357; Prankerd, 1961, p. 70).

In recent years, many facts about the structure, function and behavior of a red cell in different environments, have been revealed by using techniques of micromanipulation and osmotic swelling. Optical methods, such as X-ray

photography, electron microscopy, polarized-light microscopy, etc., have also been quite extensively used to reveal the structure of the red cell membrane and its contents. From time to time, there have been reports showing interaction between the membrane and the other constituents of a red cell. Such interaction between the different parts of a red cell seems desirable also to account for its non-sphericity in shape, as a normal cell in plasma, and in different environments.

2. The Shape and Dimensions of the Red Blood Cell

A normal human red cell has a biconcave discoidal shape. The systematic and accurate measurements of human red cell dimensions have been made by Ponder (1944, 1948). The red cells have biological variations and, even in an individual, their dimensions vary. The mean values of the main dimensions of the red cell, based on a very large number of direct microscopic measurements done by Ponder are used here to plot the red cell profile shown in Figure 1. Below the profile is a microphotograph of a red blood cell on edge. The main red cell dimensions are shown in Table 1 (Ponder, 1948).

3. The Membrane of the Red Cell

Although the fundamental characteristics of different cell membranes vary in some measure from one another, their basic structure appears to be similar. Lipids and proteins are known to constitute the main components of such membranes.

Figure 1.

(A) Profile of red cell (data from Ponder, 1944).

(B) Microphotograph of red cell on edge.

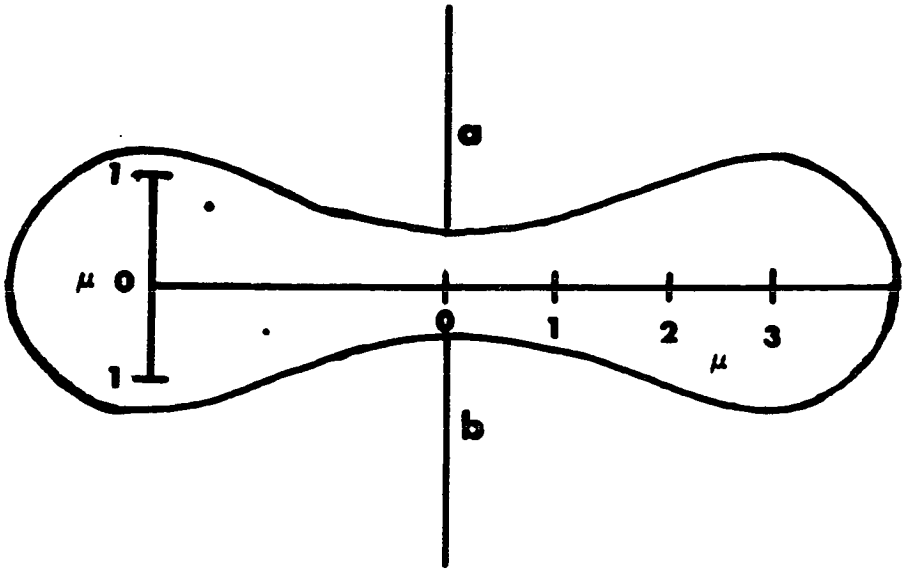

[A]

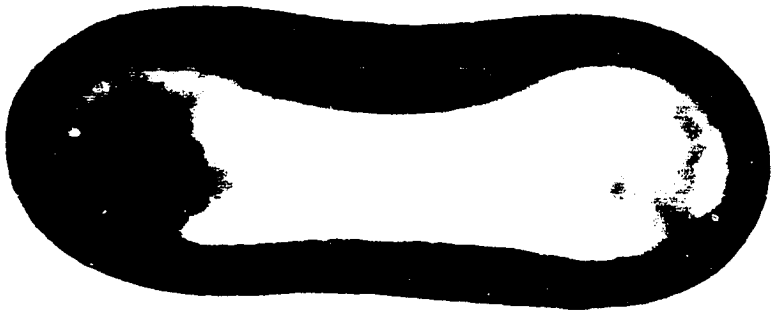

[B]

TABLE 1

The mean dimensions of the (human)normal red cell*, (Ponder 1944).

Dimension		Length/Area/Volume
Major diameter	(μ)	8.5 $\pm$ 0.41 (SD)
Greatest thickness	(μ)	2.4 $\pm$ 0.13 (SD)
Least thickness	(μ)	1.0 $\pm$ 0.08 (SD)
Surface area	(μ^2)	163
Volume	(μ^3)	87

*Recently, with improved optics the mean values of major diameter = 8.068 $\pm$ 0.547μ, Surface area = 138.1 $\pm$ 17.4μ^2, and Volume = 107.5 $\pm$ 16.8μ^3 have been reported (Canham and Burton, 1968).

The exact ultra-structural arrangement of these moieties, however, is not fully known. The 'unit membrane', which is supposed to be the fundamental structure of all biological membranes, was postulated by Robertson (Robertson, 1959, 1967). The presence of the unit membrane has, so far, been shown in many membranes, with some morphological variations according to the physiological functions of the cell membrane. Recently, the unit membrane theory has been re-evaluated in light of the data now available (Korn, 1966). Many conclusions regarding the properties of cell membranes are based on studies of the 'ghosts' of the mammalian red blood cell. This assumes similarity in the basic structure, and thus certain common properties in all biological membranes. Proceedings of two symposia (Fishman, 1962; Bell and Grant, 1963) have covered a wide field of work and have given comprehensive reviews on the plasma membrane.

(i) Molecular Arrangement and Chemical Composition

The theories of molecular structure of the cell membrane are based mainly on indirect evidence. Accordingly, the well known Davson-Danielli model of the cell membrane supposes that the lipid component of the membrane is arranged in a bimolecular sheet with the nonpolar groups on the inside and the polar groups at the two surfaces. Both surfaces of these bimolecular layers of lipids are coated with tangential layers of proteins of long chain molecules, with hydrophobic groups penetrating the lipid layer and polar groups nearly in the same plane as those of the lipids. These two

lipoprotein surfaces are also supposed to be covered by globular proteins. However, this model of the cell membrane has severe limitations. It was later proposed that the lipid phase, in the membrane, exists in the form of globular micelles, which are either embedded in a protein matrix (Sjostrand, 1963) or sandwiched between layers of protein (Lucy, 1964; Lucy and Glauert, 1964). Recently, keeping in view the complex entity of the biological membranes, a dynamic picture of the membrane structure and function has been proposed (Kavanau, 1965, 1966). Accordingly, a biological membrane transforms between several different configurations in the course of its different functions. The two dense lines enclosing a less dense line, which are seen from electron-optical studies, seem the most stable of these configurations, to which the membrane transforms automatically in the course of dehydration and exposure to cations during the initial preparative treatments.

(ii) Ultrastructure

Electron microscopy has been quite extensively used to reveal the fine structure of the red cell membrane. Electron micrographs of the red cell membranes have shown a fibrous network on their surfaces. The diameter of these fibrous structures, for human red cells, has been shown to be nearly 200Å (Hillar and Hoffman, 1953; Hoffman, 1956). Recently, the fibers of the red cell surface have been reported to be 400Å in diameter (Glaeser, 1963). These workers have further suggested that these filamentous

structures are made up of 'elinin', which is a macromolecular substance ranging in length and diameter up to 10,000Å and 125Å respectively. There is no electron microscopic evidence for a tangential protein layer between the radial lipid layer and this surface felt-like structure in either red cell or any biological membrane. However, this has been shown by optical birefringence using polarized light. All this evidence suggests that in spite of having the specific unit membrane structure, cell membranes are very labile in different environments and which may change the structure drastically before being seen under high resolution electron microscopy. Furthermore, the dimples of a red cell have been reported to reappear at the same part of its surface when a swollen or crenated cell is returned to its normal shape under normal pH (Furchgott, 1940). This suggests that the membrane at the dimple regions might be interacting with the contents of the red cell, perhaps with some dynamic long chains of protein molecules. The presence of such proteins has been recently reported in human erythrocyte stroma (Mitchell and Hanahan, 1966). Red cells in an electrical field as well as in hypertonic solution show bumps (20 to 25 per cell) of crenation (Rand, Burton and Canham, 1965). This again suggests some type of charge distribution, with fixed charge groups on the membrane.

On the other hand the probability of the membrane being different in texture and mechanical properties at its

different regions has, however, been contradicted by experiments on rubber models and micromanipulation of different parts of the red cell membrane (Rand and Burton, 1964; Rand, 1964a).

(iii) Thickness

On the basis of chemical analysis of the red cell ghosts, and by calculating the size and arrangement of the molecules of the constituents, the thickness of the red cell membrane has been estimated to be 100 to 500Å (Fricke, Parkar and Ponder, 1939; Nevo, 1960). This thickness range is also in agreement with the thickness of the red cell membrane obtained by leptoscope (which uses interference of reflected light) or by methods of measurement of the electrical impedance (Waugh and Schmitt, 1940). On the basis of leptoscope measurements it has been reported that the membrane thickness changes with pH of the cell environment.

Electron microscopy has given the thickness of the red cell membrane to be between 400 and 1000Å (Robertson, 1959, 1960; Latta, 1952). But for many reasons, this range of thickness cannot be accounted for by the red cell membrane only. The main explanation is that the hemoglobin left in the red cell ghosts, after hemolysis, which may be insignificant as regards the weight of the red cell membrane, may contribute significantly to its thickness. It has been reported that the hemoglobin is an integral part of the red cell membrane and therefore this membrane may not have definite interior boundaries (Harris, 1964, p. 198).

In general the contradiction in the data available about the thickness of the red cell membrane, is probably due to preparation of the red cell ghost by different methods, so that they contain different amounts of hemoglobin, differently distributed.

4. Electrophoresis

Electrophoretic measurements of intact red cells indicate that they are negatively charged at physiological pH. As in the case of other cells, the interior of a red cell may be negative with respect to its outer surface. The first reported isoelectric point of the red cells was roughly in the neighborhood of pH 2 (Abramson, Furchgott and Ponder, 1939). This value was considerably lower than the value of isoelectric points found for either extracted protein or lipid fractions of the red cell ghosts, yet it was concluded that the red cell surface charge is due to phospholipids. The mobility of the red cell in the electrical field has been reported to be constant between pH 6.0 to 11.0, and the mobility of human red cell ghosts is not significantly different from that of the intact red cells (Heard and Seaman, 1960). Thus, it was suggested that protein and lipid groups, which are positively charged at pH 7.4 and groups with pK's in the range of 6.0 to 11.0 must be effectively folded in the red cell membrane structure (Heard and Seaman, 1960). For the human red cells, a mean surface charge density (3280 e.s.u. per sq. cm.) over a wide range of ionic strengths was found

by Hunter in 1960. Recently, the existence of fixed charge groups in the red cell membrane has been reported (Elul, 1967; Ginzburg, Friedlander and Pouchovsky, 1967). It is quite probable that some of these charge groups may be positive and some negative. The membranes of two red cells in agglutination have been shown by electron microscopy to make contact only at few points with each other (Danon, 1967).

It has been reported that the red cells treated with receptor-destroying enzymes almost completely lose their negative charge (Stone and Ada, 1952). Later, it was reported that there is a reduction in the electrophoretic mobility of the red cells, if they are treated with neuraminidase, a receptor-destroying enzyme (Cook, Heard, and Seaman, 1961). Recently, the pH-mobility curve for OsO_4-fixed red cells has shown that these red cells are isoelectric at pH 1.6 (Glaeser and Mel, 1964). The alternative explanation for this is that the lipid and protein of the red cell membrane play a relatively minor role in the determination of the net charge on the red cell surface; since they are effectively undissociated, being far back from the membrane surfaces. On the other hand, a carboxylic group of N-acetylneuraminic acid (sialic acid) may be completely responsible for the normal charge on the surface of a red cell. Since this substance has no cation groups at pH 7.4 and it appears to have all the acid-base characteristics necessary to explain the entire pH-mobility curve from pH 0.9 to 12.3 (Glaeser and Mel, 1964; Seaman and Uhlenbruck, 1963). Harry, Wing and Seilby (1965), and

Danon, Howe and Lee (1965) have also reported sialic acid as being implicated, bearing almost the total surface charge of the red blood cells. Recently, the surface charge on the older red cells has also been reported to be less than the charge on the surface of the younger red cells (Marikovsky, Danon, and Katchalsky, 1966). The potential difference across the human red cell membrane has been measured to be 8 mV, negative inside with respect to extracellular fluid (Jay, 1968).

5. Rouleaux Formation

Rouleaux formation of red blood cells shows that under certain circumstances red cell membranes attract each other. There is experimental evidence that in the absence of long chain proteins (like fibrinogen) in the plasma the probability of rouleaux formation decreases considerably (Merrill, Cokelet, G. C., Britten, A. and Wells, R.E., 1963). This suggests that these long chain protein molecules in the electric field of surface charges, might have arranged themselves parallel to each other and normal to the red cell surfaces.

This formation of tactoids between the red cell surfaces may possibly produce an attractive force after overcoming the repulsive force between similarly charged surfaces bringing red blood cells together to form rouleaux (Weiss, 1965).

6. Hemolysis of the Red Cell

Red cells change in shape in different environments. Osmotic and chemical means are usually used to bring about a change in the environment of the red cells, which ultimately leads to hemolysis or crenation.

(i) Osmotic Hemolysis

In a hypotonic solution red cells swell due to water entry through their membranes, and if the solution is hypotonic enough, the cells become spherical in shape. At the stage of spherical shape, the membrane abruptly becomes permeable to hemoglobin and hemolysis takes place. When the concentration of hemoglobin in the cell reaches its concentration in the environment, hemoglobin stops leaking. This hemolysed cell, which is known as the 'red cell ghost', can be hemolysed more completely by transferring it into another hypotonic solution free of hemoglobin (Hoffman, 1958). In this way, by adjusting the ionic strength of the hemolysing solution as much as 99.95% of the red cell hemoglobin can be removed, apparently causing very little structural change in the membrane. After hemolysis the changes in shape of a red cell are reversible, and in the proper environment, the red cell ghost regains the biconcave shape again. In swelling up to spherical shape, the volume of a red cell nearly doubles, but there is very little increase in its surface area (Ponder, 1948; Rand and Burton, 1963). On the other hand, in hypertonic solutions, water leaks out through the membrane, the cell loses its shape, and ultimately crenations on the red cell surface occur.

Again the crenated cell regains its shape on transferring it into an isotonic environment. The crenations per cell are 20 to 25 in number and seem to have some specific spacing on the membrane.

(ii) Chemical Hemolysis

There are many surface active agents (hemolysins), such as saponin, digitonin, etc., which cause a reversible change from normal shape to sphere, without any significant change in volume of the red cell. These agents in higher concentration disrupt the cell membrane. For hemolysis, the quantity of hemolysin (sphering agent) required is even much less than that required to form a monolayer over the cell surface. This suggests that there are some specific points on the membrane of the red cell where these sphering agents act. The time for hemolysis depends upon the specific sphering agent and its concentration (Ponder, 1948). Small quantities of these sphering agents produce drastic structural changes in the cell membrane (Douramashkin, Dougherty and Harris, 1962; Husson and Luzzati, 1963).

7. The Composition of the Red Cell Interior

Normal red blood cells contain about 28% (28 gm per 100 ml. of red cells) hemoglobin. Other constituents amount to 2% (stromal meshwork of protein, phospholipids, etc., nearly all in the membrane). The rest of the volume of red cells is occupied by water molecules (about 65%), cholesterol and membrane lipid and protein (about 5%) (Harris, 1965, p.199; Kugelmass, 1959 p.298). Calculations on the basis of molecular

dimensions of the hemoglobin molecule show that there are nearly 3 x 10^8 hemoglobin molecules per red blood cell and they are very closely packed in it (Drabkin, 1945). The rest of the volume of the interior of a red cell is occupied by water, glucose and other molecules. However, the number of molecules of the glucose and other substances in the interior of the red cell is nearly the same as the hemoglobin molecules and thus contribute equally to the osmotic equilibrium of it. The red cell may be in osmotic equilibrium with its environment (Williams, Fordham, Hollander, 1959). However, according to Ponder (1940) a red cell does not always behave as a perfect osmometer, probably because of the bound water molecules with the hemoglobin molecules, and thus it may not be in osmotic equilibrium with the environment. Furthermore, the amount of the stromal protein 'Stromatin' present in a red cell is not accurately known, but the fact that as little as 0.1% suspension of stromatin can gel, shows that the red cell contents may be in gel state rather than a sol state (Fricke, et al., 1939).

8. The Interaction Between the Interior Contents and the Membrane of the Red Cell

Charges on the surface of a red cell will produce an electrical field inside the cell. This electrical field, if it is sufficiently strong, would orient molecules of the proteins and lipids present there. Elinin extracted from the red cell membranes has been found to have long molecules and seems to have a structural framework with the other

protein and lipid molecules, forming a stroma by linking laterally inside a red cell. These lipo-protein molecules seem highly oriented at the inside surface and contain little hemoglobin. The hemoglobin concentration progressively increases toward the center of the red cell, while the concentration of lipid and protein molecules decreases, so that no absolute dividing lines can be drawn. (Harris, 1965 p. 199; Prankerd, 1961. P. 16). The individual molecules of hemoglobin are fairly ordered at the surface, while the orientation progressively decreases towards the center. Nevertheless, some ordering of the hemoglobin may exist throughout the cell, since low-angle x-ray scattering shows that the molecules can individually move freely but only within their own limited spaces, packing being such that only 10Å separates one from the other (Bateman, Hsu, Knudson, Yudovitch, 1953).

It has been suggested that the orderly long-chain lipo-protein molecules, ramifying through hemoglobin molecules from one flat surface to another of a red cell, will support hemoglobin molecules and vice-versa, and thus adding rigidity to the whole supporting structure (Crosby, 1959). Moreover, the lipo-protein structure will be even stronger because of the bumpy inner surface of the membrane (Glaeser, 1963). From time to time, workers have tried to show lipo-protein meshwork electron microscopically in the red cell, but the results reported, so far, have been vague. This may be because of the subtle nature of the meshwork,

and so the chains could be easily washed away by different reagents involved in processing of red cells for experimentation. Recently, it has been reported that there exists a protein in the interior of the red cells, which is analogous to the proteins found in the muscle. This protein can be separated, and if the adenine nucleotide of this protein is added, the cell configuration changes. This suggests that an ATP-dependent contractile protein might be playing a vital role in maintaining the biconcave shape of a red cell (Nakao, Nakao and Yamazoe, 1960, 1961).

9. Summary

The red cell membrane, a lipo-protein complex, has to some extent a regular structure. The estimate of thickness of the red cell membrane varies from 100Å to 1000Å. Electron micrographs show a stroma of fibers nearly 400Å in diameter on the surface of the membrane. Specific charge groups have been reported to be present on the red cell membrane. Rouleaux formation of the red cells takes place only if some long chain protein molecules, like fibrinogen, are present in the suspension medium.

The interior of the cell contains a very highly concentrated hemoglobin solution. The hemoglobin seems to play no part in the maintenance of the red cell shape. Other proteins in very minute quantities have also been shown to be present inside the red cell.

There seems to be some interaction between the red cell membrane and its contents.

III. ATTRACTIVE FORCES WITHIN A RED CELL AND BETWEEN RED CELLS

1. Introduction

The problem of the biconcave shape of the red blood cells has been the subject of much comment and speculation. Many explanations have been suggested and theories have been proposed so far, but this biophysical problem remains unsolved. How can the biconcave shape, and indeed the whole family of shapes, from normal to spherical, of a red cell in the hypotonic solution represent physical equilibria of the membrane under the known forces acting on it? Not only the normal red cell and its different configurations in the hypotonic solution, but the ghost of a red cell again acquires a biconcave shape and maintains it, if it is transferred into an appropriate environment.

In this section we will consider whether the forces which we know acting on the membrane of a red cell are adequate and sufficient to explain its shape in the normal state, and also the infinite number of stable shapes it may acquire in hypotonic environments of different tonicities. If not, what extra forces, in addition to the forces which we know acting on the membrane, are needed to maintain a

biconcave discoidal shape? How will these forces vary from point to point on the membrane of the red cell?

2. The Mechanical Properties of the Red Cell Membrane and the Known Forces Acting Upon It

A particular shape of an object is the result of all the forces acting upon it. Therefore, the forces acting upon the membrane of an intact red cell must explain its biconcave discoidal shape. These forces may be classified into two categories:

(a) The ones which are due to the reaction of the cell membrane, i.e. which originate in the cell membrane and may be classified as 'intrinsic forces'. These forces are the components of the different stresses in the membrane.

(b) The others are the forces which originate either inside or outside of the cell membrane and may be classified as 'extrinsic forces'. The transmural pressure across the membrane of the red cell comes in this category.

Rand (1964b), by pulling a part of the red cell membrane into a micropipette, by applying very small negative pressure, and by pressing a normal red cell with this stiffer one, has shown that the tension and rigidity can develop in the membrane, and a red cell behaves like a fluid filled membrane. The fact that a red cell ghost resumes the normal red cell shape in the proper environment also supports this (Ponder, 1944).

The following properties of the red cell membrane are also mainly based on the experiments done by sucking

different parts of the red cell membrane into micropipettes of different diameters (Rand and Burton, 1964; Rand, 1964a). Katchalsky and his colleagues (1960), have also come to the same conclusions with entirely different methods. These properties of the red cell membrane which have to be considered in any theory of how the biconcave shape of a red cell is maintained appear to be:

(a) The resistance to bending of the membrane of the red cell is very small, though not negligible. Expressing the modulus of the resistance to bending in terms of interfacial tension (surface tension) it has a value of about 0.013 dynes/cm only (surface tension of water is 75 dynes/cm). This gives a very low value of red cell membrane bending moment, ensuring it a very small energy expenditure on bending, thus allowing the red cell to change shape very easily. The shape deformation is necessary for a red cell in the crowded and bumping circulation. In addition to this, the surface energy (interfacial tension) of the membrane of a red cell is about 0.014 ergs/sq.cm., which tends to resist the change of area of the membrane (like the surface tension in a soap bubble).

(b) The Young's modulus of the membrane is of the order of 10^7 dynes/sq.cm., which is less than that of collagen and more than that of elastin. This high value shows that the resistance to increase in the area of the membrane (resistance to stretch) is quite high. As little as 15% increase in the area of the membrane produces structural

changes which are reversible. At this stage, hemoglobin starts leaving the cell and hemolysis takes place. However, the shape changes up to sphere do not change surface area of the cell.

(c) The membrane creeps under stress and the time to hemolyse a red cell under a stretching stress depends upon the magnitude of that stress. The co-efficient of viscosity of the membrane is of the order of 10^7 poise. These properties give a visco-elastic nature to the red cell membrane, suggesting that the tension in the membrane must be uniform all over. The membrane can rejoin itself or another membrane, so that a broken cell is 'healed'.

(d) The transmural pressure across the cell membrane has been reported to be 2.32 mm of H_2O (nearly 227.4 dynes per sq. cm.), (Rand and Burton, 1964). This pressure not only exists in normal red cells, but also in cells osmotically swollen to biconvex shapes (short of the sphere). On the other hand, this pressure is absent in cells shrunken by hypertonic solution. The volume of the cells in a hypotonic solution increases, but it is only when the cells become spheres and the area increases that the tension rises in the membrane, the cells become rigid and their internal pressure rises greatly.

(e) The membrane appears to be uniform and thin. The electron-microscopic studies have reported its thickness to be about 100Å. Micromanipulation of the red cells has shown no difference in the behavior of the membrane at the

rim and at other parts of the cell, as at the dimple region (Rand and Burton, 1964). In an attempt to check the validity of the isotropic nature of the membrane, Rand (1964b), made many rubber models, cast in the biconcave shape, with a slightly thicker region at the dimple than at the rim and vice-versa. The behavior of these, as they were inflated, never did imitate that of the red cell, as it is osmotically swollen. For example, these models never became perfectly spherical, even with high pressure inside, and showed the 'oil-can' phenomenon, snapping from biconcave to biconvex shape at a critical pressure. Red cells never show the 'oil-can' effect and when swollen to spheres appear to be geometrically perfect.

Thus, looking at the properties of the red cell membrane as described above, we will assume the membrane to be thin, isotropic and uniform in thickness, with a uniform tension in it. This suggests that 'soap-film Physics' may be of some use in exploring the problem of its different equilibria, either as an intact normal red cell or as a swollen red cell in hypotonic solution, up to its spherical shape. It may also reveal why a red cell ghost regains and maintains the same shape as a normal red cell in an appropriate environment. In contrast, physics of rigid shells may be involved in this problem which involves, even in the simplest cases, almost intractable mathematics and complicated solutions with multiple peculiar points. Tentatively, therefore, let us try 'soap-film Physics' and see where it leads in regard to the different equilibria of a red cell membrane.

3. Geometry of the Red Cell Membrane

Any surface can be completely defined by two principal radii of curvature R_1 and R_2 for each point on the surface. The red cell membrane forms a surface of revolution about the axis shown as axis of rotation in Figure 2. On purely geometrical manipulations, the principal curvatures $\frac{1}{R_1}$ and $\frac{1}{R_2}$ at different points on the membrane can be determined from the average profile of the red cell given by Ponder in Figure 2. Geometrically, the two principal centers of curvature C_1 and C_2 of the membrane at any point on it must lie on the normal at that point. C_1 is the center of the circular arc at point X, drawn in the plane of the figure and which fits the curve of the profile at this point (Figure 2). Practically, C_1 is taken as the point of intersection of the right bisectors of the two small chords lying close to the point X. C_1X is then the radius of curvature R_1. Since the surface is one of revolution about an axis, the other center of curvature C_2 must be at the intersection of the normal to the curve at X and this axis. Thus, the other principal radius of curvature at point X of the profile is R_2. The centers of curvature C_1 and C_2 may lie on the same or opposite sides of the membrane, and thus R_1 and R_2 may be either positive or negative. Conventionally, these are positive if they lie toward the inside of the cell (i.e. tending to external convexity), and negative if they lie toward the outside (i.e. tending to external concavity).

Figure 2.

Schematic representation of the two quadrants of a red cell profile.
The cell is generated by rotation of the quadrants about the axis of symmetry.
The two principal radii of curvature, $R_1 = C_1X$ and $R_2 = C_2X$, are described in the text for different singular points on the red cell profile.

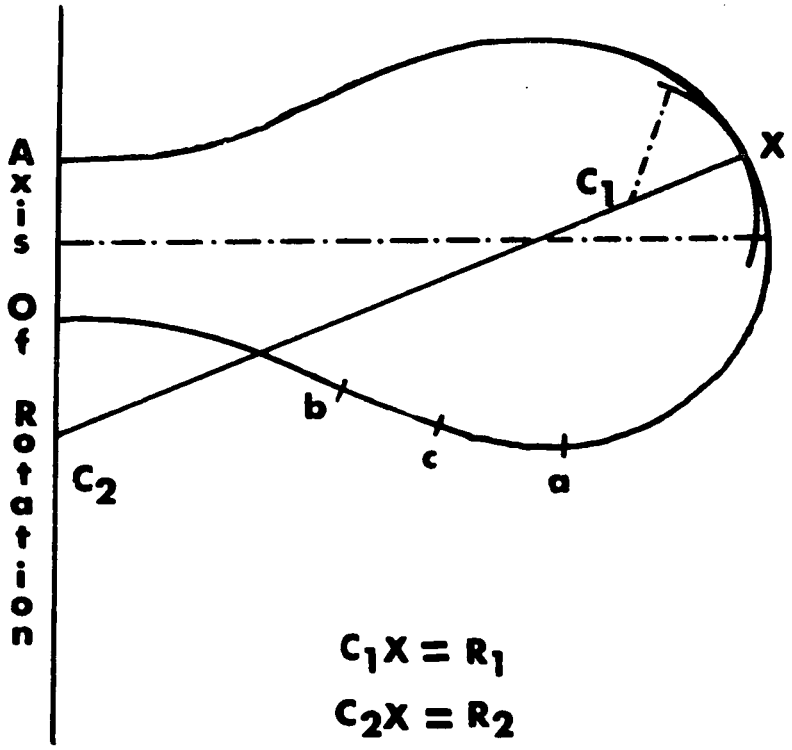

$C_1X = R_1$

$C_2X = R_2$

According to the variation of $\frac{1}{R_1}$, $\frac{1}{R_2}$ and $(\frac{1}{R_1} + \frac{1}{R_2})$, the red cell surface has several singular points and the membrane can be divided into three regions (Figure 2).

(a) From the extreme point on the rim to the point 'a' where the normal to the curve becomes parallel to the axis of revolution, making R_2 infinite (i.e. $\frac{1}{R_2} = 0$), both radii of curvature are positive. The surface is 'synclastic' and convex outward. The point 'a' where $\frac{1}{R_2} = 0$ is a singular point.

(b) From the point 'a' where R_2 is infinite (i.e. $\frac{1}{R_2} = 0$) to the point 'b' where R_1 is infinite (i.e. $\frac{1}{R_1} = 0$) which is the point of inflection of the profile, the surface is 'anticlastic', i.e. in this region R_1 and R_2 have opposite signs. The point where $\frac{1}{R_1} = 0$ is also a singular point on the profile. In this 'anticlastic' region there is a point 'c' where the two radii of curvature R_1 and R_2 are equal in magnitude and opposite in direction (i.e. $\frac{1}{R_1} + \frac{1}{R_2} = 0$). This is known as an 'isoclastic' point.

(c) From the point 'b' where R_1 is infinite (i.e. $\frac{1}{R_1} = 0$) to the point through which the axis of revolution of the profile passes, the surface is once more 'synclastic' with both radii of curvature R_1 and R_2 negative. In other words, the surface is concave outwards.

4. Theoretical Considerations

(i) The Membrane Theory of Thin Shells

The extrinsic force we know so far, acting on the red cell membrane is the positive hydrostatic pressure across its membrane, producing tangential stresses. It has already been mentioned that, although the red cell membrane is curved at its different regions, the stresses due to bending of the membrane are treated here as insignificantly small in comparison to those in reaction to the stretch in the membrane. The red cell membrane is taken as thin (about 100Å) and apparently uniform (Rand and Burton 1964b). Thus the membrane theory of thin shells (Timoshenko, 1959; and Novozilov, 1959) seems applicable to account for the shape of a red cell, if we neglect the bending moment.

Neglecting the bending stresses, the equilibrium of a point on the membrane of a red cell may be represented by the equation:

$$\Delta P = \frac{T_1}{R_1} + \frac{T_2}{R_2} \qquad (1)$$

Where ΔP is the transmural pressure (extrinsic force) acting uniformly over the membrane, T_1 and T_2 are the tensions at the point under consideration on the red cell membrane acting in the direction perpendicular to the two principal radii of curvature R_1 and R_2 at the point respectively (Figure 3). Let the comparable tensions be T_1^1 and T_2^1 at some other such point on the membrane. Therefore, on the basis of different tensions at different points, membranes can be divided into the following categories:

Figure 3.

Schematic diagram illustrating the two principal radii of curvature of an element of the membrane and some of the forces involved in its deformation.

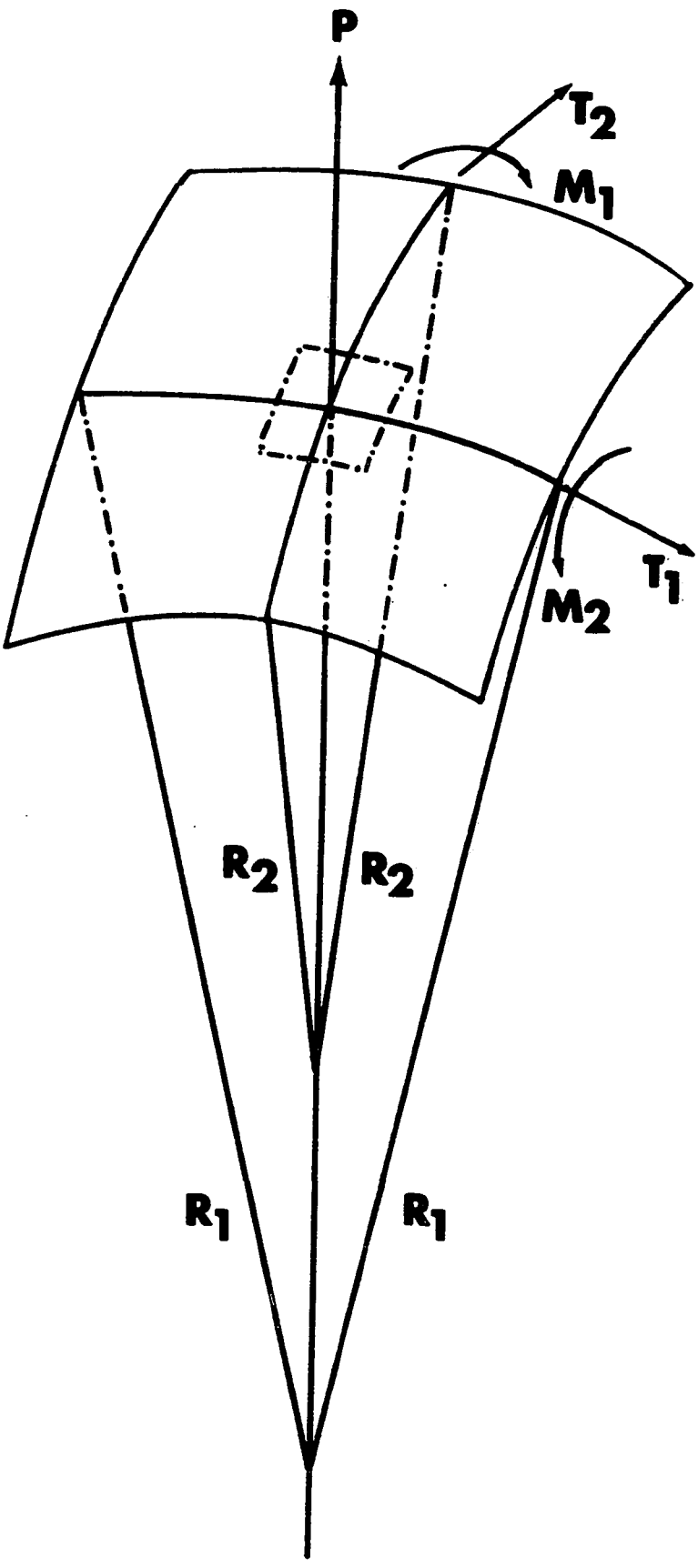
P
T2
M1
T1
M2
R2
R2
R1
R1

(a) Isotropic - if $T_1 = T_2$ and $T_1^1 = T_2^1$

(b) Anisotropic - if $T_1 \neq T_2$ and $T_1^1 \neq T_2^1$

(c) Homogeneous - if $T_1 = T_1^1$ and $T_2 = T_2^1$

(d) Inhomogeneous - if $T_1 \neq T_1^1$ and $T_2 \neq T_2^1$

For the sake of simplicity, and also knowing the visco-elastic nature of the red cell membrane where tension would always equalize, we will assume the membrane to be isotropic and homogeneous. Thus, for the membrane of the red cell we will write

$$T_1 = T_2 = T_1^1 = T_2^1 = T$$

where T is the uniform tension all over the red cell surface. Under these conditions equation (1) can be written as:

$$\Delta P = T \cdot \left(\frac{1}{R_1} + \frac{1}{R_2}\right)$$

$$\frac{(\text{dynes})}{(\text{sq. cm.})} = \frac{(\text{dynes})}{(\text{cm.})} \cdot \frac{(1)}{(\text{cm.})} \qquad (2)$$

which is the familiar law of Laplace for liquid interfaces.

It may seem that we have oversimplified the situation; however, if bending stresses are neglected then the visco-elastic nature and other properties of the red cell membrane compel us to think along these lines which, at least, lead us to familiar 'soap-film Physics'.

(ii) Equilibrium of the Red Cell Membrane

Ordinarily no soap film could take the shape of a red cell. Moreover, if we go to the equation (2) and with its help try to analyze the biconcave shape of a red cell membrane by taking, one by one, components involved in the equation, it soon appears that some force is still missing

about which we know nothing so far, and possibly the equation is not applicable. Rand and Burton (1964) concluded that ΔP and T are constant and not zero all over the membrane surface. Yet, because the principal radii of curvature R_1 and R_2 are different at different points, the term $(\frac{1}{R_1} + \frac{1}{R_2})$ varies from point to point on the membrane of the red cell.

This variation of $(\frac{1}{R_1} + \frac{1}{R_2})$ from point to point with ΔP and T being constant suggests that equation (2) is not sufficient to maintain the equilibrium of a red cell membrane. Moreover, at the isoclastic point where $(\frac{1}{R_1} + \frac{1}{R_2}) = 0$, equation (2) suggests that ΔP is zero, which does not seem correct as ΔP is constant all over the membrane of the red cell. Thus, equation (2) alone seems inadequate unless some extra force acts on the membrane. The magnitude and direction of this extra force must be such that the right-hand side of the equation (2) in spite of the variation of $(\frac{1}{R_1} + \frac{1}{R_2})$ at each point on the membrane, is always equal to ΔP.

(iii) The Need for an Attractive Force

Consider a point on the rim of a red cell membrane (Figure 4). The tension at this point produces an inward force which could balance the excess pressure ΔP at this point. However, at the axial point where the membrane is concave outward, the tension in the membrane at this point would produce an outward force, which would act on it in the same direction as excess pressure ΔP, tending to push out the membrane. This suggests that under the existing forces, which we know act on this point, physical equilibrium of the

Figure 4.

Schematic diagram to illustrate the missing normal force p^1 required to explain the equilibrium of the red cell membrane if it obeys soap-film physics.

As shown in the diagram the force p is constant, whereas the proposed force p^1 varies from point to point on the membrane of the red cell. It is a maximum at the dimple, and a minimum at the periphery of the membrane.

$$\Delta P = T \left\{ \frac{1}{R_1} + \frac{1}{R_2} \right\}$$ Cannot APPLY.

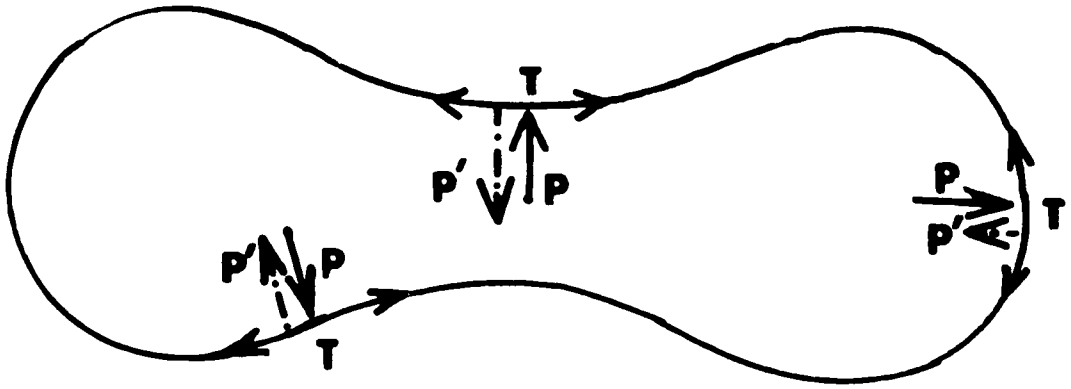

$$\Delta P = T \left\{ \frac{1}{R_1} + \frac{1}{R_2} \right\} + P'.$$

P' = Normal Attractive Force/Area.

membrane of the red cell is not possible; whereas, this point (axial point) on the membrane is in physical equilibrium and thus an extra force is required to act at this point which will balance the effect of ΔP and T on the membrane. In the same way, if we account for the equilibria of all such points which ultimately constitute the whole membrane, we will find that this extra force cannot be the same at all points on the membrane. In other words, this force has to vary from point to point on the membrane, and its variation will determine the principal radii of curvature of these points.

We therefore add, hopefully, a normal inwardly directed force per unit area p^1 (dynes/sq.cm.), (Figure 4). These considerations thus change the shape of equation (2), to account for the shape of an intact red cell, as follows:

$$\Delta P = T \cdot \left(\frac{1}{R_1} + \frac{1}{R_2}\right) + p^1 \qquad (3)$$

$$\frac{(\text{dynes})}{(\text{sq.cm.})} = \frac{(\text{dynes})}{(\text{cm.})} \cdot \frac{1}{(\text{cm.})} + \frac{(\text{dynes})}{(\text{sq.cm.})}$$

Seeing the equilibrium profile of the red cell membrane, we can assess the variation of this proposed attractive force over it. At the axis point this attractive force must be maximum, acting inwardly. From the axis point to the isoclastic point, this force should decrease steadily so that at the isoclastic point it becomes equal in magnitude and opposite in direction to the excess pressure ΔP (since at this point $\left(\frac{1}{R_1} + \frac{1}{R_2}\right) = 0$. Furthermore, from the isoclastic point to the extreme rim point, the magnitude of this attractive force appears to decrease.

5. Quantitative Estimation of the Proposed Attractive Force at Different Points on the Red Cell Profile

As has been discussed earlier, the biconcave shape of the red cell obviously suggests that this attractive force p^1 needs to be greatest at the axis, and need not be very great, if it exists at all, at the rim. With the data available about ΔP and T, and the interpretation given, we can quantitatively estimate the magnitude of this normal inward force per unit area at different points on the membrane.

The best value for the excess pressure ΔP is 2.32 mm of H_2O (Rand and Burton, 1964), while for the tension T the value can be taken as 0.014 dynes/cm (Rand, 1964b). This latter value is obtained from measurements on shrunken and crenated cells and seems to represent the interfacial (or surface) energy only of the membrane. For the normal and osmotically swollen cells the value of T is given by .037 dynes/cm., which includes the resistance to bending of the membrane also. Soap-film physics does not include any form of energy contributing to the surface tension except surface energy. Thus, it would be unjustified to use this higher value of surface tension obtained from the swollen red cells. The principal radii of curvature at the different points on the red cell profile are calculated as has been previously described in this section.

Photographs of the ten red cells on edge chosen as representing the average shape (Figure 5) were taken to find the principal radii of curvature at different points on their

Figure 5.

Examples of photographs of red cells on edge with the line profiles used for measuring radii of curvature. These radii were used to calculate p^1 at these different singular points. The line profiles are drawn on the basis of the rules laid down by Ponder (1930).

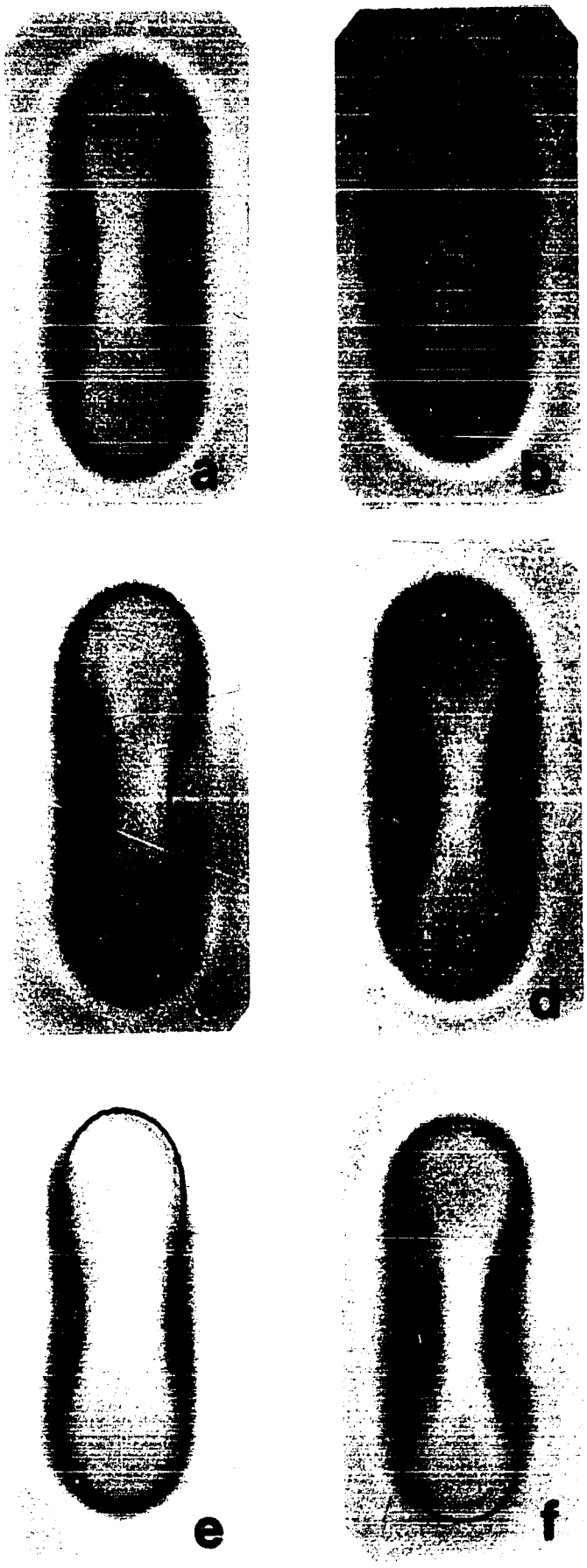
a
b
e
f

profiles. The profiles were drawn on the basis of the rules laid down by Ponder (1930).

The points of interest on the profile, where the principal radii of curvature are measured and the proposed attractive force has been calculated, are singular points as follows:

(a) There are two conjugate axial points on the profile. The principal radii of curvature R_1 and R_2 at each of these points must be equal in magnitude and negative in direction. R_1 and R_2 are measured on both of these points, and the mean of these two radii of curvature has been used for the calculation of the proposed attractive force p^1 at these points.

(b) The points where $R_1 = \infty$ are four on a red cell profile, distributed symmetrically on the membrane in each of the four quadrants. R_2 is measured separately on all of these four points and its mean has been taken in the calculations for the force of attraction p^1 at these points.

(c) Isoclastic points are also four, distributed symmetrically on the membrane in each of the four quadrants of the profile. At these points where R_1 and R_2 are equal in magnitude and opposite in direction gives $(\frac{1}{R_1} + \frac{1}{R_2}) = 0$. Thus, from the equation (3) the attractive force p^1 is equal to excess pressure ΔP at these points.

(d) The points where $R_2 = \infty$ are again four in number, distributed symmetrically on the membrane of each of the four quadrants of the profile. Normals to the profile at

these points become parallel to the axis. Again R_1 is measured separately on each of these points and mean is used to calculate the proposed attractive force p^1 at these points.

(e) There are two extreme points on the rim of the profile, where both R_1 and R_2 are positive and coincide with the major diameter of the profile. The measurements for the principal radii of curvature are done separately and the means of R_1 and R_1^1 and of R_2 and R_2^1 have been used in the calculation of p^1 at these points. p^1 at these points is supposed to be very small and minimum.

Table 2 gives the mean of the calculated value of the proposed attractive force p^1 at different points on the red cell membrane. On the axis of revolution the attractive force is maximal and is 2.82 mm of H_2O, while at the rim it is minimal and is only 0.66 mm of H_2O - the distribution we expected. If p^1 at the rim region were negative, and not an inwardly directed small quantity, it would have been difficult to explain it on the basis of the proposed attraction between the opposite membranes of a red cell.

6. The Attractive Forces in Biology

(i) Origin

What could be the origin of this attractive force of the membrane on one side of the red cell for its own membrane on the other side? The existence of such an attraction is more plausible when we remember that the membrane of one red cell evidently attracts the membrane of another

red cell as shown in rouleaux formation (but only if long chain molecules, like fibrinogen, are present in the medium). We are, thus, suggesting that the membrane similarly attracts the membrane, not only of another cell, but its own membrane across nearly the one micron distance at the axis, and the long chain molecules inside the red cell are involved in the attraction.

(ii) Long-range Attractive Forces

Speculation and imagination have been powerful tools for thinkers when stubbornly refusing to give up in the face of real theoretical difficulties. The History of Science shows that imaginative and speculative thinking, at times, has given the right direction in which to attack a problem. Thus, here we enter the field of speculation and what follows is mostly the exercise of the imagination.

There is no doubt that in Biology there is much evidence that identical cellular membranes tend to cohere, but do not adhere to membranes which are different. A mixed population of cells will aggregate with their own kind. Leaders in this field, such as Paul Weiss (1958), L. Weiss (1960; 1965; 1967), Abercrombie (1964), and Moscona (1962), have written many reviews on the subject and have produced a wealth of literature. The specific attractive forces exist, between the biological objects, and often over very large distances, yet the nature of these forces is very controversial. The two main difficulties are:

(a) How can 'like' membranes have a specific attraction for each other?

TABLE 2

Mean values of the proposed force of attraction p^1, calculated at specific points on the membrane of the red cell.

Point on the membrane	Proposed attractive force p^1 (mm. of water)
Axis of revolution	2.82
$R_1 = \infty$	2.54
Isoclastic point	2.32
$R_2 = \infty$	1.50
Rim end	0.66

Figure 6.

Schematic diagram to illustrate the force between two lines of equally spaced alternate positive and negative charges.

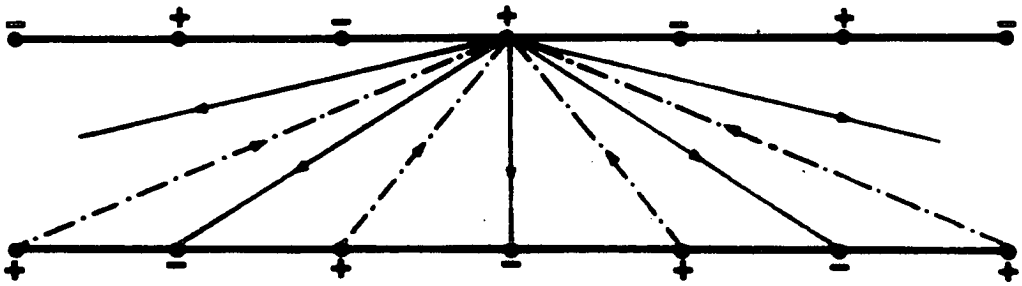

Net Attraction

Net Repulsion

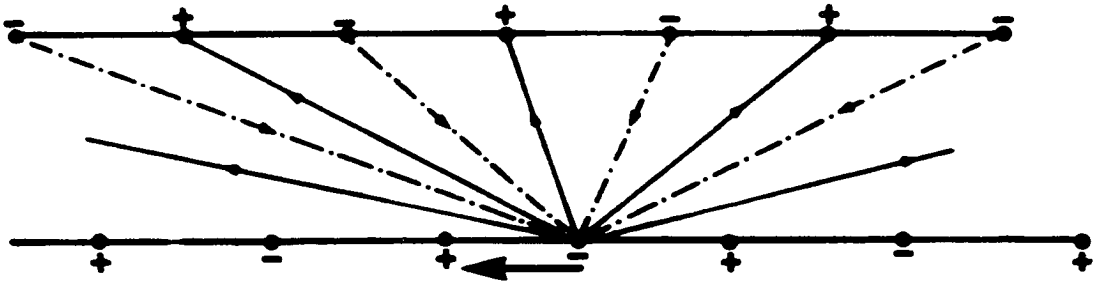

Axial Force

(b) How can the attractive forces extend over long distances (of molecular dimensions)? At distances up to 200Å London-van der Waals forces are a satisfactory explanation, but cannot operate at greater distances.

If the forces are electrostatic in nature, logic forces us to answer question (a) in terms of a regular pattern of spacing of positive and negative charges. The problem can be simplified and can be given necessary specificity as shown in Figure 6 as a line of charge. To understand the actual problem, a two dimensional picture of the membrane surface has to be imagined. As has been shown in Figure 6, the charge distribution may give rise to a significant net attraction, or repulsion between the membrane surfaces and may also produce very little attraction if the spacing of charges is not nearly identical. However, to get a significant force of attraction, the identical spacing distance between charges of opposite sign must be comparable to the distance between the two membranes. For the problem of the red cell, the charges will have to be of the order of one micron apart. In fact, it has been shown that in the crenated cells due to hypertonic solution, the crenation 'spots' are 20 to 25 in number per cell, being nearly one micron distance from each other. Similar results have also been reported about red cells under electrical fields, (Rand, Burton and Canham, 1965). These workers have shown also that these crenated spots appear and disappear at the same spot on the same cell quite reversibly. Also, in the conditions of pH approaching those that cause crenation, the cells often show

regular polygonal forms with sides of about one micron in length, so that we do not think the 'spots' or vertices of these polygons represent merely a random folding of the membrane, but rather, pre-existing points of discontinuity. They could be charge centers. In this Department of Biophysics, a computing program was also started to show whether an array of charges spaced over the surface of a wooden model of the shape of a red cell, about one micron apart, would give the distribution of the normal inward force required. For this there were two requirements. The resultant at each point must be zero in the plane of the membrane, and must have the required value along the normal. The computing problem could not be completed as we realized that we did not know whether we ought to use the inverse square law for the potential computation. This led us to experimental work on a physical model. The results of this work are presented in the next section.

We come to the second question: Whether electrostatic forces of sufficient magnitude could be produced over distances of up to one micron and more. If the intervening medium were nonconducting, we would calculate how much charge density on the plates of a parallel plate condenser would be needed to obtain a force of 2 to 3 mm H_2O (about 200 to 300 dynes/sq. cm.) at a distance of one micron. The formula is:

$$F = \frac{2\Pi}{K} (\text{Charge density})^2, \qquad (4)$$

where K is the dielectric constant. This formula is independent of the distance.

Using the value of p^1 as 2.82 mm H_2O (275 dynes/sq. cm.) the charge density required would be, for water (K = 80), nearly 60 e.s.u. per sq. cm. Now the surface charge density on the red cell, deduced from electrophoretic studies has been found to be 3280 e.s.u. per sq. cm. (Hunter, 1960). Thus, it appears that electrostatic forces seem reasonable. However, there is a very serious consideration which seems to eliminate the possibility of electrostatic forces of sufficient magnitude. It is that in a conducting medium, the force between charges is very drastically reduced by the 'ionic atmosphere' effect. In other words, instead of $\frac{e_1 e_2}{r^2}$, it becomes $\frac{e_1 e_2}{r^2} \exp(-cr)$, where the c is related to the conductivity of the medium. If we can remove this objection, the electrostatic attraction between membranes with a pattern of positive and negative charges might be worth pursuing. Goldacre (1954), has claimed the existence of long-range forces in crystalline bacterial arrays. Recently, also, the existence of such forces in Biology has been suggested at distances up to 1μ (Friedenberg, Blatt, Gallucci, Danielli and Shames, 1966; Brooks, Millar, Seaman and Vassar, 1967).

(iii) Action at a Distance by Medium Specialization

One way of obtaining 'action at a distance' is to specialize the medium between the two points concerned. There is abundant evidence, particularly from electron microscopy, of 'fibers' of oriented protein molecules within cells.

These dynamic organizations of oriented fibers, representing linear arrays of dipoles, with long chain molecules from the medium joining and leaving the array freely, play a major role in Biology. This phenomenon is called 'tactoid organization'. Very accurate studies of birefringence have shown such chains, known as 'spindle fibers', in living cells during cellular mitosis (Inoue and Dan, 1951).

Could the orientation of chains of protein molecules (stromatin) within the red cell, between groups of charges distributed over the surface, account for the long range attractive forces necessary to explain the equilibrium shapes of the red cell? Would this orientation of dipoles take place even in saline? At any rate, such orientation does take place in the cytoplasm of cells. Again, what happens to the force between the charges if they are connected by 'bridges' or by oriented long molecules? In particular, how the force would vary with the distance between charges when connected by dynamic long chains is a question which is to be explained in the next section of this thesis.

7. Summary

There seems to be an attractive force between the two surfaces of a red cell as there is between adjacent surfaces of red cells in rouleaux. This extra attractive force, along with positive hydrostatic pressure and stresses due to mechanical properties of the membrane may account for the equilibria of a normal and osmotically swollen cell.

The specialization of the medium inside a red cell,

by long chain-like protein molecules, in the form of dynamic tactoids might produce an attractive force between the interior surfaces of a red cell.

The red cell shape demands this type of attractive force, varying in magnitude from point to point on the membrane. Calculation shows that this force is a maximum at the dimple center and a minimum at all points on the rim.

IV. THE RED CELL AND ITS ELECTRICAL ANALOGUE

1. Introduction

Because of the charged membrane a red cell may be considered as an electrical capacitor of very small capacity. Therefore an electrical model of a red cell may be represented by a parallel plate condenser, charged with an appropriate potential difference across the plates. The net charge inside a red cell is very small. However, because of the small size and short distance between its two surfaces (about 1.3μ apart) (Table 17) the electrostatic field inside a red cell seems to be high. The effect of a high electrostatic field inside a red cell is greatly reduced by the 'ionic atmosphere' effect due to the conducting medium.

Due to the presence of the electrostatic field in a red cell, the formation of dynamic tactoids from long chain protein molecules, which are present inside, is quite probable. From time to time, workers in this field have also tried to show the presence of such long chain molecules inside red cells. The physical equilibria of a red cell in different environments seem to demand the presence of such dynamic tactoids inside it. We hopefully wait for some electron-microscopic evidence for these proposed dynamic tactoids in

Figure 7.

The absolute electrometer used to measure force of attraction between the charged plates.

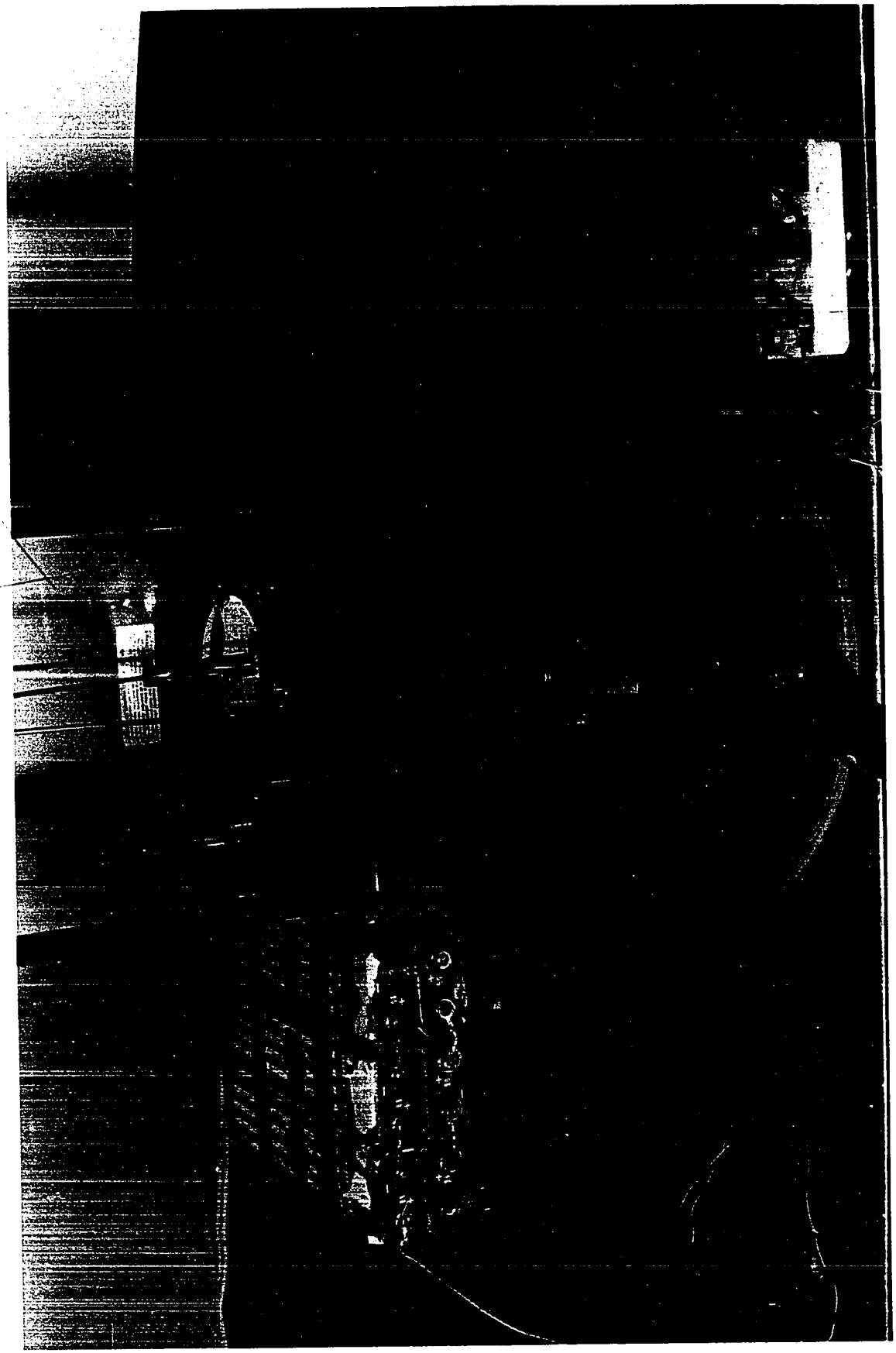

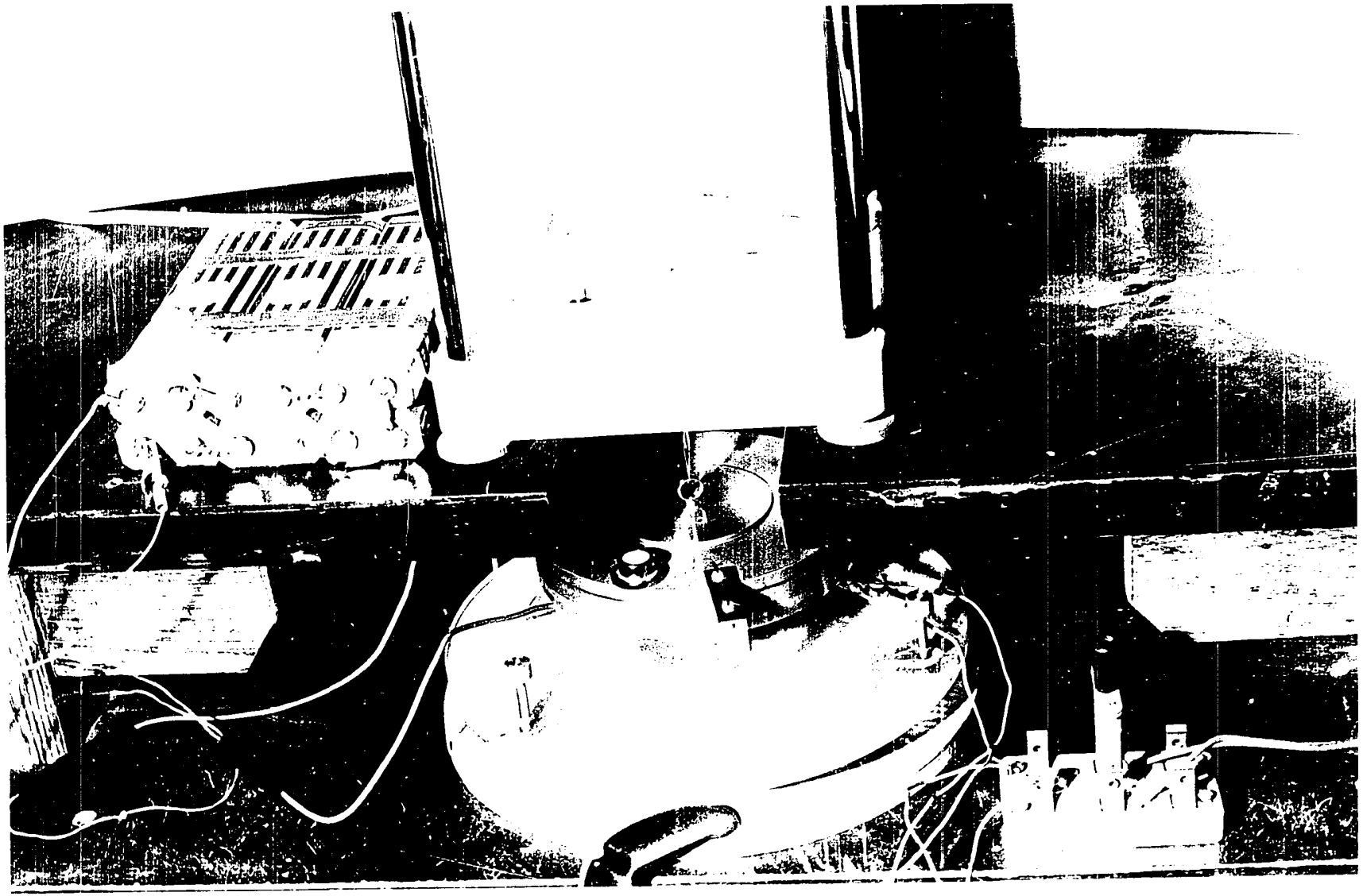

the red cell.

In view of the probable existence of tactoids in red cells, it is very desirable to know the nature and behavior of artificially created tactoids in an electrical model. Therefore, in this section, model experiments have been presented, and it has been shown that the presence of 'tactoids' may affect the classical laws of electrostatics. Whether the results we obtained from model experiments have any connection with the biological problems remain debatable, but at least, we have learned some unexpected features of the model for which there seems no simple explanation at present.

2. Absolute Electrometer

(i) Description

The apparatus used for experimentation was an absolute electrometer made by constructing a parallel plate capacitor. The lower circular plate of the electrometer was 1.0 cm. thick, having a radius of 8.0 cm. The upper plate was 0.7 cm. thick, having an effective radius of 3.6 cm. (the effective radius means the actual radius of the plate plus half of the width of the air gap between the guard-ring and the plate). The guard-ring, which was used to avoid the electric field distortion at the edge of the upper circular plate, was also 0.7 cm. thick. The radius of the lower circular plate and guard-ring was the same. All of these were made of aluminum. A nylon fiber was used to hang the upper circular plate, by a hook provided at its center, to a pan of a balance accurate to 0.1 mg. (Model No. 182372,

Figure 8.

Schematic diagram of the absolute electrometer. Below is the circuit diagram with battery (DC), showing charging and discharging of the parallel plates of the electrometer.

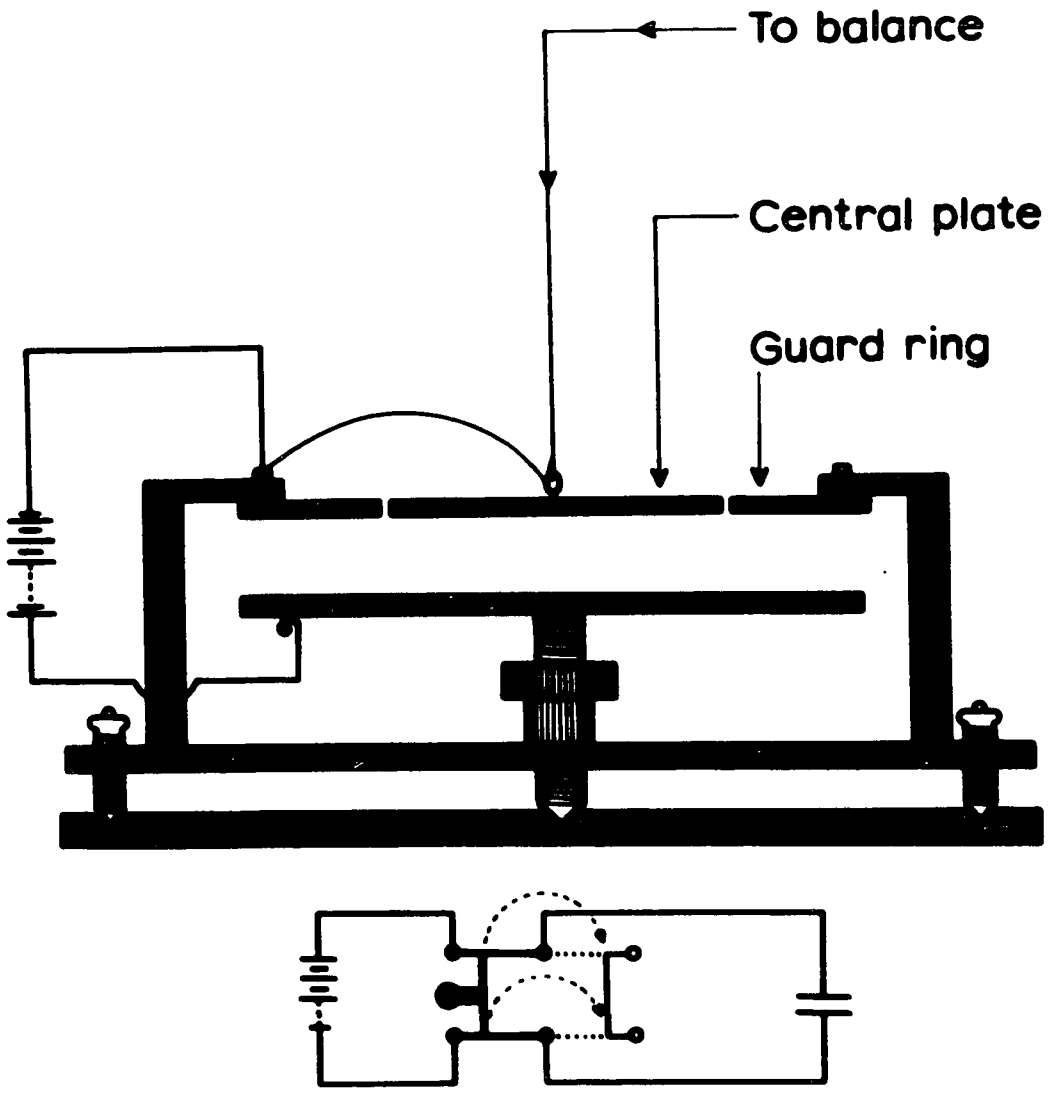
To balance
Central plate
Guard ring

Mettler & Co.), so as to suspend it freely in the circular gap of the guard-ring. In the freely suspended position, both plates were parallel to each other. The air gap between the guard-ring and the upper circular plate was about 0.2 cm. wide. The guard-ring was rigidly fixed and was supported by three pillars as shown in Figures 7 and 8 . Further, the guard-ring and the upper circular plate were electrically connected to each other by a flexible thin copper wire. The lower circular plate was fixed in its position on a supporting circular base-plate having the same radius so that it could be taken out and placed again in its position. At its center there was a circular area marked, which, in its resting position on the base-plate, was just under the upper circular plate. The base-plate was rigidly fixed on a pillar at the center of the instrument, having a graduated movable screw. With the help of this screw, the lower circular plate along with its base-plate could be accurately lowered or raised as desired. This arrangement made it possible to achieve different distances of separation between the two plates of the electrometer. The whole instrument was provided at its base with three levelling screws so that the two plates could be made parallel to each other. These screws were also used to raise or lower the whole instrument to bring the hanging upper circular plate into the plane of the guard-ring. To charge the plates, one pole of a battery was connected through a switch to the lower circular plate. The other pole was connected with guard-ring and the upper circular plate, which

were already connected to each other with a copper wire. Figure 7 shows the photograph of the absolute electrometer, while it is shown diagrammatically in Figure 8.

(ii) Theoretical Consideration

Theoretically, the force on the charged parallel plates of area A is given as:

$$\text{Force} = \frac{KAE^2}{8\pi} \text{ dynes}$$

where K is the dielectric constant of the medium between the plates, and E is the potential gradient between plates in the electrostatic units (e.s.u.). We may take $E = \frac{V}{r}$, where V is the potential difference between the two charged plates in e.s.u., and r is their distance of separation in cms. If the medium between the plates is air K = 1, and since the hanging upper plate is circular having radius R, we can write $A = \pi R^2$. Thus, the above equation becomes

$$F = \frac{R^2}{8} \left(\frac{V}{r}\right)^2 \text{ dynes} \qquad (2)$$

Changing V from e.s.u. to Volts, we have

$$F = \frac{R^2}{8} \left(\frac{V}{300r}\right)^2 \qquad (3)$$

since 300 e.s.u. = 1 volt.

Furthermore, in terms of gms. the force F in dynes can be written as

$$F = mg \text{ (dynes)}$$

where m is in gms. and g = 980 cm. per sec.$^{-2}$.

Thus, the force experienced by a charged plate of radius R is given in gms. as

$$m = \frac{R^2}{8g} \left(\frac{V}{300r}\right)^2$$

$$= \frac{R^2}{8 \times 980 \times 9 \times 10^4} \left(\frac{V}{r}\right)^2$$

$$= 142 \times 10^{-11} R^2 \left(\frac{V}{r}\right)^2 \text{ gms.} \qquad (4)$$

where R and r are in cms. and V is in volts. These three quantities involved in the above expression could be measured for a particular setting of the absolute electrometer, and thus the absolute force experienced by the upper hanging plate can be calculated.

(iii) Control Experiment (Method)

The balance and the absolute electrometer were levelled separately, with nothing but air between the parallel plates. The upper circular plate was hung freely in the plane of the guard-ring, so that it was not touching it. In this position the weight of the freely suspended upper circular plate in air was recorded. Again, after connecting a battery (DC) of 540 volts across the plates of the electrometer, the weight of the upper circular plate was recorded. The difference of these two readings gave the force of attraction between the two charged plates in gms.

Further, the force of attraction was measured at different distances of separation from 1.6 mm. to 7.2 mm. between charged plates. For statistical evaluation, five such sets of force vs distance of separation were taken. Even at 1.6 mm. distance, the shortest distance of separation of

the two charged plates, the leakage current never exceeded 0.2 milliampere.

(iv) Results and Discussion

Table 3 shows the force of attraction between the charged plates of the absolute electrometer obtained experimentally and the corresponding values of force of attraction calculated theoretically, at different distances of separation with nothing but air between the plates. The results serve to indicate the degree of accuracy of the experiments. The lines on the graphs 9A and 9B are those from theory and dots give the experimentally observed values of the force of attraction, corresponding to the given distances of separation of the charged plates.

Theoretically, the force of attraction F can be calculated as has been discussed before. The fit to the curve 9B, representing force vs $(\frac{1}{\text{distance}})_2$, and also to the curve 9A, representing force vs distance is excellent except for the point where the distance between the charged plates is so small that it could not be measured with much percentage of accuracy.

3. Absolute Electrometer With Specialized Medium Between Its Plates

(i) Method

Nylon fibers of three different lengths, approximately 1.0, 0.5 and 0.3 mm. and of about 0.05 mm. in diameter

Figure 9.

Diagram illustrating inverse square law.

(A) Force vs distance between the 'empty' charged plates of the absolute electrometer.

(B) Force vs $\frac{1}{(\text{distance})^2}$ between the empty charged plates of the absolute electrometer.

The lines are calculated on theoretical grounds.

The dots are the experimental points.

Except for the points where the distance between the charged plates is difficult to measure accurately the experimental points fall on the curve.

The data to plot these points have been taken from Table (3).

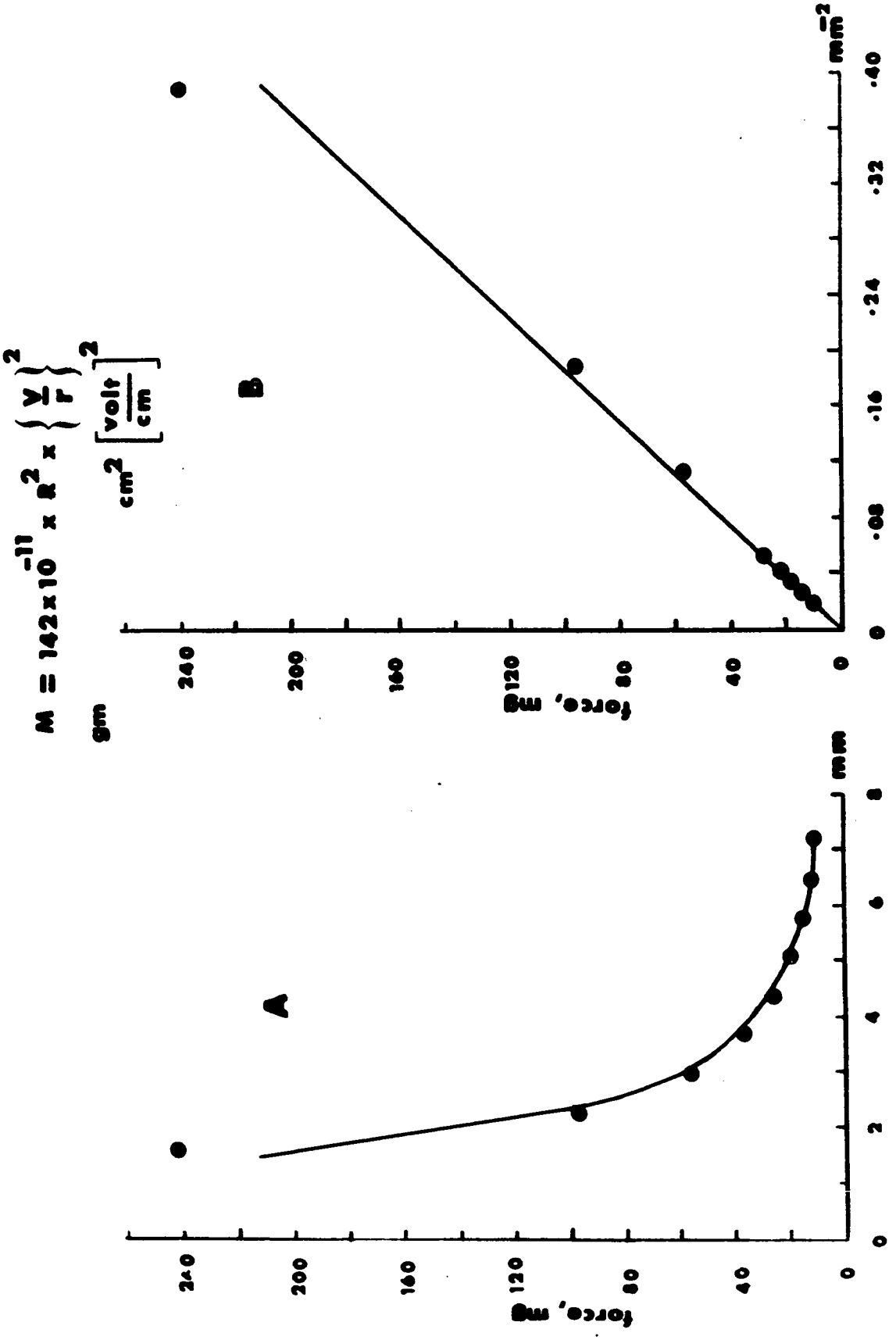
A
force, mg
0
40
80
120
160
200
240
0
2
4
6
8
mm
B
force, mg
0
40
80
120
160
200
240
0
.08
.16
.24
.32
.40
mm⁻²
$M = 142 \times 10^{-11} \times R^2 \times \left\{\frac{V}{r}\right\}^2$
gm
$cm^2 \left[\frac{volt}{cm}\right]^2$

TABLE 3

Table showing force of attraction obtained experimentally and calculated theoretically, between the charged plates of the absolute electrometer with air between the plates. Potential difference between the plates was 540 volts.

Distance of separation between the plates in mm.	Force of attraction obtained experimentally in mg. with SEM	Force of attraction calculated theoretically in mg.
1.6	241.4 ± 1.5	209.2
2.3	95.4 ± 3.1	101.2
3.0	54.7 ± 1.2	59.4
3.7	36.1 ± 0.5	39.1
4.4	26.0 ± 0.4	27.6
5.1	19.4 ± 0.3	20.5
5.8	15.3 ± 0.2	15.9
6.5	12.3 ± 0.1	12.6
7.2	10.0 ± 0.1	10.3

Figure 10.

Histograms showing scatter in the lengths of the nylon fibers used to create 'bridges' between the charged plates of the electrometer.

(A) for fibers of mean length 1.0 mm.

(B) for fibers of mean length 0.5 mm.

(C) for fibers of mean length 0.3 mm.

The fiber yarn in each case was 4.5 denier (denier is the weight of the yarn in gms. per 9,000 meters of length).

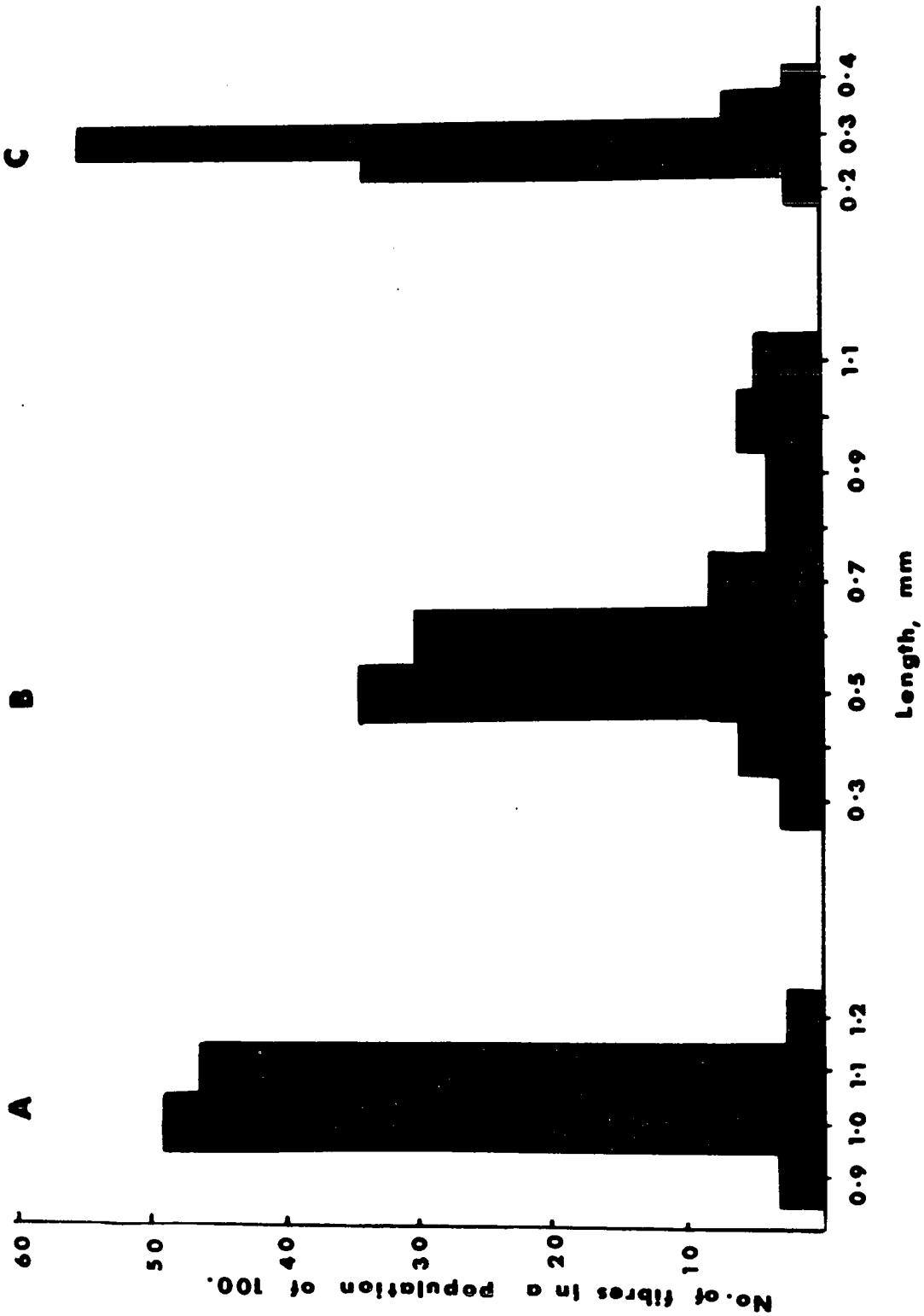
A
B
C
No. of fibres in a population of 100.
60
50
40
30
20
10
0·9 1·0 1·1 1·2
0·3 0·5 0·7 0·9 1·1
0·2 0·3 0·4
Length, mm

were used. To measure the length, these fibers of different length were photographed separately. The length measurement was done on one hundred of each range of length from their enlarged photographs and by using a half mm. scale. The histograms of the length of these fibers give their mean length and the scatter of their length about it (Figure 10).

A known, but small, amount of one kind of these fibers was spread uniformly on the lower plate of the absolute electrometer. After adjusting the whole instrument, a potential difference of 540 volts was created between the two electrometer plates by connecting a battery through an off and on circuit. Initially, the distance between the two plates was kept at 1.6 mm. The electrostatic field between the plates caused most of the nylon fibers to orient along the field direction. Charging and discharging of the plates several times repeatedly organized the fibers well into bridges. In each bridge, there were nearly six to ten fibers standing on each other, and bridging the air gap between the two plates. As these experiments were done when the humidity of the weather was very low, the leakage current never exceeded 0.5 milliamperes. The leakage current through plates having nothing but air in between, but under other similar conditions was always about 0.2 milliamperes. In each case, the volume of the nylon fibers used at a time was negligible in comparison to the volume of the space between the plates of the electrometer. By increasing the distance of separation, step by step, between the charged plates, the fiber bridges

followed the increased gap by becoming longer and thinner. Once the bridges between the plates were intact, they did not break even after the plates had been discharged for several hours.

(ii) Observation by Photography of the Nature of the Fiber 'Bridges'

The first investigation performed was to find the nature of the fiber bridges between the two charged plates. A small apparatus having two circular plates parallel to each other was constructed. Both plates were cut at a chord, so that the cut surfaces were in one plane. A screw was provided in the apparatus to vary the distance of separation between the parallel plates. The bridges were formed between the two plates by a constant distance of 1.8 mm. The fibers used were 1.0 mm. long. The quantity of the fibers used was 0.8, 1.6, 2.4, 3.2, 4.0, 4.8, 5.6 and 6.4 mg. per ml. of the space between the plates. Each time, after spreading the fibers uniformly on the surface of the lower plate, they were completely removed except from a strip like surface covering an area 0.5 x 6.0 cm. parallel to the cut surface of the plates. When a potential difference of 540 volts was applied between the plates, the fibers oriented in the field direction forming a thin wall of bridges. Photographs of these fiber bridges with increasing concentration of the nylon fibers per unit of the space between the plates were taken (Figure 11). Two observers independently estimated the number of intact

Figure 11.

Photographs of the nylon fiber bridges as a function of fiber density (mg/ml) with constant plate spacing and charge.

Length of each fibre is 1 mm approx.

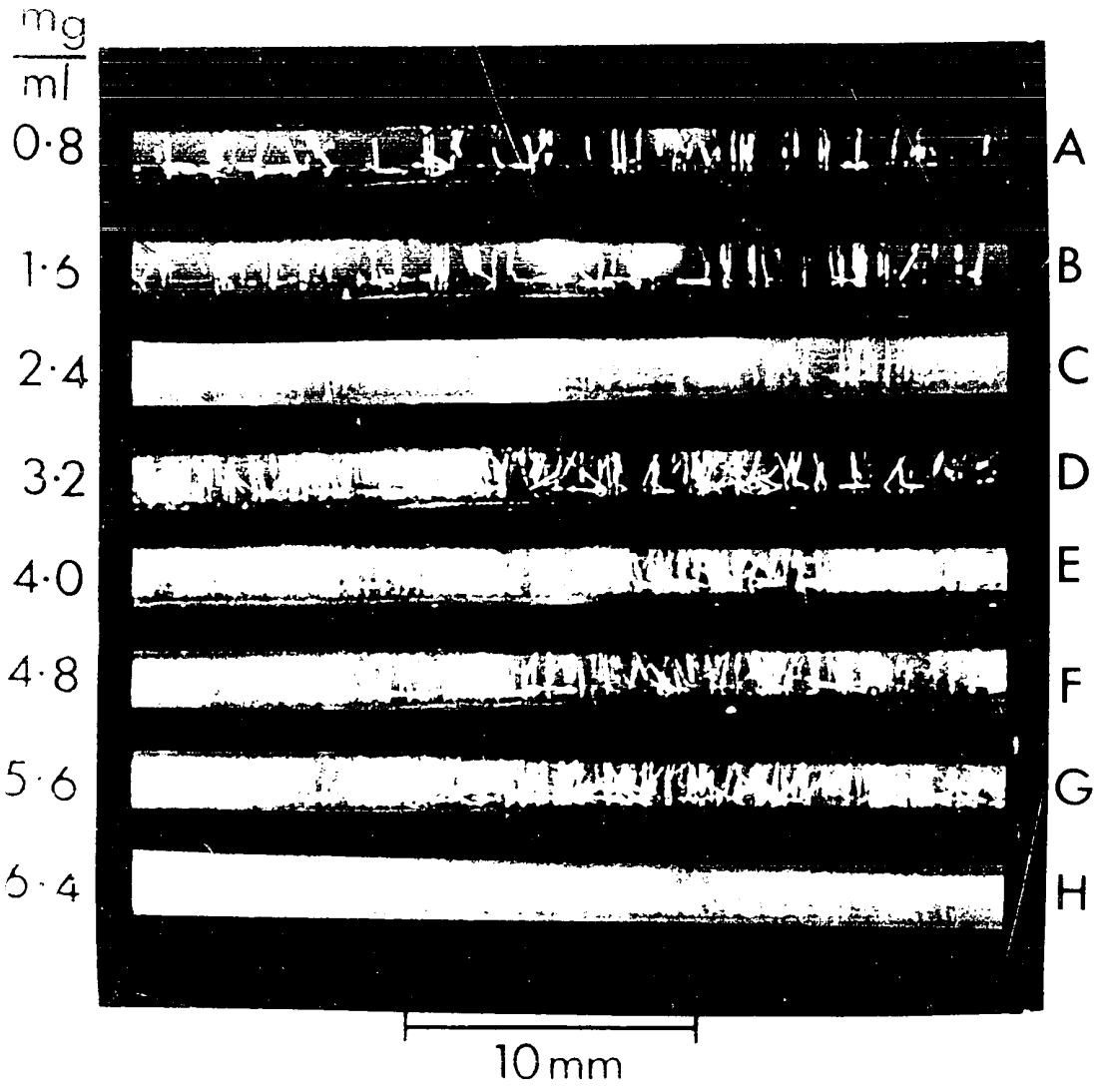

Figure 12.

Number of intact bridges as a function of fiber density with constant plate spacing and charge (as counted by two observers). Both curves show a tendency to saturation at higher density.

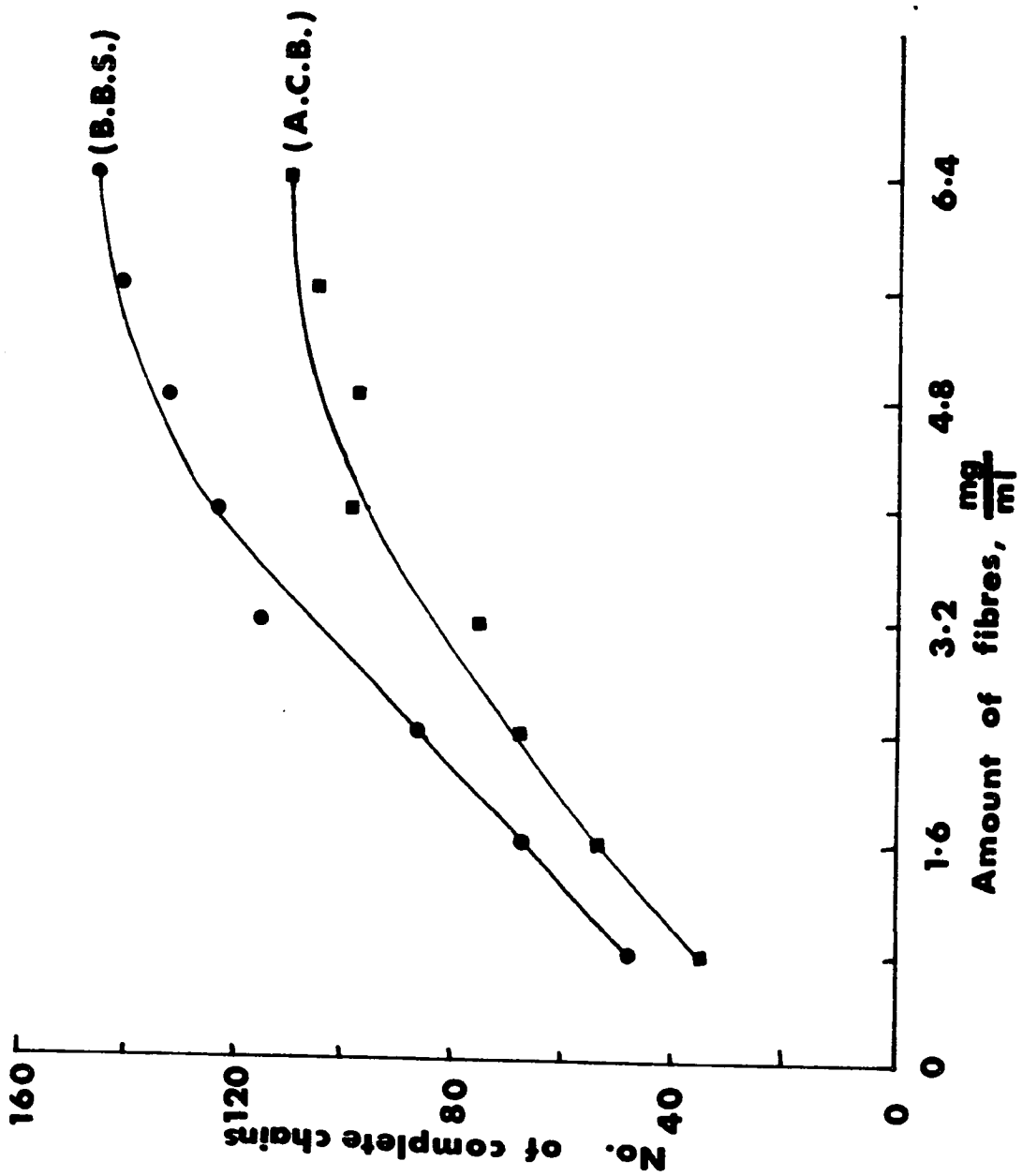
(B.B.S.)
(A.C.B.)
No. of complete chains
160
120
80
40
0
0
1·6
3·2
4·8
6·4
Amount of fibres, mg/ml

fiber chains between the plates as the quantity of the fibers per unit space was increased. While the number of bridges counted by the observers differed, as would be expected, both agree that the number of bridges does not increase proportionately but tends to a maximum (Figure 12). This suggests that there is an energy of interaction between the parallel bridges, as well as an energy of formation of each bridge so that a final stationary pattern of organization results as the quantity of fibers is increased. The increased quantity after a certain limit is not utilized in forming new bridges and fibers can be seen left lying on the lower plate (Figure 11).

Furthermore, to study the linkage between the fibers of a bridge between the two charged plates, the bridges were formed again, using a constant amount of 1.0 mm. long fibers. The constant amount of the fibers used was 3.5 mg. and were spread uniformly on a strip of area 0.5 x 6.0 cm. on the lower plate as has been described before. After applying a potential difference across the plates, the distance of separation between them was increased, step by step, to 2.4, 3.0, 3.6, 4.2, 4.8, 5.4, 6.0, 7.2, 7.8, 8.4, and 9.2 mm. respectively. This gave a decreasing amount of fibers per unit volume of the space. At each distance of separation between the plates, a photograph of the bridges was taken. Figure 13 gives these photographs of the fiber bridges at different stages of separation between the plates. The fibers in a bridge successively mount on each other as

Figure 13.

Photographs of the nylon fiber bridges as a function of plate spacing. The fiber mass and charging voltage were constant. At a critical separation (F) breaks appear in the bridges which constitute about 5 fibers each. The longest bridges in picture (L) contain about 10 fibers.

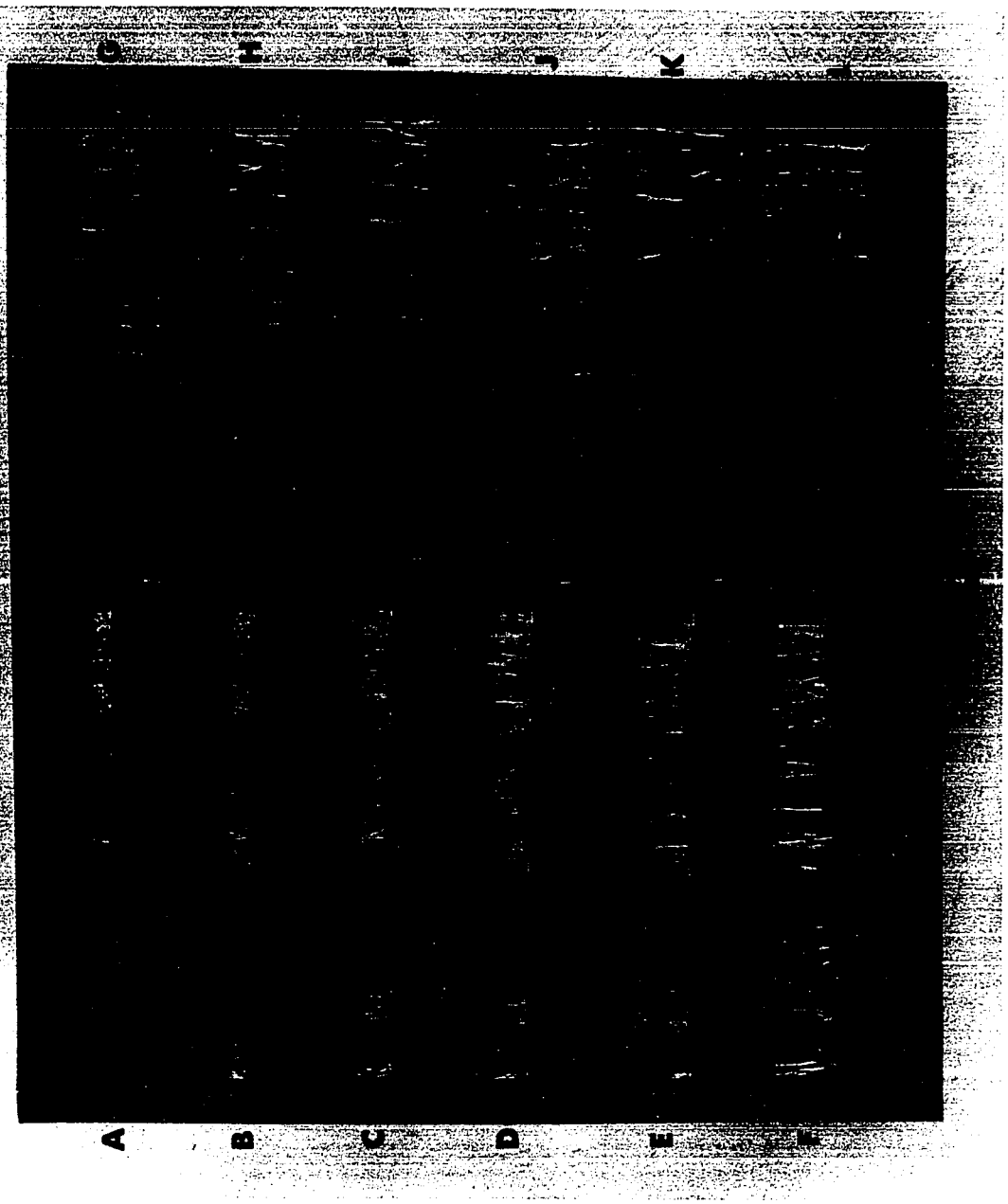
Length of each fibre is
A
B
C
D
E
F
G
H
I
J
K
L

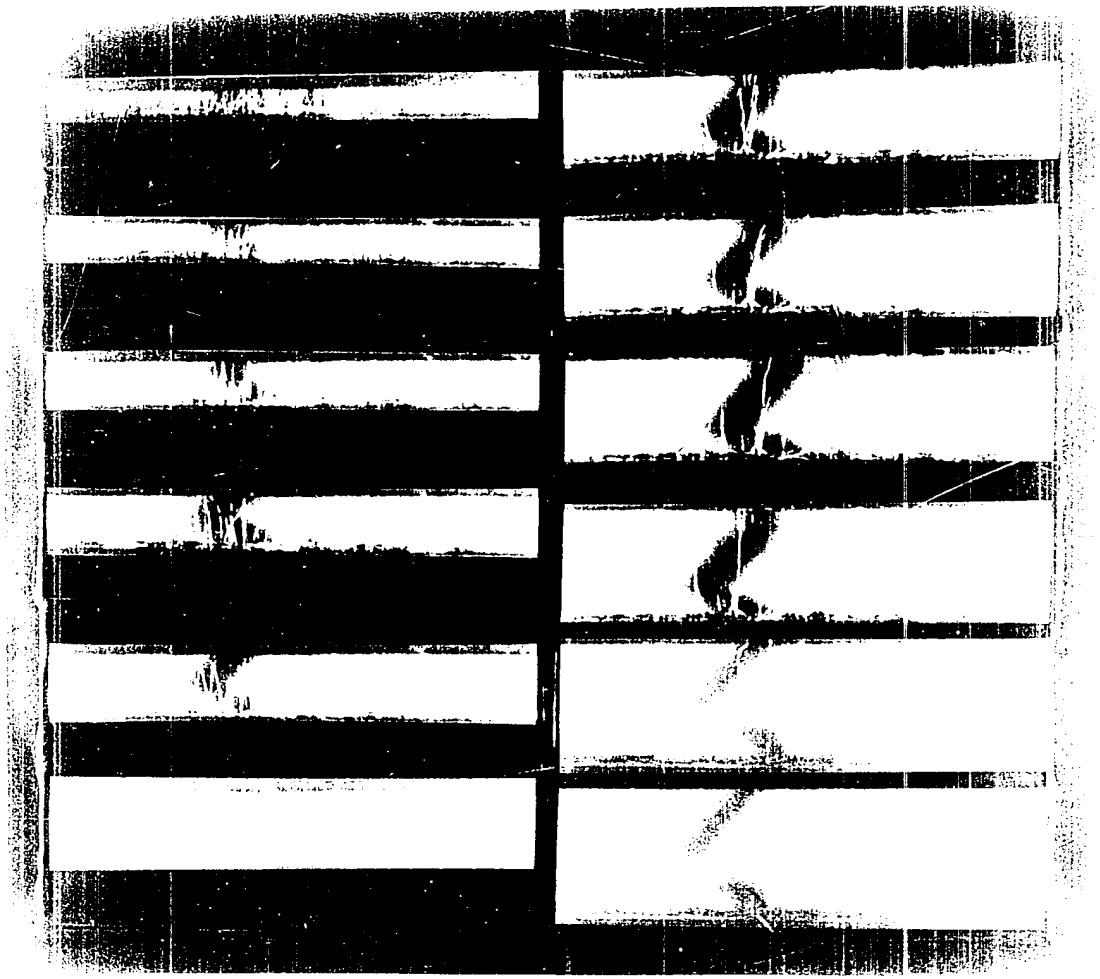

it is elongated by increasing separation of the plates. At the same time, these bridges become thinner and thinner until a chain of single fibers is reached. Beyond this limit, breaks occur in the bridges leaving fiber 'palisades' on both plates.

(iii) General Experimental Procedure

A known amount of one type of nylon fibers was taken and intact bridges were formed between the plates of the absolute electrometer. Keeping the fiber bridges intact between the discharged plates, the weight of the upper plate was recorded. Then the weight of this plate was again recorded after charging the plates of the electrometer. The difference of these two readings gave, in each case, the force of attraction between the charged plates, with the fibers in the form of bridges present in the space between them.

Distance between the plates was altered and a set of forces of attraction for different distances of separation was obtained. The distance of separation between the charged plates was varied from 1.6 mm. to 7.2 mm. For statistical analysis, such five sets of force of attraction vs distance of separation of the charged plates were recorded for each of the five known (5, 10, 15, 20 and 25 mg.) amounts of the nylon fibers of 1.0 mm. and 0.5 mm. length. At distance of separation of the plates lower than 1.6 mm. it was not possible to record observations within tolerable experimental error due to increase in leakage current between the plates.

It should be noted that increasing separation gave a decreasing concentration of fibers per unit of space between the two plates.

4. Model Experiments

PART A. Force vs Distance of Separation Between the Charged Plates Having a Constant Potential Difference

(i) Experimental Results

The results of the force of attraction vs the distance of separation between the plates are presented in Figures 14 and 15. The force actually increases to a maximum as the distance between the plates is increased. At greater distances of separation of the plates, the force follows the inverse square law obtained for the 'empty' experiment, but remains slightly higher. The maximum seems to correspond to the point of separation of the two plates at which the chains of the fibers begin to break. Further increase in the separation distance starts breaks at the middle of the bridges leaving an air gap between the fiber 'palisades' left on both plates. These fiber palisades remain attached to the plates on further increasing separation, thus reducing the effective distance of separation between the two plates by a constant amount. In other words, beyond the maxima the electrometer behaves as if it were empty (having only air between the plates) but with less distance of separation by a constant amount than the actual distance between its parallel plates.

Figure 14.

Plots of:

(A) force vs distance between the empty charged plates of the electrometer.

(B) force vs distance, with 15 mg of 1.0 mm long nylon fibers between the charged plates of the electrometer.

In both cases vertical lines indicate the standard error of the mean.

The data for curve (B) are presented in Table 3, Appendix I.

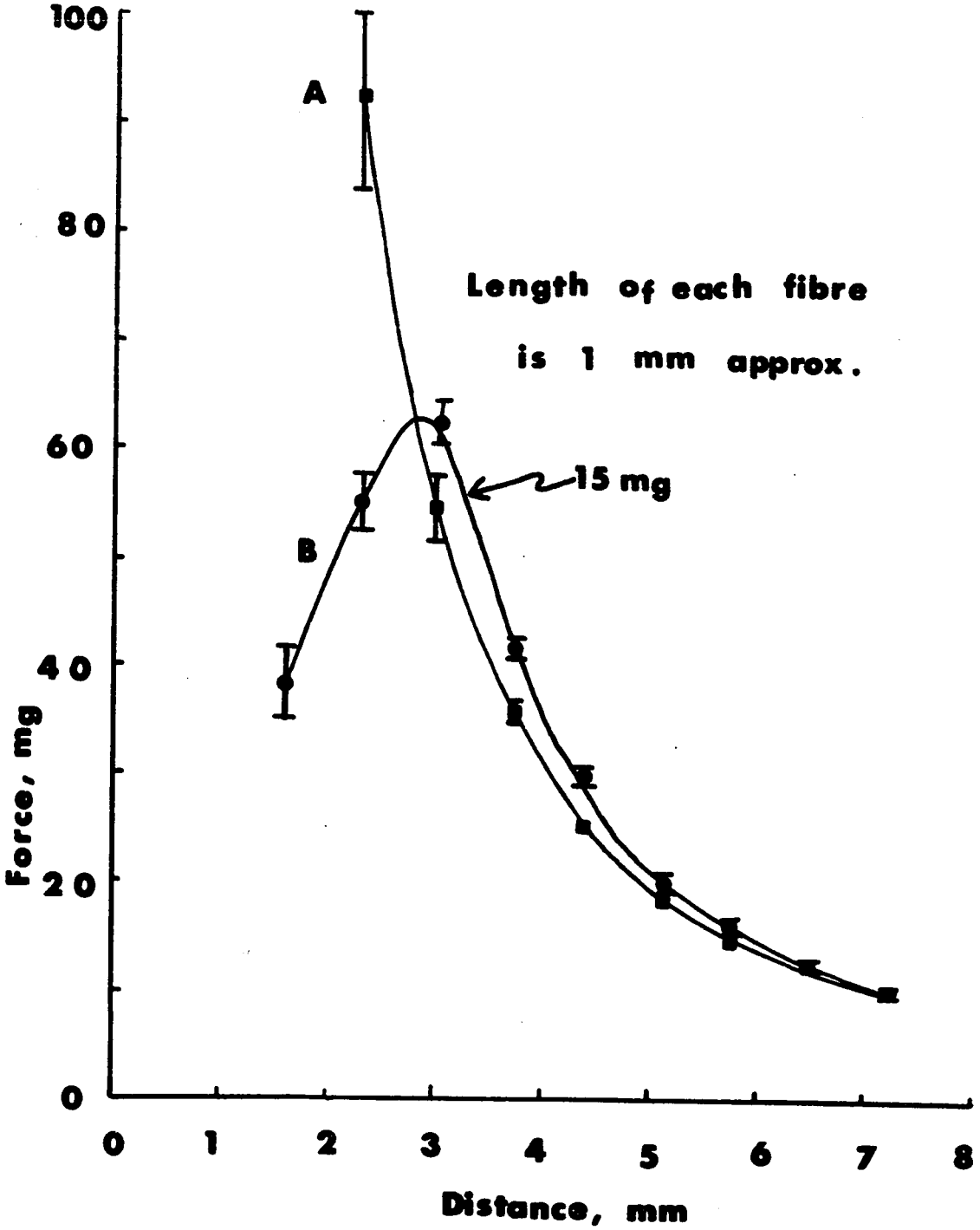
100
80
60
40
20
0
Force, mg
A
B
Length of each fibre
is 1 mm approx.
15 mg
0
1
2
3
4
5
6
7
8
Distance, mm

Figure 15.

Plots of:

(A) force vs distance between the empty charged plates.

(B) force vs distance, with 20 mg of 0.5 mm long nylon fibers between the charged plates of the electrometer.

In both cases vertical lines indicate the standard error of the mean.

The data for curve (B) are presented in Table 5(e), Appendix I.

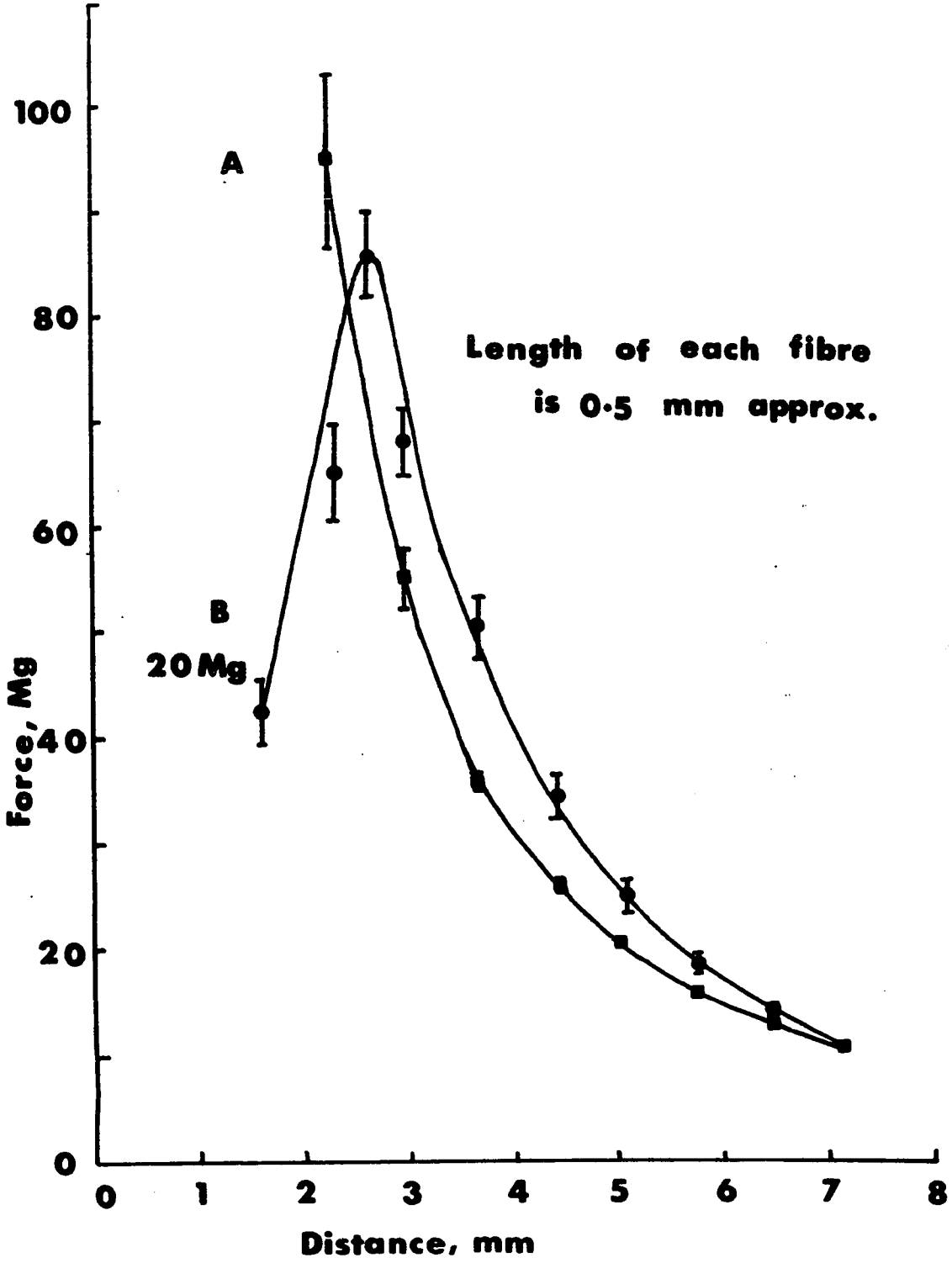
100
80
60
40
20
0
Force, Mg
A
B
20 Mg
Length of each fibre
is 0·5 mm approx.
0
1
2
3
4
5
6
7
8
Distance, mm

Figures 16 and 17 present the two families of curves (corresponding to 1.0 mm. and 0.5 mm. long fibers respectively) of force versus distance between the charged plates as a function of fiber mass.

(ii) Conclusions

The following are the conclusions drawn from these curves:

(a) There seem to be no maxima if 5 mg. or less of the fibers were used. In other words, a certain minimum number of fibers is needed to form chains effectively. On the other hand, a too great quantity of fibers (beyond 25 mg. in this case) may produce difficulties in measurements because the upper plate of the electrometer does not move freely in such situations.

(b) With an increasing number of fibers, the maxima decrease successively in magnitude, but they occur at a slightly greater distance of separation of the plates. This suggests that the interaction between neighboring dipoles stabilizes each fiber chain.

(c) Before the maxima are reached, an increase in the number of fibers decreases the force of attraction between the plates.

(d) The energy of the parallel plate capacitor for a constant separation of the plates and constant voltage across them is constant. Therefore, on the basis of conservation of energy the increase in number of fiber bridges between the plates

Figure 16.

Plots of:

(A) force vs distance between the empty charged plates of the absolute electrometer.

(B to F) family of curves of force vs distance between the charged plates of the electrometer as a function of fiber mass (1.0 mm long nylon fibers).

The data for curves (B) to (F) are presented in Tables 1, 2, 3, 4 and 5(a), Appendix I.

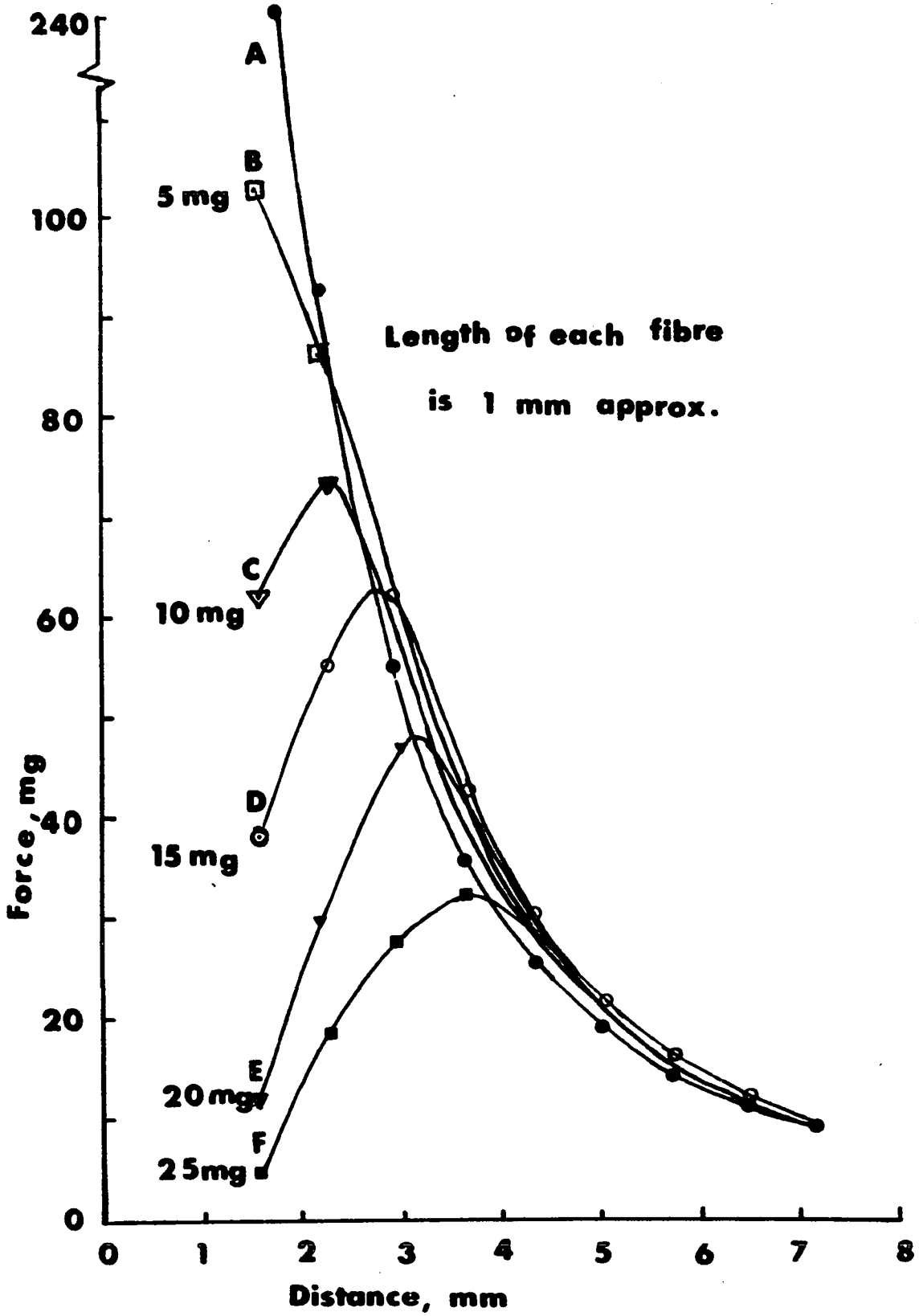
240
100
80
60
40
20
0
Force, mg
A
B
5 mg
C
10 mg
D
15 mg
E
20 mg
F
25 mg
Length of each fibre
is 1 mm approx.
0
1
2
3
4
5
6
7
8
Distance, mm

Figure 17.

Plots of:

(A) force vs distance between the empty charged plates of the absolute electrometer.

(B to F) family of curves of force vs distance between the charged plates of the electrometer as a function of fiber mass (0.5 mm long nylon fibers).

The data for curves (B) to (F) are presented in Tables 5 (b, c, d. e and f), appendix I.

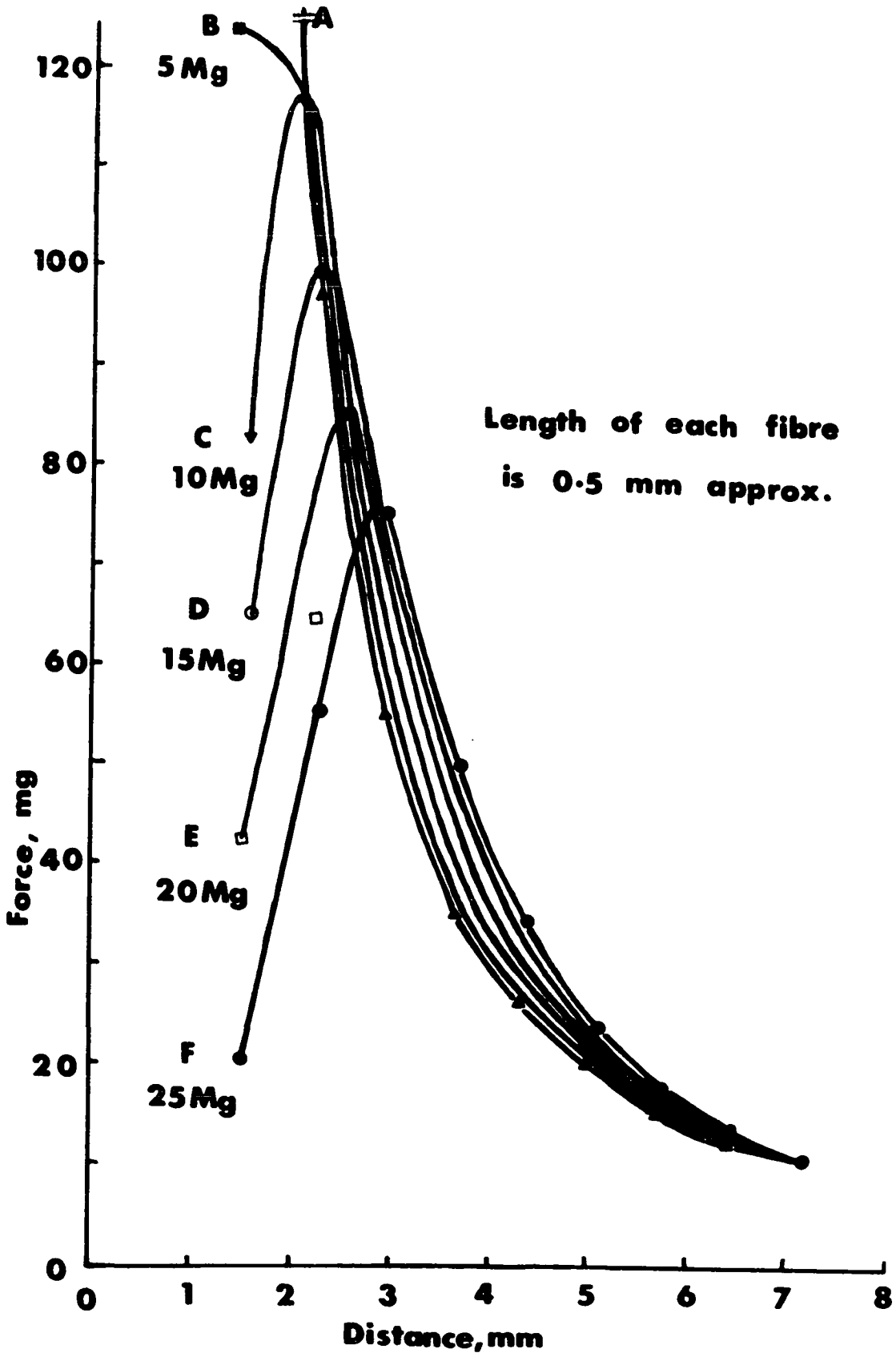
A
B
5 Mg
C
10 Mg
D
15 Mg
E
20 Mg
F
25 Mg
Length of each fibre is 0·5 mm approx.
Force, mg
Distance, mm
0
20
40
60
80
100
120
0
1
2
3
4
5
6
7
8

will decrease energy of the electrical field between them. Consequently the two plates will experience less force of attraction.

(e) Comparing figures 16 and 17, the maximum force for a given weight occurs at a smaller distance of separation for shorter than for the longer fibers, and the maximal force produced is greater for shorter than for longer fibers. This may be because of the fact that more shorter fibers are needed to bridge a given gap than the longer fibers and thus more electrical energy might be required to orient them in a chain.

We also tried to repeat these experiments with 0.3 mm. long nylon fibers, and we were unable to find a maximum in these curves. The maxima would be expected to occur at shorter distances with these shorter fibers. These short distances would make the leakage current high.

The effect of vibrating the lower plate of the electrometer on fiber bridges was also investigated. A 50 cycle/sec. electrically driven small vibrator was mounted on the lower surface of the lower plate. Vibrating the plates in this way, when they were charged, organized the bridges better. Also, some new bridges were seen to be formed from the fibers left unutilized without vibration. To see the effect on the force of attraction between the charged plates of more and better organized bridges due to vibrating the lower plates, observations for the force of attraction vs corresponding distance of separation of the charged plates were recorded. The data have been plotted in

Figure 18.

Force vs distance between the charged plates of the absolute electrometer, before and after vibrating the plates, with the vibrator mounted on the lower plate.

(A) force vs distance between the empty plates of the electrometer.

(B) force vs distance between the charged plates of the electrometer having nylon fiber bridges (before vibrating the plates).

(C) force vs distance between the charged plates of the electrometer, having nylon fiber bridges (after vibrating the plates).

The data for curves (B) and (C) are presented in Tables (6), appendix I.

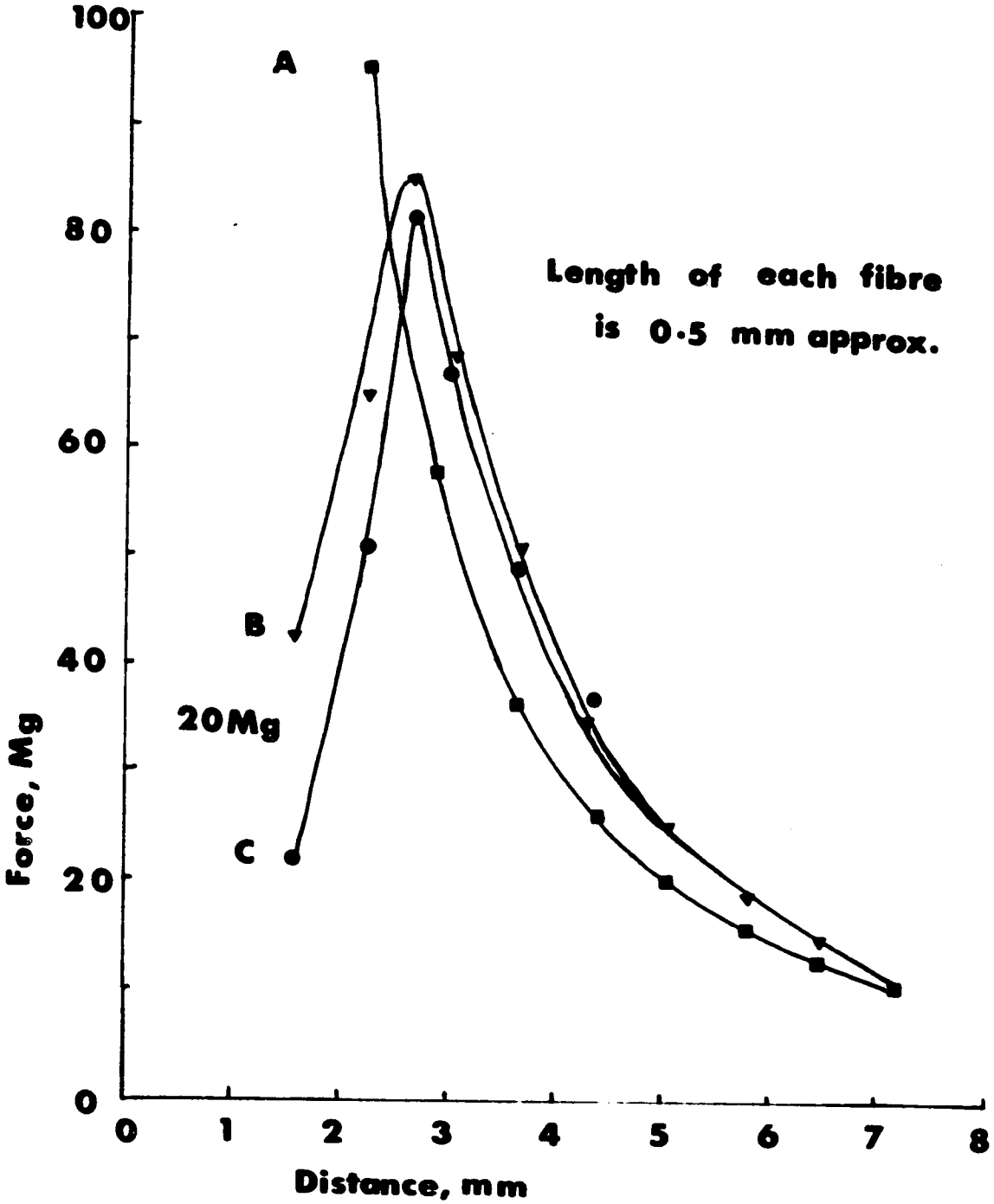
100
80
60
40
20
0
A
B
C
20Mg
Length of each fibre
is 0·5 mm approx.
Force, Mg
0
1
2
3
4
5
6
7
8
Distance, mm

the Figure 18, which shows that more and better organized fiber chains between the plates lower the maximum force (as discussed before).

PART B. Force vs Distance of Separation Between the Charged Plates Having Constant Charge Instead of Constant Potential Difference

(i) Theoretical Considerations

Total charge Q across the plates of a capacitor is given by the relation

$$Q = CV \qquad (5)$$

where V is the potential difference across the plates, and C is the electrical capacity which,in the case of a parallel plate capacitor,is given by the relation

$$C = \frac{KA}{4\pi r} \qquad (6)$$

where A is the area of the plate separated by a distance r, and K is the dielectric constant of the medium between the plates.

Thus, in the case of a parallel plate capacitor, the charge Q across its plates can be written as

$$Q = \frac{KA}{4\pi}\frac{V}{r} \qquad (7)$$

This relation shows that at different distances of separation of the plates, charge across a parallel plate capacitor can

be maintained constant by keeping the ratio V/r constant. In other words, if the distance between the plates is doubled, charge between the plates can be maintained constant by doubling the potential difference across them.

From the classical laws of electrostatics, we know that the force of attraction between two charged plates, maintained at constant charge, at their different distances of separation, is given by the relation

$$F_Q = \frac{2\pi Q^2}{KA} \tag{8}$$

This F_Q is independent of the distance between the charged plates. Here, however, we are concerned about how the force F_Q varies with the distance of separation when the medium between the two plates, having been maintained at constant charge, is specialized by bridges of nylon fibers.

At constant charge let Vo and V be the potential differences applied across the plates of the parallel plate capacitor, separated by distances r_o and r respectively. Thus, charge being constant on the plates, we can write

$$\frac{V}{r} = \frac{Vo}{r_o}$$

or

$$V = \frac{Vo}{r_o} r \tag{9}$$

Again, from the classical laws of electrostatics, when the distance of separation between the charged plates is kept constant, we know

$$F \propto V^2 \tag{10}$$

where F is the force of attraction between the charged plates having a potential difference V. This relation is also

Figure 19.

Plot of force between plates as a function of square of the charging voltage. Plate separation and fiber mass were constant.

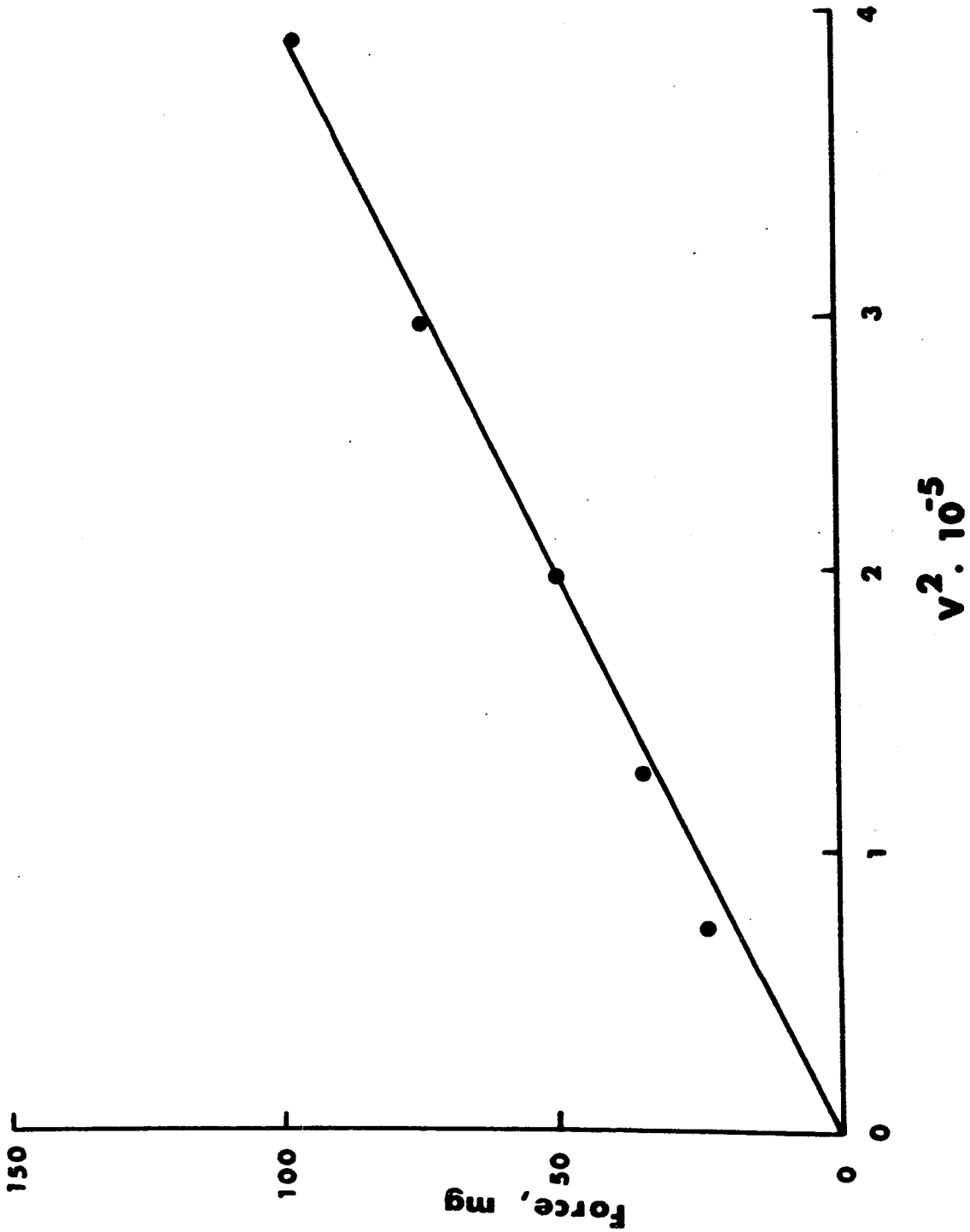
Force, mg
150
100
50
0
0
1
2
3
4
$v^2 \cdot 10^{-5}$

true when the nylon fibers are present in the form of bridges between the two charged plates as shown in Figure 19 from experimental data.

Thus, combining equations 9 and 10, we get

$$F_Q \propto \left(\frac{Vo}{r_o}\, r\right)^2$$

$$\propto \left(\frac{Vo}{r_o}\right)^2 r^2$$

$$\propto F.r^2 \qquad (11)$$

where, as has been said before, F is the force of attraction between the plates having a constant potential difference between them. Thus, expression 11 gives a way of deriving F_Q from F and the corresponding distance of separation r. From Figures 16 and 17, which are the families of the curves for force of attraction vs distance of separation between the parallel plates, we can derive the quantities proportional to F_Q at different distances of separation r of the plates.

Tables 7(a) to 7(f) and 8(a) to 8(f), shown in appendix I, give values of F_Q which are proportional to $F.r^2$ for distances of separation r between the charged plates with fiber bridges between them. These values of F_Q have been calculated from families of curves (16) and (17), representing forces of attraction vs distances of separation for 1.0 mm. and 0.5 mm. long fibers respectively used for bridges formation between the plates.

Figure 20.

Family of curves representing force F_Q (for constant charge on the plates) vs distance between the plates of the absolute electrometer.

(A) F_Q vs distance between the charged empty plates of the electrometer. The curve is independent of the distance of separation between the plates in accordance with the theory of electrostatics.

(B) to (F) F_Q vs distance between the charged plates of the electrometer as a function of fiber mass (1.0 mm. long nylon fibers).

The data for these curves are presented in Tables 7 (a, b, c, d, e and f), appendix I.

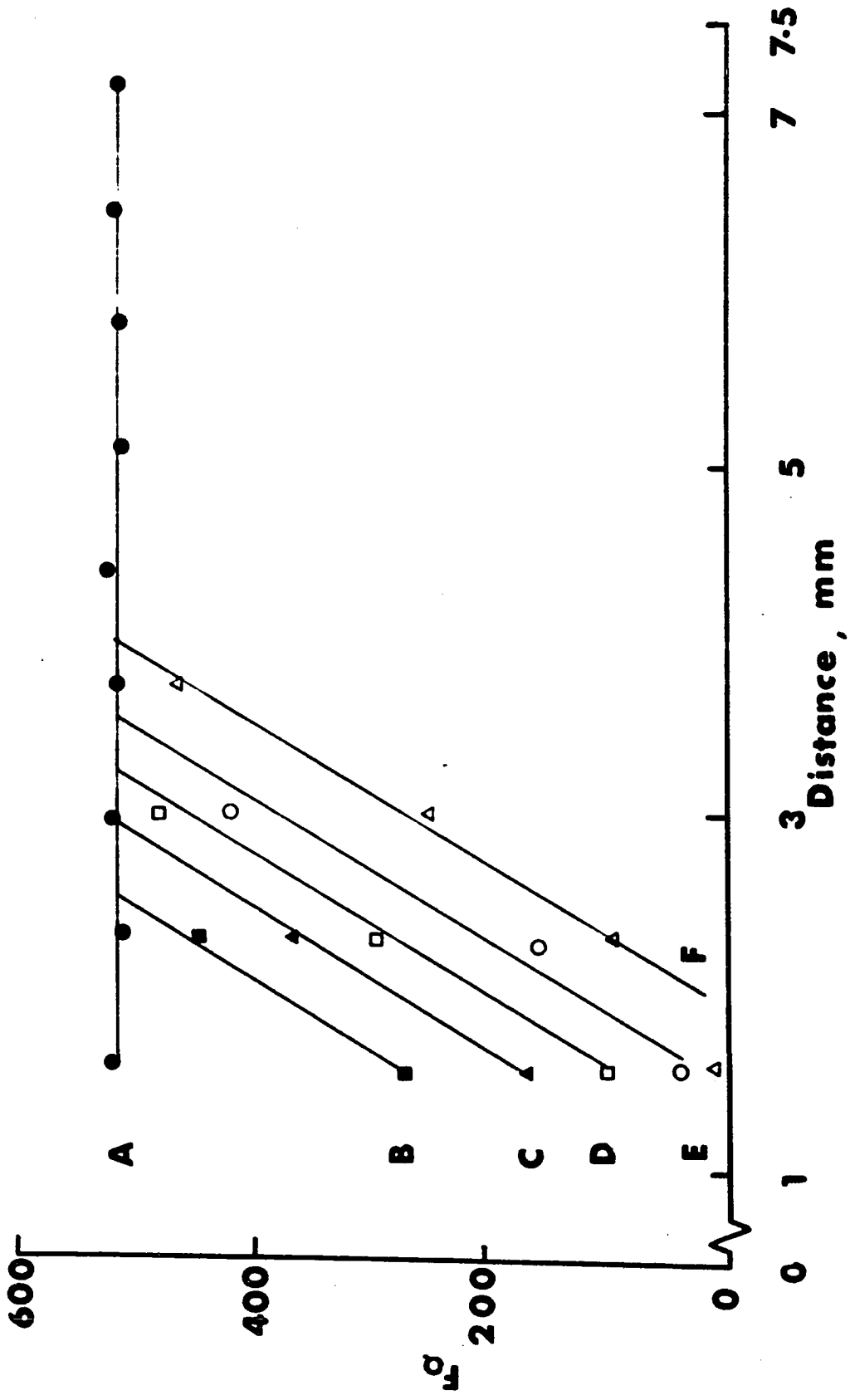
600
400
200
0
σ_F
A
B
C
D
E
F
0
1
3
5
7
7.5
Distance, mm

Figure 21.

Family of curves representing force F_Q (for constant charge on the plates) vs distance between the plates of the absolute electrometer.

(A) F_Q vs distance between the charged empty plates of the electrometer. The curve is independent of the distance of separation between the plates in accordance with the theory of electrostatics.

(B) to (F) F_Q vs distance between the charged plates of the electrometer as a function of fiber mass (0.5 mm. long nylon fibers).

The data for these curves are presented in Tables 8 (a, b, c, d, e and f), appendix I.

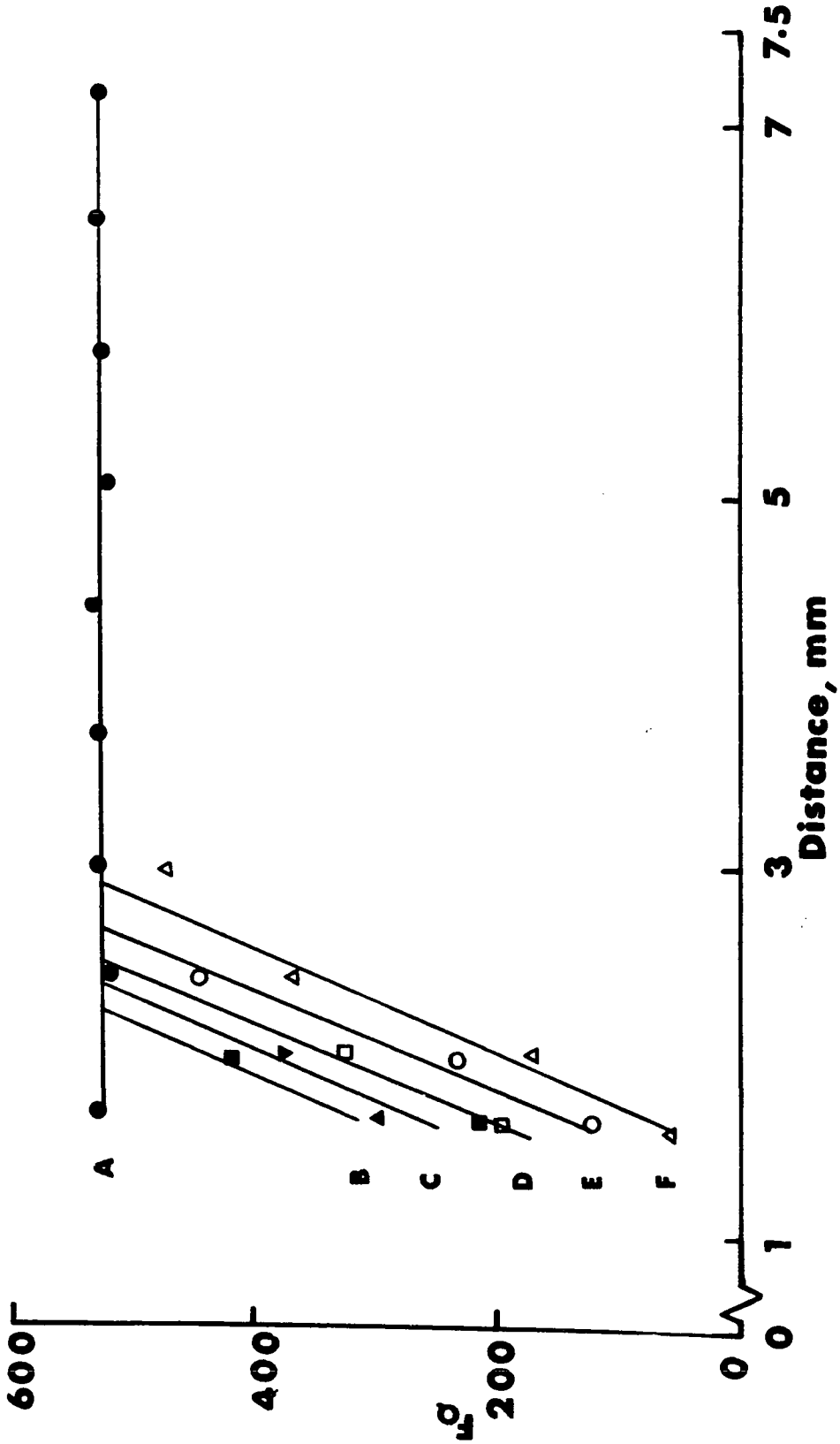
600
400
200
0
D_F
0
1
3
5
7
7.5
Distance, mm
A
B
C
D
E
F

(ii) Conclusions

Plotting F_Q vs distance of separation r for a constant charge on the plates with an empty space between them gives a straight line, independent of distance of separation between the plates, just as the classical theory of electrostatics says it should (Figures 20 and 21). If there are fiber bridges present in the space between the charged plates (for 1.0 mm. and 0.5 mm. long fibers), F_Q increases as the distance of separation between the plates increases until the bridges are no longer intact and effective. Beyond this, the curves follow the curve for the empty space between the plates (Figures 20 and 21).

5. Analogy Between the Red Cell and the Electrical Model

(i) Introduction

In section 3, we have proposed the existence of an attractive force p^1 acting normally on the inner surface of the membrane of the red cell. The magnitude of this force has been calculated to be maximal at the dimple region, and minimal at the rim. Such an attractive force, acting on the red cell membrane, seems to be indispensable to maintain the biconcave discoidal shape if the membrane is uniformly thin and has a positive transmural pressure. As has already been proposed by us in the preceding sections, the molecular organization in the form of 'tactoids' could create this attractive force p^1 between the similarly charged opposing membranes of the red cell.

A parallel plate capacitor, with nylon fiber bridges between its charged plates, was next used in an attempt to simulate a red cell in reference to the foregoing hypothesis. The properties of this electrical analogue, studied with increasing distance between the charged plates, were compared to the response of intact red cells suspended in solutions of decreasing tonicity. Observations made on these swelling red cell series are presented in the following pages.

The opposing membranes, which constitute the two flat faces of a red cell, are not exactly flat and parallel (due to the dimple in the membranes) like the charged plates of its electrical analogue. However, when a red cell is transferred into a hypotonic environment, its membranes at the dimple region move apart, and acquire a new equilibrium position. This new equilibrium position of the red cell membrane depends on the tonicity of the hypotonic solution to which it is transferred. Thus, swelling of the red cell membrane in a hypotonic solution is similar, to some extent, to an increase in the distance between the charged plates of its electrical analogue. The unique feature of the electrical model of the red cell is that the force of attraction between its charged plates first increases with an increase in the distance between them and attains a maximum at a certain separation distance. Beyond this, the force

decreases on further increasing the distance (Figure 14). This is equivalent to the existence of an elastic component in the system, i.e. elasticity can be thought of as the property of resisting an increase in the distance between two connected points. Surface energy of the cell membrane, and the positive transmural pressure across it are the other two main forces that act on the red cell membrane to maintain its equilibrium shape. Neither of these two forces appear to change due to swelling of the cell membrane until the cell becomes spherical and starts leaking hemoglobin. Therefore, the only force that must change in order to maintain the new equilibrium of a swollen red cell membrane in the hypotonic solution is the proposed force p^1.

The swelling series of individual red cells on edge were obtained by Dr. P. Rand. We have measured the radii of curvature at the center of the dimple region of these swelling red cell series to calculate the magnitude of the force p^1 at their various swollen stages. The red cell profiles were obtained by drawing lines on each of the photographs of these series in accordance with the rules laid down by Ponder (1930).

(ii) Theoretical Considerations and Measurement of the Proposed Attractive Force p^1 for the Swelling Red Cell Series

For an idealized red cell shape, the 2 radii of curvature at the center of both dimple region are equal, i.e.

$$R_1 = R_2 = R_1^1 = R_2^1$$

Therefore, the proposed attractive force p^1 at the

center of the cell dimple regions may be expressed by the equation

$$p^1 = \Delta P - T\left(\frac{1}{R_1} + \frac{1}{R_2}\right) = \Delta P - \frac{2T}{R_1} \qquad (12)$$

where ΔP is the positive transmural pressure across the cell membrane and T is the surface energy of the cell membrane. Since, in nature perfect symmetrical shapes are very rare to come by, and thus, in the case of red cells also, in general, we observe only that the

$$R_1 = R_2 \text{ and } R_1^1 = R_2^1 .$$

In other words, the two dimple regions of a red cell are parts of two spheres of different radii. Therefore, the proposed attractive force p^1 at the two dimple regions, in general, is separately expressed by the two equations

$$p_1^1 = \Delta P - \frac{2T}{R_1}$$

$$p_2^1 = \Delta P - \frac{2T}{R_1^1} \qquad (13)$$

and the average of these two quantities, as the mean representative of the proposed force p^1 at the center of the dimple of a red cell, is given by the following equation:

$$p^1 = 1/2(p_1^1 + p_2^1) = \Delta P - T\left(\frac{1}{R_1} + \frac{1}{R_1^1}\right) \qquad (14)$$

In other words, instead of taking the arithmetic mean of the radii of curvature, we have taken the harmonic mean.

Compasses were used and the radii of curvature at the center of both of the dimple regions of a red cell profile were measured by 'circle fitting' method. The line profile of the cell in each of the serial photographs, magnified to

10,000 times the actual size, was traced on white sheets of paper. The curves of known radii of curvature were then fitted to them on both sides of the dimple region of the line profiles. For each series this method was repeated five times independently and the force p^1 was calculated for each pair of the measured radii of curvature. Lastly, the standard error of mean for each series was determined. The radii of curvature for both dimple regions of a red cell are negative until its both opposite faces at dimple regions become parallel (i.e. both R_1 and R_1^1 are infinite) in its swelling series. Beyond this equilibrium stage of the cell both radii of curvature are positive. For calculating p^1, the transmural positive pressure ΔP was taken to be 227.36 dynes/cm^2 (or 2.32 mm. of H_20), and surface energy T (exclusive of the bending energy) was taken to be 0.014 dynes/cm. These values of ΔP, T, and radii of curvature R_1 and R_1^1 were substituted in equation (14) to calculate p^1.

(iii) Discussion

The calculated force p^1 for each stable equilibrium of the red cell series was plotted against the corresponding distance of separation between the cell membranes at the dimple region. Figure 22 shows these plots for each red cell series, and the data are presented in Table 9*. As is evident from the plots, the force p^1 at dimple center of a red cell increases during the initial stages of the cell swelling. After reaching a maximum the force p^1 falls as the cell swells further. In other words, the variation of the p^1 with an

*See Appendix I

Figure 22

Plots showing variation of the proposed force p^1 versus distance of separation between the opposite membranes of a red cell at the dimple region. The bars show the standard error of the mean. The cells were individually swollen, step by step, in a soltuion of decreasing tonicity. The data for these curves were presented in Table 9, Appendix I.

(A) Major Diameter 8.0μ

(B) Major Diameter 8.6μ

(C) Major Diameter 9.1μ

(D) Major Diameter 8.8μ

In each plot the dotted line represents the stages of the cell series from planar (where membranes at the dimple region of a red cell are parallel to each other) to the spherical swollen shape of the red cell. The broken lines represent the extrapolation of these curves by joining to their origins (with reference to model experiments, Figures 16 and 17). The squares with dots are the points representing the proposed attractive force p^1 at the center of the dimple region of the red cells treated with Tween 80 against the mean separation distance between the two membranes at the dimple center (i.e. 2.32 mm. H_2O against 0.767μ; discussed in section VI*). This point seems to fall on extrapolated part of these curves.

*Page 140

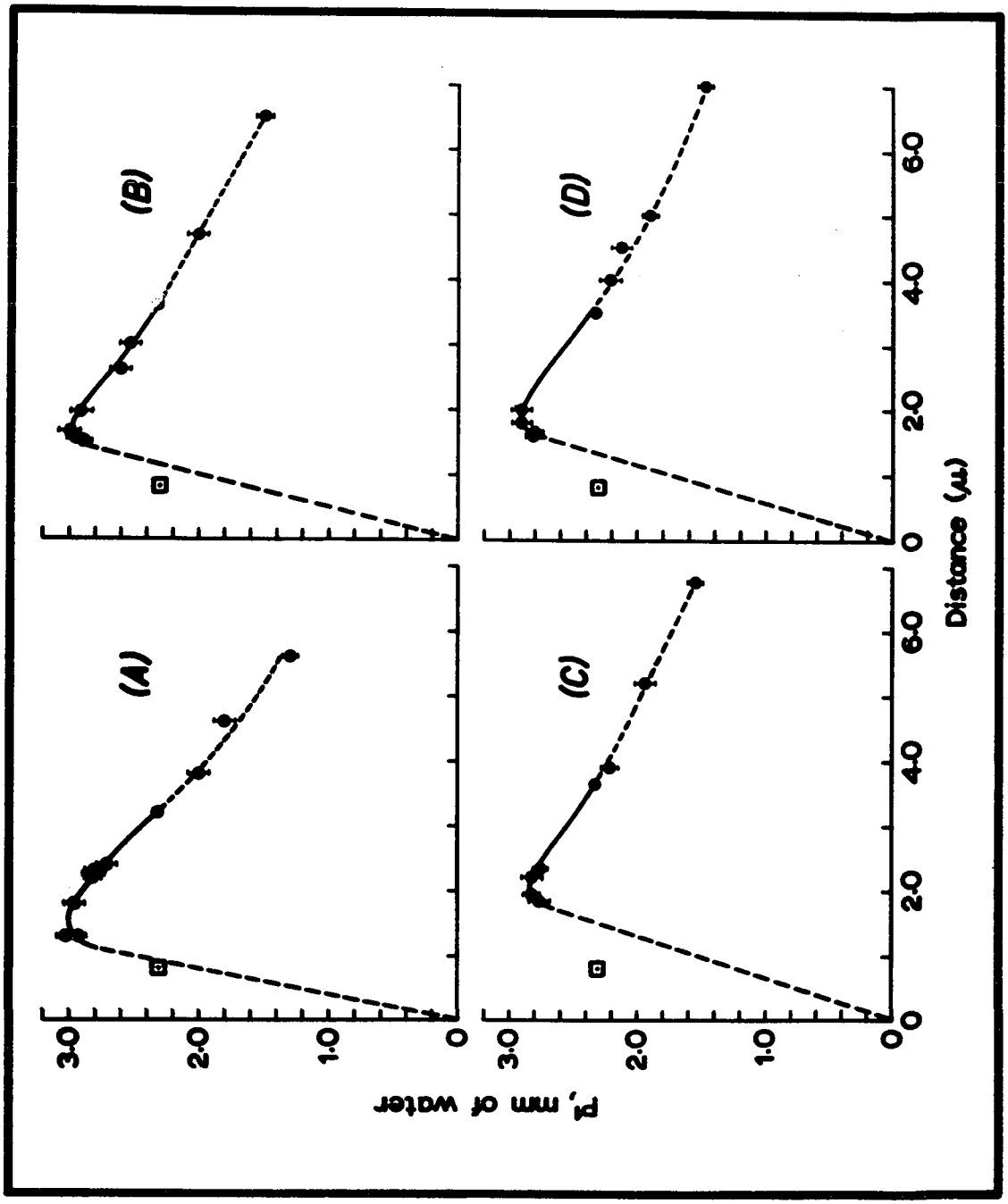
(A)
(B)
(C)
(D)
P_f, mm of water
Distance (μ)
0
1.0
2.0
3.0
2.0
4.0
6.0

increase of the distance between opposite membranes of a red cell at its dimple region, resembles the variation of the force of attraction with an increase of the distance between the charged plates of the previously described electrical analogue, (Figures 22 and 14).

An increase of p^1 in the initial stages of the red cell swelling implies a decrease of the radii of curvature (that is, an increase in the curvature) at the dimple region. Therefore, in keeping with the viscoelastic nature of the red cell membrane, a decrease in the radii of curvature at the dimple region during the initial stages of swelling of a red cell seems to be explained only by invoking the presence of a molecular organization, between the membranes, linking them together at the dimple region. These molecular chains may be comparable to the nylon fibers that are aligned parallel bridging the gap between the charged plates of the electrical analogue of the red cell. Therefore, as the cell starts swelling, the molecular organization resists the outward movement of the membranes at the dimple regions which, in turn, makes the cell membranes at the dimple more curved. As the stress on the molecular organization, on further swelling of the red cell, increases and passes through the maximum point for p^1, the molecular organizations seem to give way, and the force p^1 starts decreasing from then on. Here again, it is very tempting to draw an analogy to the nylon fiber bridges which start breaking, when the charged plates are separated beyond the maximum force of attraction between them. Thus, it is concluded that the molecular chains

between the charged membranes of a red cell at the dimple region seem to provide the necessary attractive force p^1 for the stable equilibrium of the biconcave discoidal red cell membrane shape.

6. Summary

A parallel plate capacitor of appropriate capacity, and having a specialized medium between its charged plates, may be considered an electrical analogue of a red cell.

The oriented nylon fibers in a charged parallel plate capacitor greatly modify the classical laws of variation of force resulting from a change in the distance between the plates. The force actually increases to a maximum as the distance between the plates is increased. The magnitude of the maximum force and the distance of separation at which it occurs depend upon the length of the fibers used, their quantity per unit space between the plates and also on the charge across the plate.

Lastly, the variation of p^1, the proposed attractive force at the dimple region of the red cell in relation to the degree of swelling of the cell has been investigated. Like the force of attraction between the charged plates of the electrical analogue of the red cell, the force p^1 increases during the initial stages of swelling of a red cell, attains a maximum, and on further swelling starts to decrease.

This behavior of the red cell membrane in hypotonic solutions of different tonicities suggests the presence of tactoids between the charged opposite membranes at dimple

region. The tactoids appear to function in a manner similar to the nylon fiber bridges between the charged plates of the electrical analogue of the red cell.

V. POLARIZATION MICROSCOPY OF THE RED CELL INTERIOR

1. Introduction

Polarization microscopy has contributed much to our knowledge of ultrastructures and their function in biological systems. In some respects it has advantages over x-ray and electron microscopic techniques. For example, polarization microscopy has been used to illustrate the dynamic nature of molecular organizations, such as the contractile nature of living muscle cells, mitotic spindles in dividing cells, etc. (Hughes and Swann, 1948; Mazia, 1961; Inoué, 1964; Forer, 1965, 1966). Thus, for understanding biophysical aspects of cellular physiology, polarization microscopy has been extremely useful.

In general, structural anisotropy of an object is associated with its optical anisotropy, making the object birefringent*. Also,ultrastructures and function of a cell are usually very closely related to each other. Therefore, the occurrence of birefringence in contractile elements of living cells seems to have a deeper significance than the mere localization of oriented molecules or micelles (Inoué, 1964). On thermodynamic grounds also, it has been argued that in order to convert chemical energy (a scalar quantity) directly

*See appendix III.

to contractile energy (a vector quantity), structural anisotropy is required (Katchalsky, 1963). In other words, the molecular organization causing a contractile force or a particular structural stability in a cell, cannot be randomly arranged, but must form an organized structure, whose properties should vary in different directions.

In this section of the thesis are described some polarization microscopic techniques which we have used to reveal the presence of ultrastructures in the form of molecular chains (tactoids) in the interior of the red cell.

2. Instrumentation

(i) Polarization Microscope

The polarization microscope used for these studies was 'Zetopan-Pol', manufactured by Reichert (kindly lent to us by Prof. G.H. Reavely). The light source attached to it was a HBO-200 mercury vapor lamp with heat and UV absorption filters. The microscope has a polarizer and an analyzer of high quality polaroids, which, on being crossed, give nearly perfect extinction. The strain-free objective and eyepiece used were 100X oil immersion with 1.25 NA and 10X, respectively. The numerical aperture of the light condenser was kept 0.38 to get a nearly parallel beam of incident light.

The rotating circular stage provided with the instrument could be adjusted with an accuracy of 0.1° with the help of the vernier scale attached to it. An attached mechanical stage on the circular rotating scale made the

Figure 23

Polarization microscope used in the investigation.

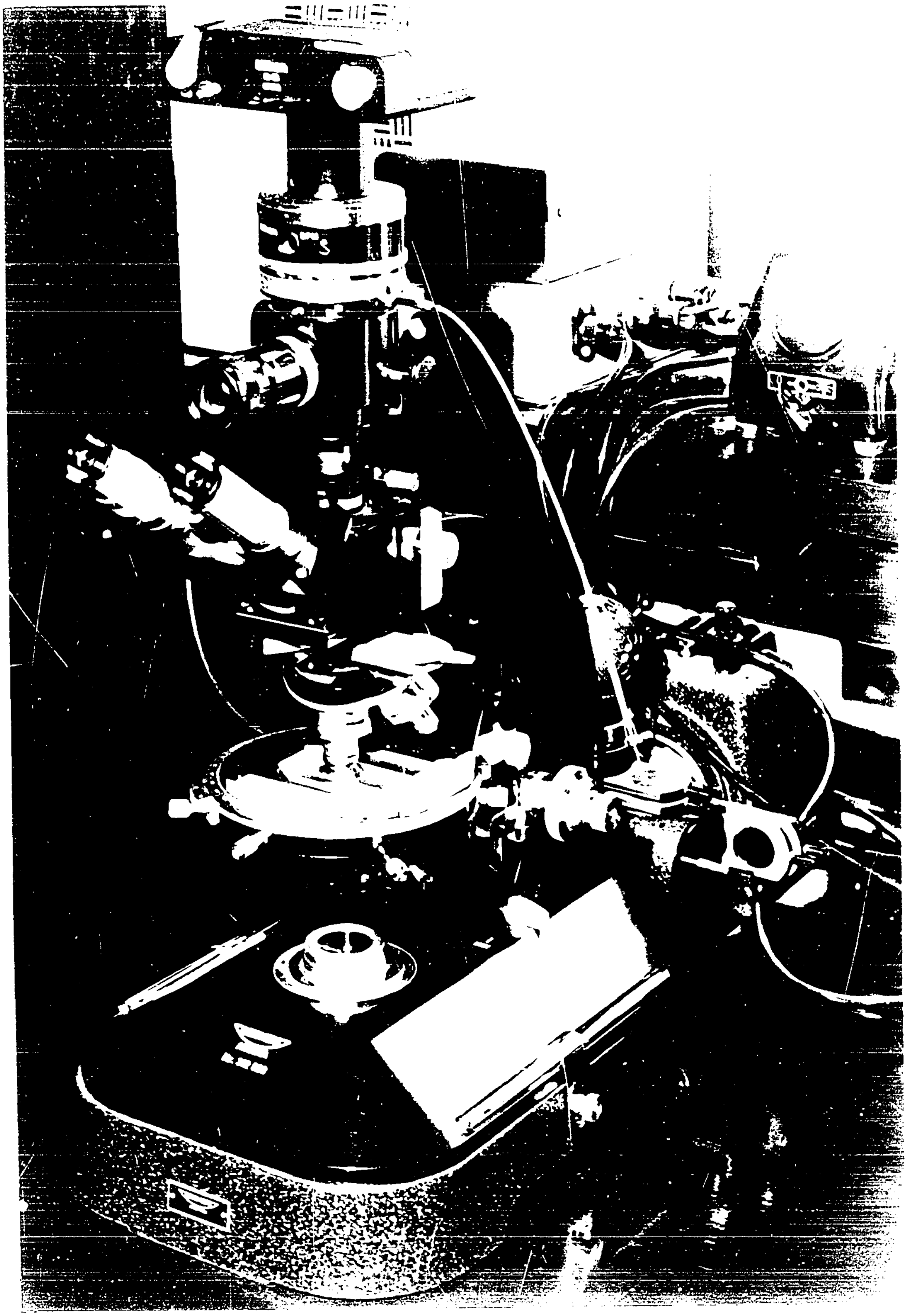

arrangement versatile to work with. The photographic equipment, microflex model EFM (Nikon), was coupled with the microscope and was used for microphotography of the red cells on edge. The microscope with its other accessories is shown in Figure 23.

(ii) Theoretical Consideration

Figure 24 shows an arrangement of the crossed polarizer and analyzer with a birefringent object between them, the optical axis of which makes an angle θ with the polarizer axis. If the amplitude vector of polarized light passing through the polarizer is equal to A, the amplitude vector of light passing through the birefringent object, which is a component of A, is

$$= A \cos \theta$$

and the amplitude vector of light passing through the crossed analyzer, and which is a component of A cos θ is

$$= A \cos \theta \cos (90-\theta)$$

$$= A \cos \theta \sin \theta.$$

Since the intensity of light is proportional to the square of the amplitude vector, the light intensity coming out of the crossed analyzer and detected by the detecting device placed above it is

$$I = A^2 \sin^2 \theta \cos^2 \theta.$$

As can be seen from this expression, the intensity coming out of the crossed analyzer will be zero in the absence of a birefringent object between the polarization axes.

Figure 24

Schematic representation of the crossed polarizer and analyzer. The birefringent object is between these polaroids.

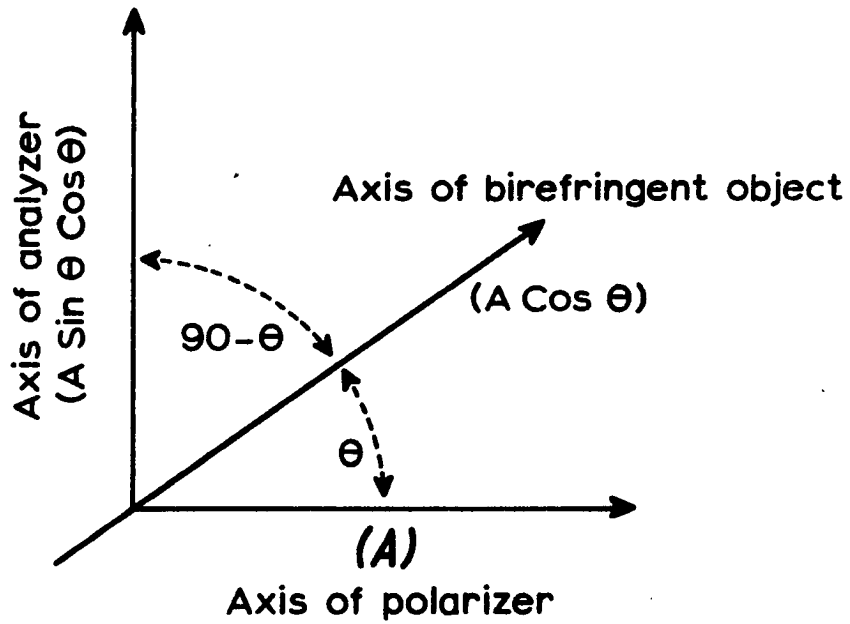

Amplitude vector through polarizer..... = A

Component of A through birefringent object.. = A Cos θ

Component of A Cos θ through analyzer..... = A Cos θ Sin θ

Intensity of light passing through analyzer, due to the presence of birefringent object between the polarization axes..... = A^2 Sin $^2\theta$ Cos $^2\theta$

(iii) Densitometer

A simple densitometer was constructed using a 1.0 x 0.5 mm. spot size. The scanning motor and the recorder motor were synchronized. The light transmitted by the positive photographic print was incident on a photoconductive cell whose output was plotted by a recorder.

3. General Procedure

Blood of very low hematocrit, diluted either with isotonic or hypotonic solution (to swell the cell) was put on a microscope glass-slide having a polished spherical cavity 0.8 mm. deep. The filled cavity was then covered with a coverslip, and the excess red cell suspension was cleaned from the slide. The coverslip was held firmly over the cavity by surface tensional forces. The glass-slide was then inverted to sediment a few red cells onto the surface of the coverslip. After leaving the slide in this position for one or two minutes, it was again inverted. This left many red blood cells hanging on edge on the coverslip surface. These red cells, hanging on edge, could be individually focussed and seen with the microscope.

The slide was fixed at the center of the circular rotating table of the polarizing microscope. Single red cells on edge, with the help of the mechanical stage, were brought exactly to the center of the uniformly illuminated field of view of the microscope. The red cell to be photographed, was thus perfectly centered so that rotation of the circular stage

did not alter its centered position.

Not enough light to expose the film emerged from the analyzer when the polaroids were crossed. Therefore, the analyzer axis was set to 89.5° relative to the axis of the polarizer. The red cell was then photographed with its major axis at 0°, 15°, 30°, ---- 360° relative to the polarizer axis.

The film used for photography was 35 mm. Kodak Tri-X Pan. This fine-grain film ordinarily has exposure index (ASA) 400,and is very sensitive for black and white photography, where very sharp images, high speed and enlargeability are required. The exposure time in each case was kept at one-half of a second. The exposure index of this film was increased to 2400, by developing it in 'diafine', a special Kodak developer. The positive prints were made on Kodabromide F-5 paper so that the final magnification was 5000. To ensure similar conditions for each cell series, time exposure, developing and printing processes were maintained the same for each photograph.

The positive prints for each red cell series were cut to a proper size to fit in the place provided on the moveable platform of the densitometer. Finally, to scan different regions, these cut positive prints were positioned properly against the light slit. The scanning of all prints was done in the linear region of the response of the densitometer. This procedure, in general, was uniformly followed for all experiments described in the section.

4. Experimentation

Polarization microscopy of the red cell interior

The polarization microscopic studies of the interior of the red cell were done to explore the problem of the biconcave discoidal shape of the red cell with an entirely different approach. So far we have concluded that the missing attractive force between the opposite membranes of a red cell at its dimple region might be due to the presence of long chain molecules forming 'tactoids' and linking the two opposite membranes of the cell with each other.

This section has been divided into three parts. The first part deals with the polarization microscopy of the interior of the normal red cells, while the second and the third parts deal with the polarization microscopy of the red cells swollen in hypotonic environments of different tonicities.

PART A. Polarization Microscopy of the Interior of the Red Cell, Hanging on Edge in Buffered Ringer Solution.

(i) Procedure

Normal blood from a finger-prick was collected in a one cc plastic syringe, having some Tris buffered Ringer solution (pH = 7.4, and tonicity = 310 mOsm). To make the hematocrit of the cell suspension very low it was further diluted with the same Ringer solution. A microscope slide, as has been described before, was made, and red cells hanging

on edge on the coverslip surface were obtained. Thirty-two red cell series at different orientations of each red cell with respect to the polarizer axis were photographed between crossed polarizer and analyzer (as described before). The scanning of each positive print was done at the dimple and rim regions separately by the densitometer. The light intensity through the white, unexposed part of the positive print, was kept constant in each case to serve as the fixed maximum level on the records. Scanning at a particular region of each positive print of a red cell series gave intensity variation profiles, in arbitrary units, of the polarized light coming out of that particular region of the red cell. The general features of the intensity variation profile at the dimple region are shown in Figure 25. In the profiles '$\bar{B}$' represents the mean intensity of the polarized light passing through the suspending medium adjacent to the red cell (i.e. mean background intensity), and 'I' represents the intensity of the polarized light passing through the interior of the red cell at its dimple region. Therefore, $(I-\bar{B})$ may be called the relative intensity of the polarized light coming out of the red cell interior with respect to the mean background intensity '$\bar{B}$'. This quantity may be positive or negative, and will depend on the optical nature of the red cell interior and the orientation of the red cell with respect to the polarization axes. In other words, if the quantity $(I-\bar{B})$ for a particular region of a red cell, oriented at some angle to the polarizer axis is negative, the

Figure 25.

Curve drawn by densitometer of the light transmitted through a positive photograph of a red cell. These photographs were exposed by the polarized light transmitted by the red cell in different orientations relative to the plane of polarization. '$\overline{B}$' is the mean intensity of the polarized light passing through the surrounding medium adjacent to the red cell. 'I' is the intensity of the polarized light passing through the red cell dimple interior. The quantity ($I-\overline{B}$) is called the relative intensity of the polarized light passing through the red cell interior with respect to the mean background intensity '$\overline{B}$'. 'M' in the curve represents the cell membrane.

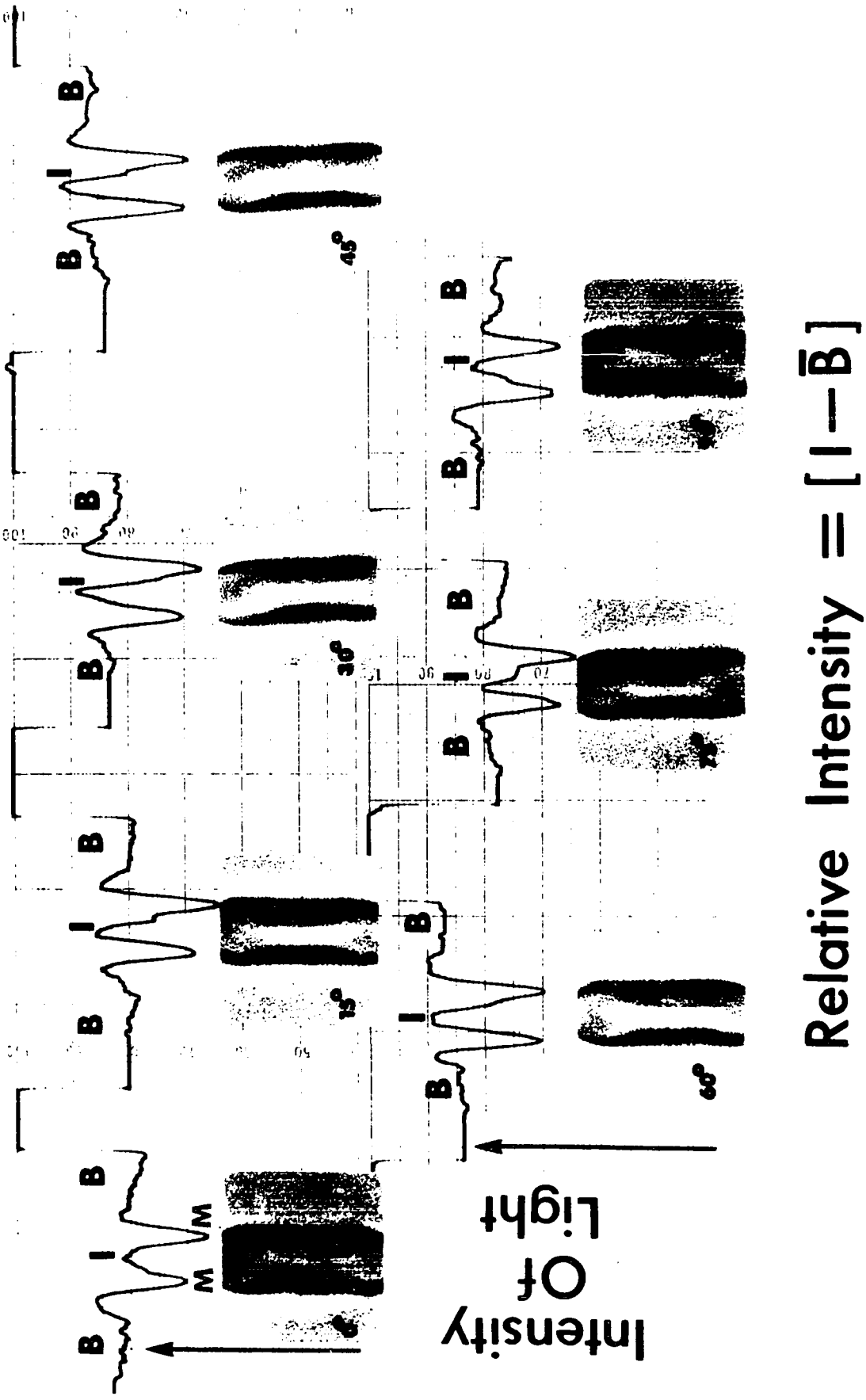
Intensity
Of
Light
Relative Intensity = [I − B̄]
B
I
M
0°
15°
30°
45°

red cell interior may be said to absorb polarized light. On the other hand, if the quantity $(I-\bar{B})$ is positive for the same region of the red cell interior when at some other angle of orientation to the polarizer axis, the cell interior may be said to emit polarized light rather than to absorb it. According to the theory of birefringence this will happen only when the red cell interior in that particular region is birefringent.

The aforesaid three quantities (i.e. I, $\bar{B}$, and $(I-\bar{B})$) were computed in the arbitrary units from each of the intensity variation profiles and for all red cell series.

Probable artifacts which might affect the results are discussed later.

(ii) Experimental Results

When the relative intensity $(I-\bar{B})$ versus cell orientation was plotted separately for each of the 32 normal red cell series, the curves did not show whether or not the relative intensity varies with the cell orientation. With the view to eliminate random errors from the data the red cell series were randomly divided into eight groups having four series each. Mean relative intensity was calculated by averaging corresponding values of relative intensities for each orientation of the cell and for each group. The data is presented in Table 10*. A variation of the relative intensity with the cell orientation is suggested by the

*See appendix II.

Figure 26

Illustrating variation of the relative intensity $(I-\bar{B})$ at dimple interior region of the normal red cell at different orientations to the polarizer axis. Each curve represents an average of four cell series together. A variation of the relative intensity with the cell orientation is suggested by these curves. The error present in the data for $(I-\bar{B})$ is mostly independent of the cell orientation, and can be eliminated by averaging as shown in Figure 27.

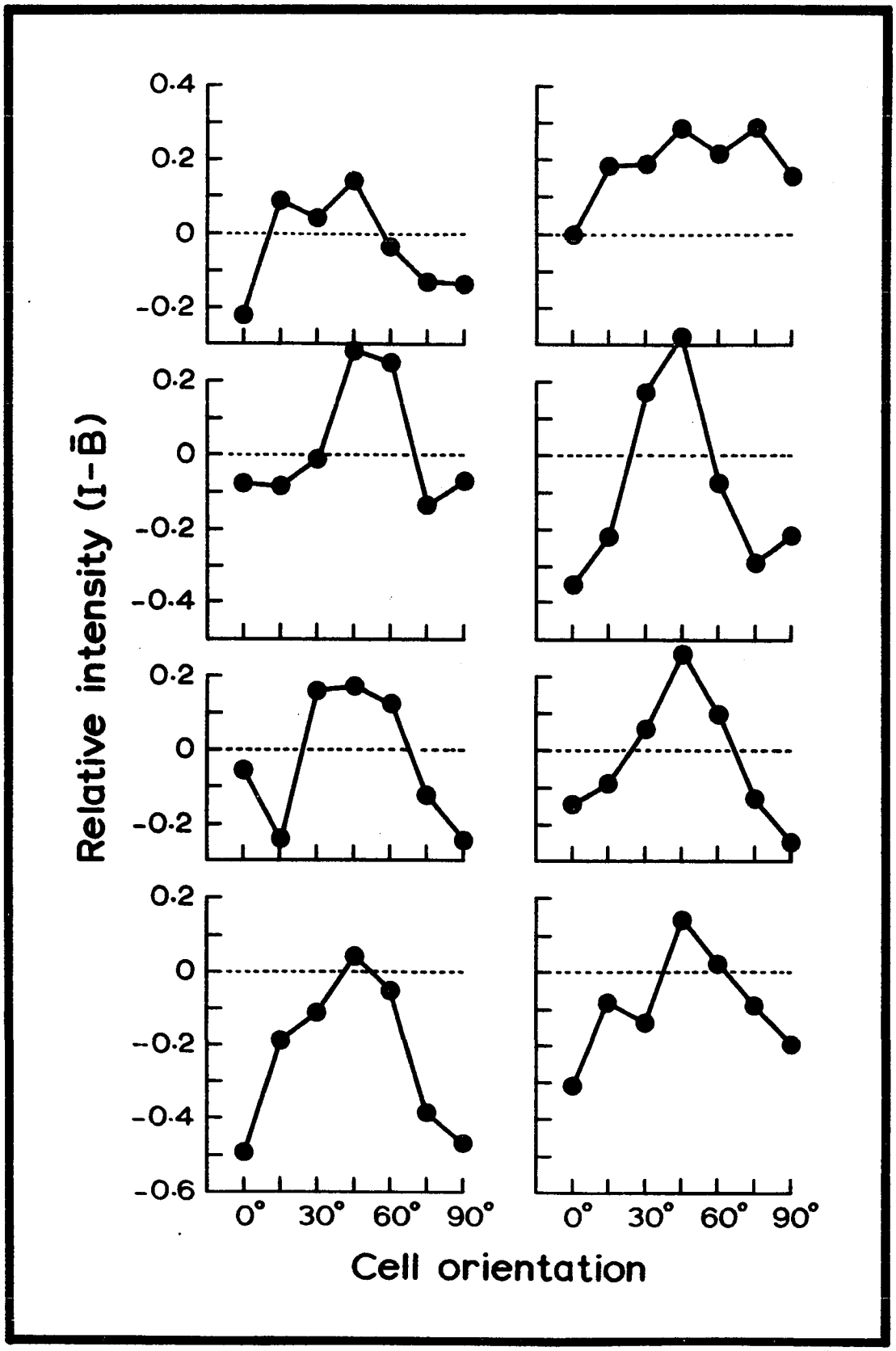
Relative intensity (I-B̄)
0·4
0·2
0
-0·2
0·2
0
-0·2
-0·4
0·2
0
-0·2
0·2
0
-0·2
-0·4
-0·6
0°
30°
60°
90°
0°
30°
60°
90°
Cell orientation

curves plotted for the data (Figure 26).

Finally, to eliminate random errors completely, all the 32 red cell series were pooled together and the mean of the relative intensity for each orientation of the cell was calculated. The data are presented in Table 11*. The plot for mean relative intensity versus cell orientation is shown in Figure 27. The curve shows that the variation of the relative intensity with the cell orientation is a periodic function.

Similarly, the mean relative intensity at the rim region was calculated for each orientation of the cell. The data are shown in Table 12*. The variation of this mean relative intensity with the cell orientation is presented in Figure 28. The curve does not seem to show any significant variation of the relative intensity with the cell orientation.

(iii) Possible Sources of Errors

The red cell membrane is a uniaxial birefringent structure with the optic axis along the normal to its surface. Since, in even an anisotropic medium, the velocities of the ordinary and extraordinary rays along the optic axis are equal, then the red cell membrane would not be expected to exhibit birefringence to the polarized light normally incident to it and, therefore, along its optic axis. When a red cell, hanging on edge, is viewed by a microscope, the light beam which passes through the interior of its dimple is always incident nearly normally to the membrane where it enters and leaves the cell rim. (See Figure 27). Thus, the anisotropy of the membrane does not seem to interfere with

*See Appendix II.

Figure 27

(A) Illustrating variation of the mean relative intensity $(I-\bar{B})$ of the normal red cell interior at dimple region as a function of the cell orientation to the polarizer axis. The circles represent the experimental points for the mean $(I-\bar{B})$, while the bars represent the SEM. The line represents a periodic function $(-0.2 + 1.6\ \mathrm{Sin}^2\ \theta\ \cos^2\ \theta)$, where θ is the angle of the cell orientation to the polarizer axis. Data of the mean $(I-\bar{B})$ as a function of cell orientation are presented in Table 11, Appendix II.

(B) Illustrating a red cell hanging on edge from a coverslip. The polarized beam of light, which passes through the dimple interior region of the cell, is normally incident to the cell rim membrane (i.e. incident in a direction parallel with the optic axis of the membrane).

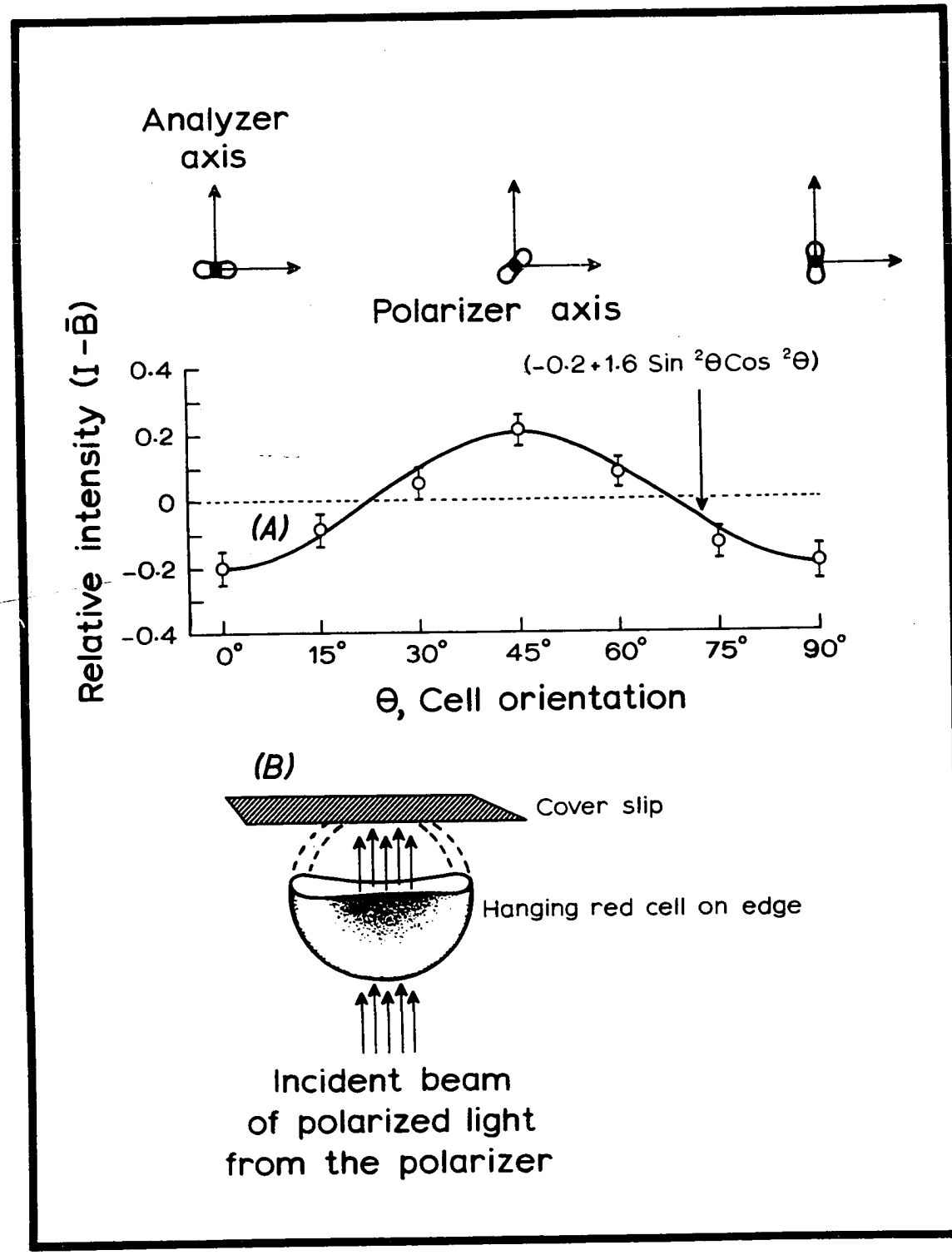
Analyzer axis
Polarizer axis
(-0.2+1.6 Sin ²θCos ²θ)
Relative intensity (I-B̄)
0.4
0.2
0
-0.2
-0.4
(A)
0°
15°
30°
45°
60°
75°
90°
θ, Cell orientation
(B)
Cover slip
Hanging red cell on edge
Incident beam
of polarized light
from the polarizer

the optical effects of the dimple interior of the red cell to the polarized light.

On the other hand, the beam of polarized light which passes through the rim interior region of the red cell is not normally incident to the membrane where it enters or leaves the cell rim. Thus, the small variation in the relative intensity (if there is any) for the rim region may be accounted for by the anisotropy of the red cell membrane rather than by the cell rim interior (Figure 28).

The other main sources of error may be summarized as follows:

(a) The red cell hanging on edge is not motionless. It is a common observation that red cells in good condition are in constant 'shimmering motion'. This may be due to Brownian motion, more likely to metabolic factors. When a red cell is photographed its shimmering motion tends to distort the photograph (Kavanau, 1965).

(b) The cells tend not to hang vertically but rather to tilt slightly in a random fashion. This artifact causes the intensity variation profiles to be assymetrical (Figure 25).

(c) Mechanical movements of the rotating table cause slight changes in the cell's position relative to the coverslip.

(d) Uncertainties in maintaining similar conditions in developing and printing processes of each photograph of the series may also lead to random error in the data.

(e) The other effects on the light, such as reflection, refraction and diffraction at the different interfaces are also important sources of error in the relative intensity data.

All these errors (except the reflection of the polarized beam of light) are independent of the cell orientation at different angles to the polarizer axis. However, the error due to reflection* of the polarized beam of light from the interior surfaces of the membrane at the dimple region seems to be small and does not seem to interfere with the relative intensity of the light passing through the center of the dimple region. In general, all these errors, which may be called the 'noise-level' are mostly independent of the cell orientation and, therefore, can be eliminated from the relative intensity data by averaging.

(iv) Discussion

Figure 27 shows the variation of the relative intensity of the red cell interior at its dimple region as a function of the cell orientation to the polarizer axis. The circles represent experimental points, while the curve represents a periodic function $(- 0.2 + 1.6 \text{ Sin}^2 \theta \cos^2 \theta)$, where θ is the angle of cell orientation to the polarizer axis. As can be seen from Figure 27, the curve fits the experimental points very well. Thus, the variation of the relative intensity of the polarized light, after passing

*Discussed on page 120, after discussion on swollen red cells.

Figure 28

(A) Illustrating variation of the mean relative intensity ($I-\bar{B}$) of the normal red cell interior at rim region as a function of the cell orientation to the polarizer axis. The circles represent the experimental points, while the bars represent the standard error of the mean. Data for mean ($I-\bar{B}$) as a function of cell orientation are presented in Table 12, Appendix II.

(B) Illustrating a red cell hanging on edge from a coverslip. The polarized beam of light, which passes through the rim region of the cell, is not normally incident to the cell membrane.

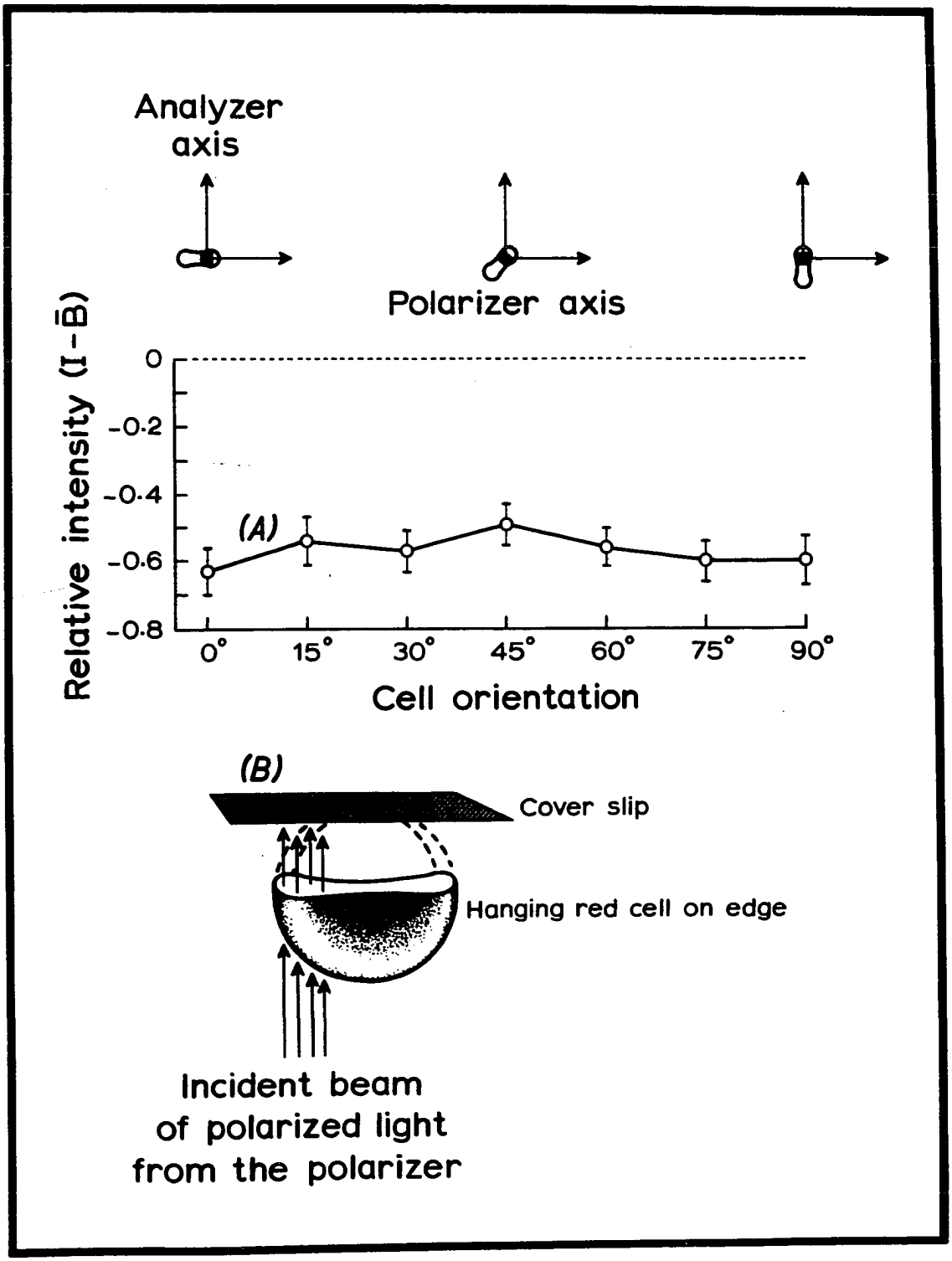
Analyzer axis
Polarizer axis
Relative intensity (I-B̄)
0
-0.2
-0.4
-0.6
-0.8
(A)
0°
15°
30°
45°
60°
75°
90°
Cell orientation
(B)
Cover slip
Hanging red cell on edge
Incident beam of polarized light from the polarizer

through the dimple interior region along the major axis of the red cell, is a periodic function of the cell orientation to the polarization axes. In other words, when a red cell hanging on edge is viewed and photographed between crossed polarizer and analyzer the light intensity through the red cell interior at the dimple region changes as the cell is rotated about the vertical axis. The relative intensity $(I-\bar{B})$ is a maximum of about 0.20 arbitrary units when the cell is oriented at an angle of 45° to the polarizer axes, Figure 27), and is a minimum of about - 0.20 arbitrary units when the cell is parallel to either of the two polarization axes. In other words, when the cell is either parallel or perpendicular to the polarizer axis, its dimple interior region transmits minimum light so that $I < \bar{B}$. If the red cell is viewed at those orientations between 0° and 90° it will appear brighter at the dimple region than it does at 0° and 90°. Between 22.5° and 67.5° $(I-\bar{B}) > 0$ which indicates that the dimple region is emitting polarized light. At all other orientations between 0° and 90° $(I-\bar{B}) < 0$ indicating that the dimple region is absorbing polarized light.

Therefore, the red cell interior at the dimple region is birefringent. This anisotropy of the red cell interior may be accounted for by the presence of long chain molecules in the dimple region either parallel to or perpendicular to the short axis. The red cell could, therefore, show form birefringence when viewed between crossed polarization axes at different orientations. The model experiments which we

Figure 29.

Schematic diagram illustrating (under ideal conditions), the birefringent and isotropic nature of the red cell dimple and rim interior regions respectively. P and A are the crossed polarizer and analyzer. The red cell on edge is shown in cross-section between the crossed polarization axes. The direction of the optical axes of the polarizer and analyzer are shown by arrows p and a respectively. Other thick arrows indicate the direction of the parallel beam of incident light, while the thin arrows show the plane of polarization of the light rays.

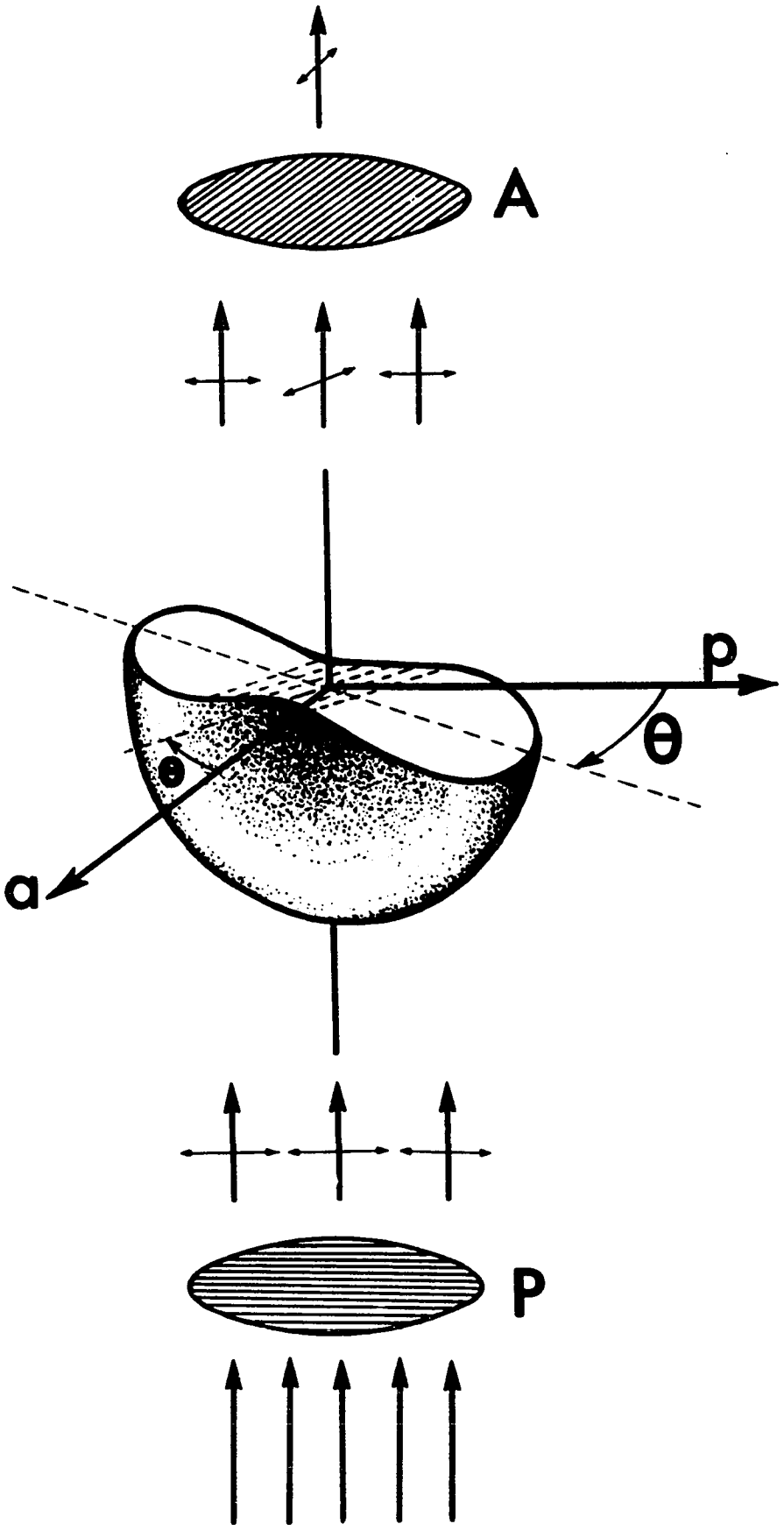
A
p
θ
θ
a
P

have described before, and some additional experiments on individual swollen red cells with polarized light which will be described later in this section, suggest that the long chain molecules are aligned along the short axis and serve to link the two membranes together at the dimple region of the red cell.

Thus, we conclude that the red cell interior at the dimple region is birefringent due to the presence of long chain molecules which link the two opposite membranes of a red cell together. These molecules would provide the missing force needed to stabilize the biconcave discoidal shape.

PART B. Polarization Microscopy of the Dimple Interior of the Red Cell, Hanging on Edge, in 240 mOsm Diluted, Buffered Ringer Solution

After completing polarization microscopy of the interior of normal red cells, it was decided to examine the effects on polarized light of these molecular chains when the cell is swelled in hypotonic solutions of different tonicities. Before describing the experimental procedure, we would like to discuss the intensity variation profiles at the dimple region of swollen red cells in 240 mOsm diluted, buffered Ringer solution. Figure 30 shows the general features of the intensity variation profiles at the dimple region of a swollen red cell in 240 mOsm buffered Ringer solution. In the figure, two regions, which may be called

Figure 30.

Intensity variation profiles at the dimple region of a swollen red cell in 240 mOsm diluted buffered Ringer solution.
Two regions of the red cell interior, which are called here 'membrane-adjacent-interior' or ('MAI') regions are separated by a lower intensity region, which is called here 'middle-interior' (or 'MI') region.

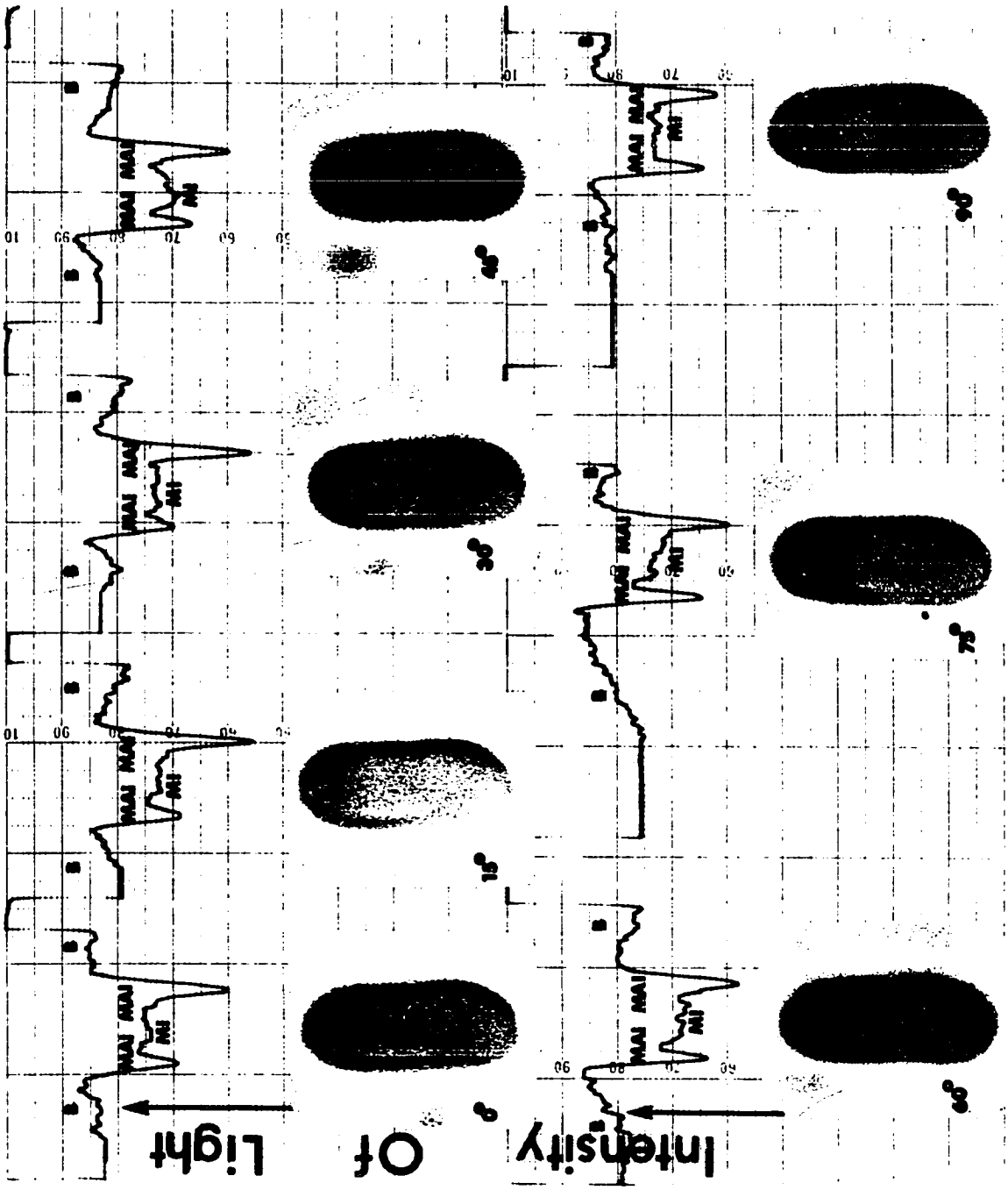
Intensity Of Light
0°
15°
30°
45°
60°
75°
90°

'membrane-adjacent-interior' (or in short MAI) are separated by a lower intensity region, which may be called the 'middle-interior' (or MI) region of the red cell dimple interior.

These regions of different intensity of the red cell dimple interior in the hypotonic environment may be accounted for as follows:

(a) In a hypotonic environment a red cell swells, which causes its adjacent membranes at the dimple region to move away from each other until they again acquire an equilibrium position at some increased distance of separation. This new equilibrium position of the cell membrane and its separation at the dimple region depends on the tonicity of the surrounding hypotonic environment of the red cell. The lower the tonicity of the surrounding hypotonic environment, the more is the swelling of the red cell, and the more is the separation of its two adjacent membranes at the dimple region. Therefore, the receding membranes of a red cell at the dimple region, when the cell is suspended in a hypotonic environment, might have created some stress on molecular chain organization, stretching and causing some of them to break. This gap in the molecular chains might correspond to the lower intensity region of the intensity variation profile, i.e. MI region in the Figure 30. The membrane-adjacent-interior, or 'MAI' regions in the intensity variation profiles might be due to palisades of the long chain molecules which are still left and attached at their one end to both interior

surfaces of the red cell membranes. These palisades of molecular chains would still be birefringent and thus would represent higher intensity MAI regions in the intensity variation profiles. If this is true, polarization microscopy could distinguish these two regions. In other words, the MI region should behave as an isotropic medium, while the 'MAI' regions, still having molecular chains, should be birefringent, and thus change the intensity of the transmitted polarized light as the cell is rotated.

(b) The second possibility seems to be that the dilution of the red cell interior, due to hypotonic surroundings, might have changed the nature of molecular chains drastically. In particular, the molecular chains might have split into smaller units, reorganized themselves differently, or scattered randomly. This possibility would demand that the two distinct regions at the dimple of a red cell in hypotonic environment should not exist, and the whole dimple interior should transmit uniformly the incident polarized light.

This region of the cell interior should show intensity variations of the transmitted polarized light if the molecular chains still exist in some organization but not if these split chains have scattered randomly.

(i) Procedure

Distilled water was added to Tris buffered Ringer solution to make 240 mOsm buffered Ringer solution. As has

been described before, a drop of fresh blood from a finger-prick was collected in a one cc plastic syringe and diluted with hypotonic solution to make blood of a very low hematocrit. The general procedure of obtaining the hanging cell and positioning discussed before was followed completely. The general features of the intensity variation profiles which have three distinct regions are shown in Figure 30. From these intensity variation profiles at the dimple region the following quantities were computed:

(a) The mean of the background intensity '$\bar{B}$'.

(b) The intensity for the middle-interior region 'MI' was computed. By subtracting the corresponding mean background intensity from this quantity, the relative intensity for middle-interior region, i.e. $(MI-\bar{B})$, was calculated for each of the cell orientations and for each cell series. Further, the corresponding values of $(MI-\bar{B})$, representing the particular cell orientation were averaged together. The mean values of $(MI-\bar{B})$ for different cell orientations are presented in Table 13*.

(c) The mean intensity for the membrane-adjacent-interior region, i.e. MAI was calculated by averaging intensities of both membrane-adjacent-interior regions of each intensity variation profile. From these quantities and background intensities, the relative intensity for membrane-adjacent-interior region, i.e. $(MAI-\bar{B})$, was calculated for

*See Appendix II.

each case. Further, by averaging, the mean (MAI-$\bar{B}$) was calculated for each cell orientation in all series. The data for the mean (MAI-$\bar{B}$) are presented in Table 13*.

(d) The relative intensity for the membrane-adjacent-interior region with respect to the middle-interior region, i.e. (MAI-MI), was calculated for each cell orientation from the corresponding mean values of intensities of MAI and MI regions. The data are presented in Table 13*.

(ii) Experimental Results

Figure 31A shows the variation of the mean relative intensity for the middle-interior region, i.e. (MI-$\bar{B}$), as a function of the cell orientation. The curve does not seem to be periodic, though it shows some decrease and increase in the relative intensity with the cell orientation.

Figure 31B shows the variation of the mean relative intensity for membrane-adjacent-interior region, (MAI-$\bar{B}$) as a function of the cell orientation. This curve seems to show a small variation in the relative intensity as a function of the cell orientation.

Finally, the curve (Figure 31C) was plotted for the relative intensity of the membrane-adjacent-interior region, with respect to the middle-interior region, i.e. (MAI-MI), as a function of the cell orientation. This curve is periodic in nature, and reveals that the relative intensity (MAI-MI) varies significantly with the cell orientation.

*See Appendix II.

Figure 31.

Illustrating variation of the relative intensity as a function of the cell orientation between crossed polarization axes, of the different regions of the dimple interior. The cell is swollen in 240 mOsm diluted buffered Ringer solution.

(A) Variation of the relative intensity (MI-$\overline{B}$)

(B) Variation of the relative intensity (MAI-$\overline{B}$)

(C) Variation of the relative intensity (MAI-MI)

The data for these curves are presented in Table 13, appendix II.

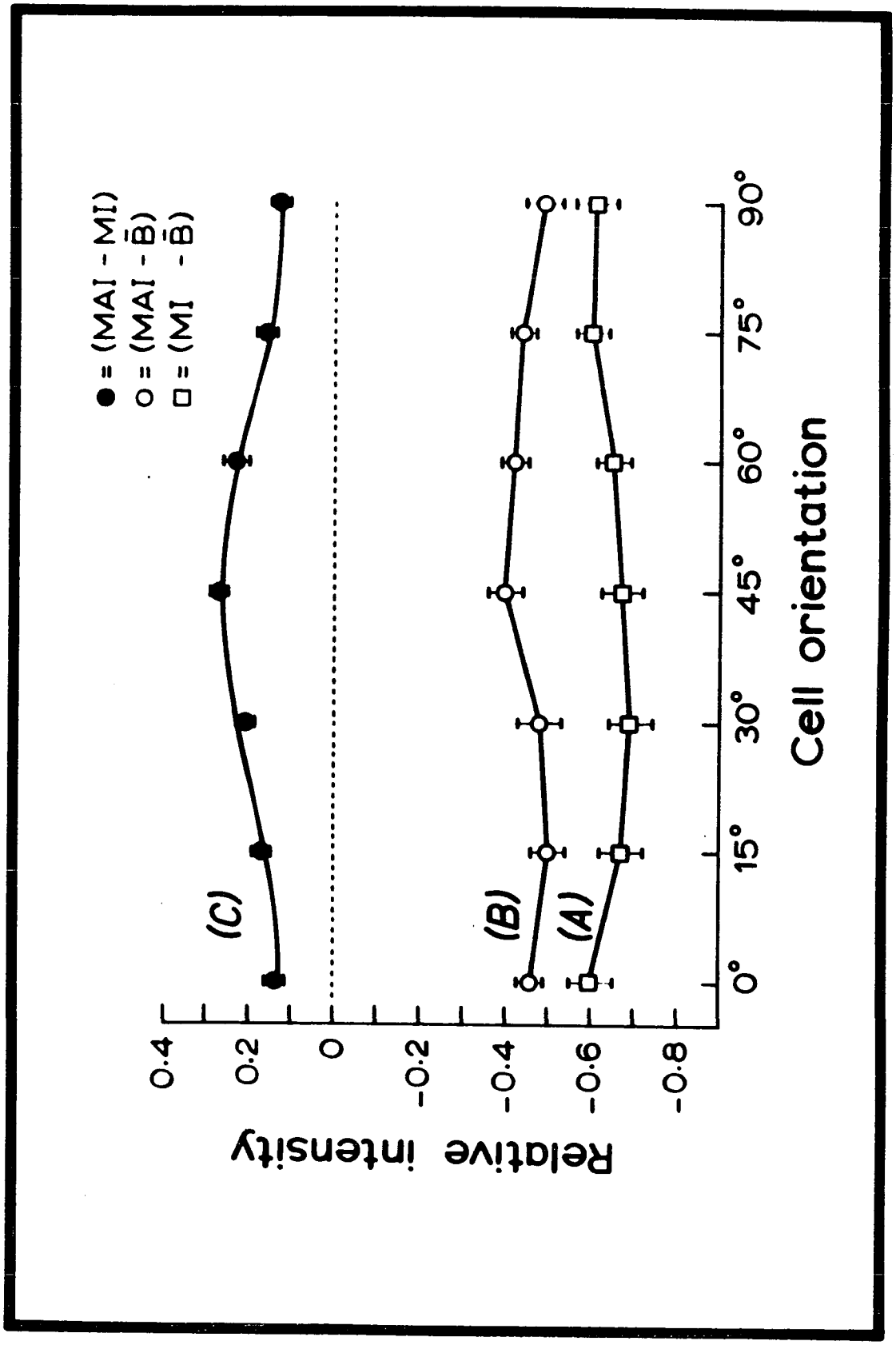
● = (MAI - MI)
○ = (MAI - B̄)
□ = (MI - B̄)
(C)
(B)
(A)
0.4
0.2
0
-0.2
-0.4
-0.6
-0.8
Relative intensity
0°
15°
30°
45°
60°
75°
90°
Cell orientation

(iii) Discussion

The Figure 31A shows the variation of the relative intensity for the middle-interior region, (MI-$\bar{B}$), vs the cell orientation. The relative intensity seems to decrease with orientation angle from $0^{o}$to nearly 30^{o} . After reaching a minimum at this orientation of the cell, the intensity increases up to a cell orientation of 90^{o}. It is, therefore, inferred that the molecular chains in the middle-interior region of the swollen cell seem to be reorganized, if they are present at all. However, the decrease in the relative intensity up to 30^{o} and then its increase up to 90^{o} of the cell orientation indicate that the molecular chains present in this region seem to have some type of alignment.

On the other hand, the relative intensity for the membrane-adjacent-interior region seems to increase with orientation angle from 0^{o} to 45^{o}. After attaining a maximum at 45^{o} the relative intensity decreases up to cell orientation of 90^{o}, Figure 31B. Thus, the variation of (MAI-$\bar{B}$) with the cell orientation, seems like the variation of the relative intensity of the dimple interior of the normal red cell. This similarity in the relative intensity variations shows that the molecular chains in the membrane-adjacent-interior regions of a red cell in hypotonic environment are intact, though their number seems to be decreased. The third curve, Figure 31C shows the variation of the relative intensity (MAI-MI) as a function of the cell orientation. In fact, this curve is the difference of the curves 31B and 31A showing the

variation of (MAI-$\bar{B}$) and (MI-$\bar{B}$). The quantity (MAI-MI) increases as the cell orientation increases from 0^{o} to 45^{o}. It then decreases as the cell orientation increases to 90^{o}. This curve seems to follow the periodic function (0.13 + 0.56 $Sin^{2}\ \theta\ cos^{2}\ \theta$), where θ is the angle of the cell orientation with the plane of the incident polarized light.

Thus, in conclusion, it can be said that the middle-interior region at the dimple interior of a red cell in 240 mOsm diluted, buffered Ringer solution, is more like an isotropic medium than the membrane-adjacent-interior regions of the same cell.

PART C. Polarization Microscopy of the Dimple Interior of the Red Cells, Hanging in 163 mOsm and 194 mOsm Diluted, Buffered Ringer Solution

(i) Procedure and Experimental Results

It was further decided to investigate the effects of more diluted environments on the anisotropy of the red cell dimple interior. Twenty series of red cells in 163 mOsm and sixteen series in 194 mOsm diluted, buffered Ringer solution were considered. The general procedure described before was followed. The general features of the intensity variation profiles for red cells suspended in 163 mOsm buffered Ringer solution are shown in Figure 32.

Computation of the mean background intensity '$\bar{B}$', middle-interior intensity MI, and the mean of the membrane-

Figure 32.

General features of the intensity variation profiles at the dimple region of a swollen red cell in 163 mOsm diluted buffered Ringer solution. The intensity variation profiles at the dimple region of red cells swollen in 194 mOsm diluted buffered Ringer solution also have the same general features (discussed later).

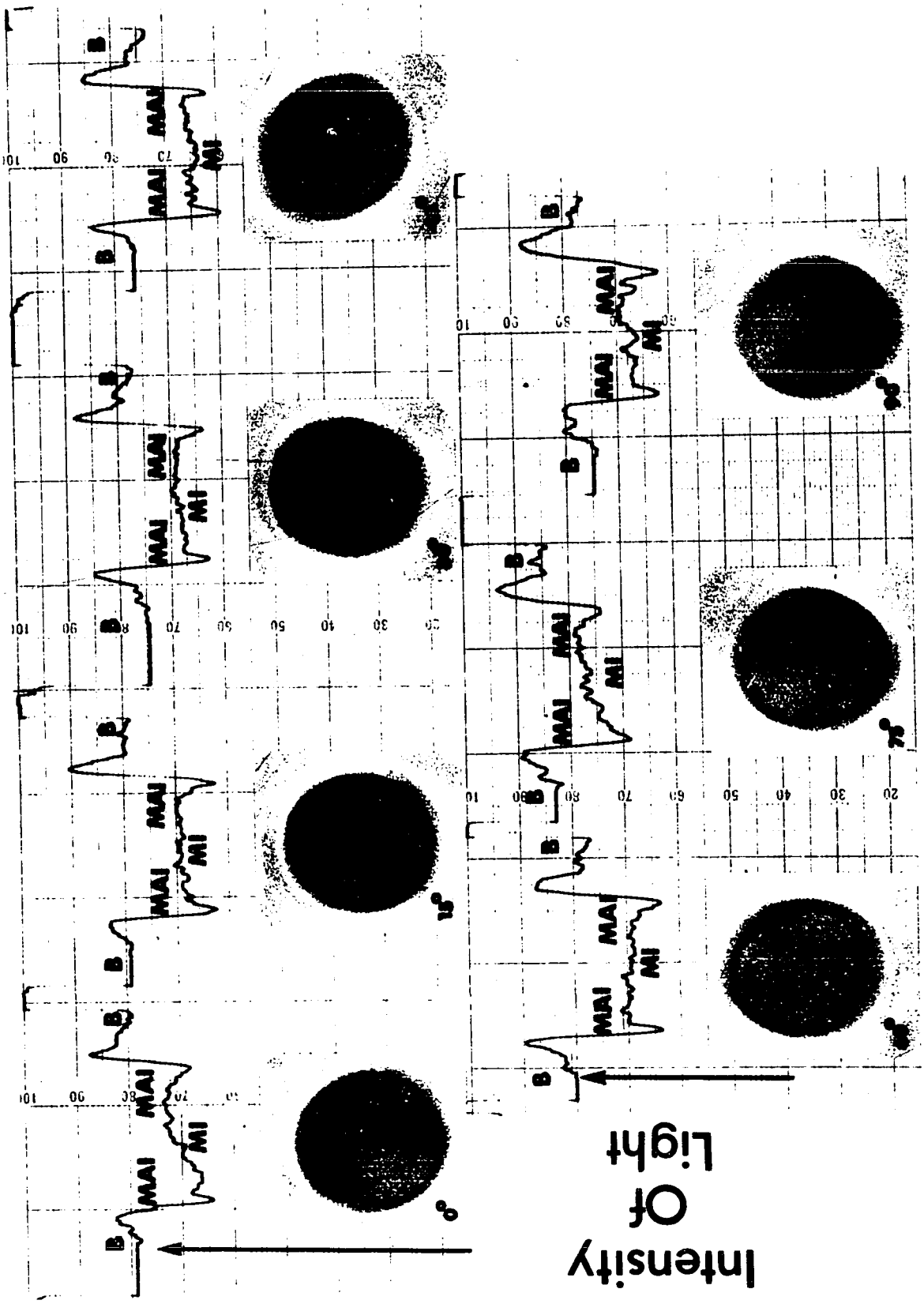
Intensity
Of
Light
B
MAI
MI
0°
15°
30°
45°
60°
75°
90°

adjacent-interior intensity MAI, were done from each of the intensity variation profiles and for both the cases. Relative intensities were calculated and then mean relative intensities $(MI-\bar{B})$, $(MAI-\bar{B})$ and (MAI-MI), were calculated for both the cases. The data of relative intensities for both the cases are given in Table 14* and Table 15* respectively. The variation of these quantities with the cell orientation has been shown in Figures 33 and 34. These curves are not periodic.

(ii) Discussion

Figure 33 shows the variation of the relative intensities $(MI-\bar{B})$, $(MAI-\bar{B})$ and (MAI-MI), as a function of the cell orientation for the red cell suspended in 163 mOsm diluted, buffered Ringer solution. The curves for $(MI-\bar{B})$ and $(MAI-\bar{B})$ are indistinguishable. This shows that the middle-interior and membrane-adjacent-interior regions at the dimple of a very swelled red cell do not exist separately. This can also be seen from the intensity variation profiles and from the curves for $(MI-\bar{B})$, $(MAI-\bar{B})$ and (MAI-MI). All of these show that the different intensity zones at the dimple interior region have not only merged into each other, but also that the whole region has become isotropic. Therefore, it seems that in a suspension of 163 mOsm diluted, buffered Ringer solution, the molecular chains, after being split into smaller units have scattered randomly. The excessive dilution

*See appendix II

Figure 33.

Illustrating variation of the relative intensities $(MI-\bar{B})$, $(MAI-\bar{B})$ and (MAI-MI) of the dimple interior regions as a function of the cell orientation to the axis of the polarizer. The red cell is suspended in 163 mOsm diluted buffered Ringer solution.

(A) Variation of the relative intensities $(MI-\bar{B})$ or $(MAI-\bar{B})$.
(B) Variation of the relative intensity (MAI-MI). Because $(MAI-\bar{B})$ and $(MI-\bar{B})$ are equal then their difference is zero, or the plot coincides with the x-axis of the plot. The bars indicate the SEM.

The data are presented in Table 14, appendix II.

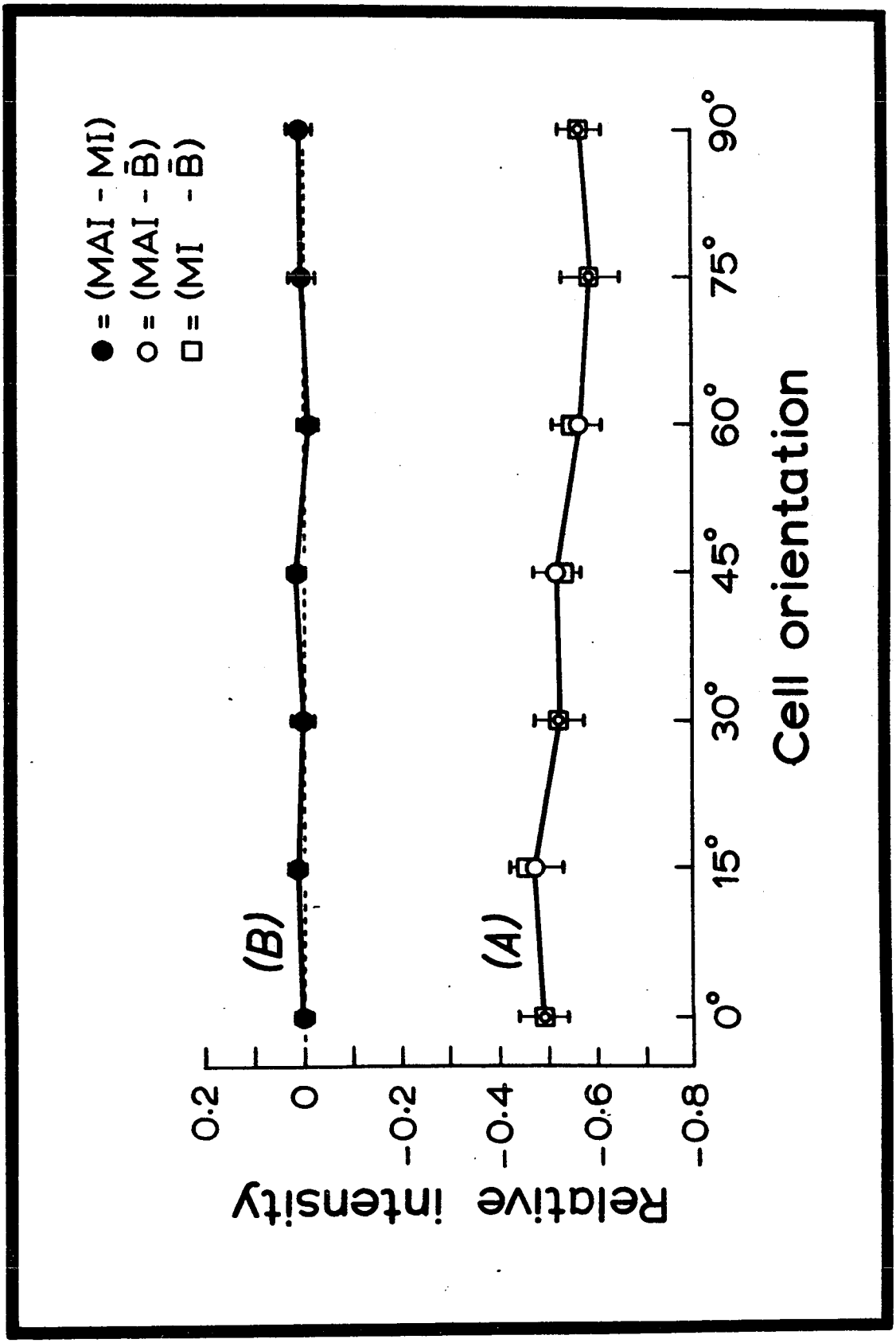
● = (MAI - MI)
○ = (MAI - B̄)
□ = (MI - B̄)
(B)
(A)
0.2
0
−0.2
−0.4
−0.6
−0.8
Relative intensity
0°
15°
30°
45°
60°
75°
90°
Cell orientation

Figure 34.

Illustrating variation of the relative intensities $(MI-\bar{B})$, $(MAI-\bar{B})$ and (MAI-MI), with the orientation of the cell to the axis of polarizer at the dimple interior region. The red cell is suspended in 194 mOsm diluted, buffered Ringer solution.

(A) Variation of the relative intensity $(MI-\bar{B})$

(B) Variation of the relative intensity $(MAI-\bar{B})$

(C) Variation of the relative intensity (MAI-MI)

Since the curves for $(MI-\bar{B})$ and $(MAI-\bar{B})$ seem to coincide to each other, the curve for (MAI-MI) nearly coincides the x-axis of the plot. The data are presented in Table 15, appendix II.

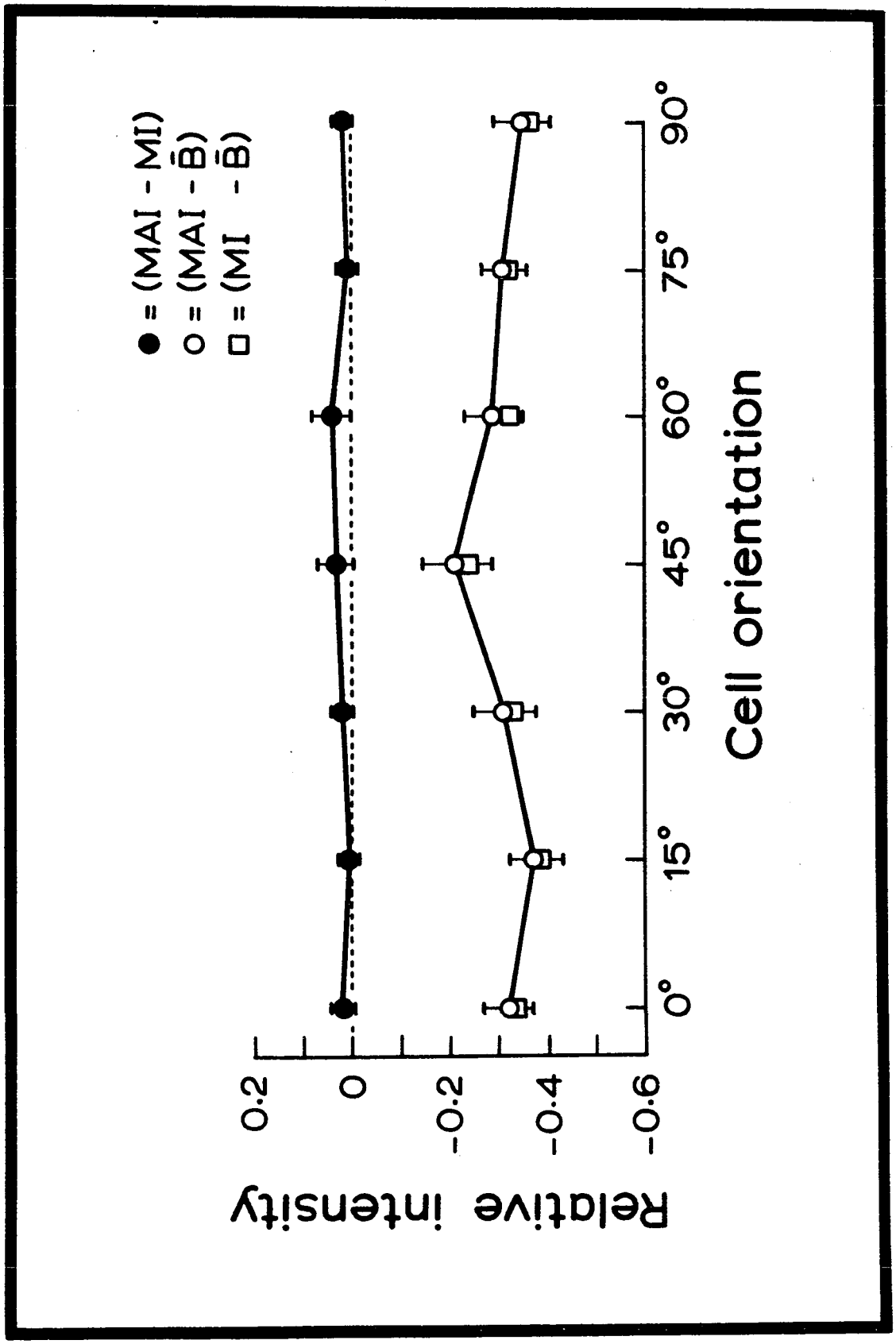
● = (MAI - MI)
○ = (MAI - B̄)
□ = (MI - B̄)
Relative intensity
0.2
0
-0.2
-0.4
-0.6
0°
15°
30°
45°
60°
75°
90°
Cell orientation

of the red cell interior makes a random migration of these split smaller units of the molecular chains from the dimple region to the rim region possible. The dilution of the cell interior and the resulting random scattering of these split units results in the isotropy of the region.

The variation of the relative intensities (MI-$\bar{B}$), (MAI-$\bar{B}$) and (MAI-MI) as a function of the cell orientation when the cell is suspended in 194 mOsm diluted, buffered Ringer solution is shown in Figure 34. The curves for the variation of (MI-$\bar{B}$) and (MAI-$\bar{B}$) as a function of the cell orientation are nearly identical, showing the merging of the two regions into each other. The curve for (MAI-MI) against the cell orientation seems to show only slight birefringence.

Thus, in conclusion, the dilution of the red cell interior by suspending it in 163 mOsm and 194 mOsm diluted, buffered Ringer solution seems to disrupt the molecular organization of the normal red cell which links opposite membranes to each other at the dimple region of the cell.

5. Possible Errors Due to Reflection of Light at the Different Interfaces of the Red Cell Membrane

The beams of polarized light incident on the dimple and rim regions of the membrane of the red cell have different angles of incidence. In the dimple region the angle of incidence is nearly zero (Figure 27B) whereas it is not for

the rim region (Figure 28B). Therefore, the amount of the light reflected at the membrane surface in these two cases will be different. Since the incident light is polarized, the reflection of the light will vary with the cell orientation. Thus it is important to establish the magnitude of this periodic error in the data of relative intensity versus cell orientation.

(a) The results for the rim region can serve as a control. The curve for the relative intensity of the light versus cell orientation for the rim interior region of the red cell did not show a variation with the orientation (Figure 28A). It is in this region that the variation of the reflection of light from the membrane surface with angle of orientation should be a maximum. In other words, the error due to light reflection at the membrane surface of the rim region is very small. Further, we can expect this error to be smaller in the dimple region where light is normally incident on the membrane surface.

(b) A second argument concerns the swollen red cell. The effect of rotation on the light reflection at the bottom of the hanging red cell should still exist, yet we find no relative intensity variation with angle in the center of the dimple region (Figures 33A and 34A). This suggests that reflection effects, at least at the point where the light enters the cell, are insignificant.

The other possibility of error is due to reflection of light from the two inner surfaces of the dimple region of

Figure 35.

Illustrating variation of the mean relative intensity ($M-\bar{B}$) of the membrane of the red cell at dimple region, as a function of the cell orientation to the polarizer axis. The circles represent the experimental points, while the bars represent the standard error of the mean. The curve does not show variation of ($M-\bar{B}$) with the cell orientation. Data for mean ($M-\bar{B}$) as a function of cell orientation are presented in Table 16, appendix II. Where M is the mean intensity of the polarized light passing through the cell membrane at dimple region, and $\bar{B}$ is the mean background intensity.

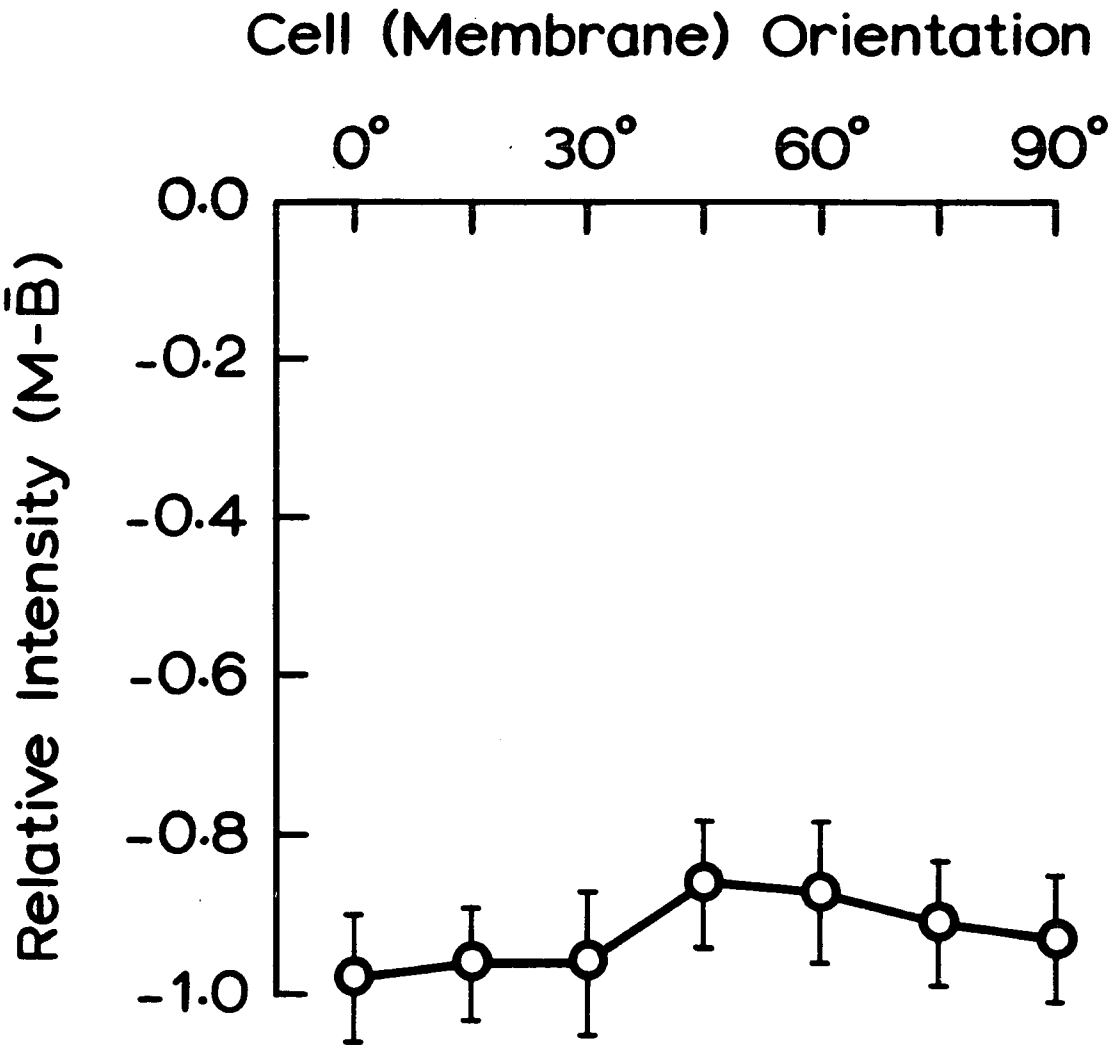
Cell (Membrane) Orientation
0°
30°
60°
90°
0.0
-0.2
-0.4
-0.6
-0.8
-1.0
Relative Intensity (M-B̄)

the red cell membrane. If this error was significant, we would expect a variation with angle of the intensity of the red cell membrane in this region, which was not present (Figure 35). Therefore, it is most unlikely that the error due to reflection of light at different interfaces of the red cell membrane contributes significantly to the data of the relative intensity of light of the red cell interior.

6. Summary

Quantitative measurements of the relative intensity variation of the transmitted polarized light through the different interior regions of a red cell have been presented in this section. Analysis of data indicates that the red cell interior at the dimple region is birefringent, whereas the rim region is isotropic. The anisotropy of the red cell dimple interior has been explained on the basis of the presence of long chain molecules bridging the gap between the two opposite membranes of a red cell. This type of molecular organization at the dimple region of a red cell would provide stability to its biconcave discoidal shape.

Suspending red cells in hypotonic environments of different tonicities disrupts the molecular organization. In moderately hypotonic environments the palisades of the broken molecular chains, left on the interior surface of the membrane at dimple region, seem to show weak birefringence. In very hypotonic environments the whole red cell interior seems to be isotropic.

VI. EFFECT OF LOW CONCENTRATION OF A SURFACTANT ON THE EQUILIBRIUM OF THE MEMBRANE OF THE RED CELL.

1. Introduction

We have been considering the equilibrium between the resultant force due to interfacial tension T (dependent on curvature), positive transmural pressure ΔP, and the proposed attractive force p^1 of the red cell. The role of bending moment of the red cell membrane is recognized. However, for the simplification of the problem of the equilibrium of the biconcave discoidal shape of the membrane of the red cell, we have not considered its bending moment along with the other three aforesaid forces.

The importance of interfacial tension of the red cell membrane in maintaining its biconcave discoidal shape has been recognized from time to time. Gough (1924) noticed that red cells washed a few times in normal saline become spherical. He also found that these washed red cells resume a normal biconcave shape if some plasma was added to their suspension medium. These observations, further, were confirm by Ponder (1925). Both of these workers have suggested that these shape transformations of the red cells

are due to changes in interfacial tension of the cell membrane. However, Ponder (1948) has described how changes in shape of washed red cells occur when they come in contact with the surface of either slide or its coverslip. These red cells crenate and become perfect spheres. If this change of red cell shape is associated with the increase in pH of the cell suspension near the coverslip surface, it may well be possible that this increase in pH increases the interfacial tension of the red cell membrane, thus changing its shape finally to a sphere. Later it was reported that the red cells sphered by repeated washing in normal saline buffered to 7.4 pH were immediately recovered to biconcave discs by transferring them to buffered saline containing RP 3300 (a surface-active agent), in concentrations of 1 in 10,000 to 1 in 80,000 (Chaplin, Crawford, Cutbush and Mollison, 1952). They also reported that this effect could be removed by washing the red cells again in normal saline.

The surface tension of buffered Ringer solution, like that of saline, is greater than that of the blood plasma. However, this surface tension can be decreased below the surface tension of the plasma by adding very small quantities of surface-active agents like polyoxyethylene (20) sorbitan monooleate* (Tween 80), in buffered Ringer solution.

Antonoff's relation states that the interfacial tension of two liquids in equilibrium (mutually saturated) is equal to the difference between their individual surface

*Obtained from Fisher Scientific Company, New Jersey, U.S.A.

tensions. If T_1 and T_2 refer to surface tension against air of two mutually saturated liquids (say water and an organic compound respectively), and if T_1 is higher than T_2, Antonoff's relations may be written as $T_{12} = T_1 - T_2$, where T_{12} is the interfacial tension between the two liquids, (Davies and Rideal, 1961). Assuming that Tween 80 changes T_1 more than T_2, the interfacial tension of the red cell membrane can be decreased by suspending them in buffered Ringer solution with Tween 80.

In this section, therefore, we will describe some experiments which we have performed on the change in the shape of red cells by suspending them in buffered Ringer solution (pH = 7.4 and tonicity = 306 mOsm) having one part of Tween 80 in 25,000 parts (0.004% by volume).

2. Surface-active Agents

Surface-active agents are many and varied. These substances, on the basis of their action on the red cell membrane, have broadly been divided into two categories (Seeman and Weinstein, 1966).

(i) Specific hemolysins (such as digitonin, saponin, etc.), which may be considered as specific in the sense that they have a very high affinity for cholesterol, and therefore, presumably, hemolyse the red cells even if they are in low concentration.

(ii) A wide variety of surface-active agents, such as oleyl derivatives of Tween, steroids, and alcohols are said to be non-specific hemolysins. These substances have biphasic effects on the membrane of the red cells. In low concentrations these substances protect or stabilize the red cell membrane against hypotonic hemolysis, while high concentrations of most of these cause direct hemolysis. Seeman (1966a, b) has studied this phenomenon in detail and has compared it with the effects of tranquilizers and anesthetics on the cells. Tween 80 (polyoxyethylene (20) sorbitan monooleate), which we have used in these experiments is a nonionic surface-active agent.

3. Control Experiments

(i) Variation of the surface tension and interfacial tension with surface-active agent Tween 80.

Surface-active agents are known to decrease surface

tension of the solvent in which they are dissolved. As the concentration of such a substance increases, the surface tension of the solvent decreases rapidly and reaches a minimal value at some higher but still very low concentration. When a surface-active agent is dissolved in water, the attraction between its own two molecules is less than the attraction between the two molecules of water. Therefore, to minimize the surface energy the molecules of water move into its interior, and their place in the outer layers is taken up by more molecules of solute, resulting in a decrease in the surface tension of the solution.

The measurements of surface tension and interfacial tension were done with the de Nouy tensiometer, in which the force required to lift a platinum ring out of the surface of a liquid or interface between two liquids is measured. The surface tension of the buffered Ringer solution was measured to be 74.5 dynes/cm.

If an amount of 0.004% by volume of Tween 80 is added to this Ringer solution, its surface tension reduces to 42.4 dynes/cm., which is lower than the measured surface tension 52.5 dynes/cm of the blood plasma. The surface tension of distilled water was measured to be 73.1 dynes/cm. Figure 36A presents the variation of surface tension we have measured of the buffered Ringer solution with different percentages of Tween 80 dissolved in it.

Just as Tween 80 can lower the surface tension of buffered Ringer solution, so it can lower the interfacial

Figure 36.

Illustrating the variation of:

(A) Surface tension of buffered Ringer solution with Tween 80.

(B) Interfacial tension between buffered Ringer solution and oleic acid, a lipid, with Tween 80.

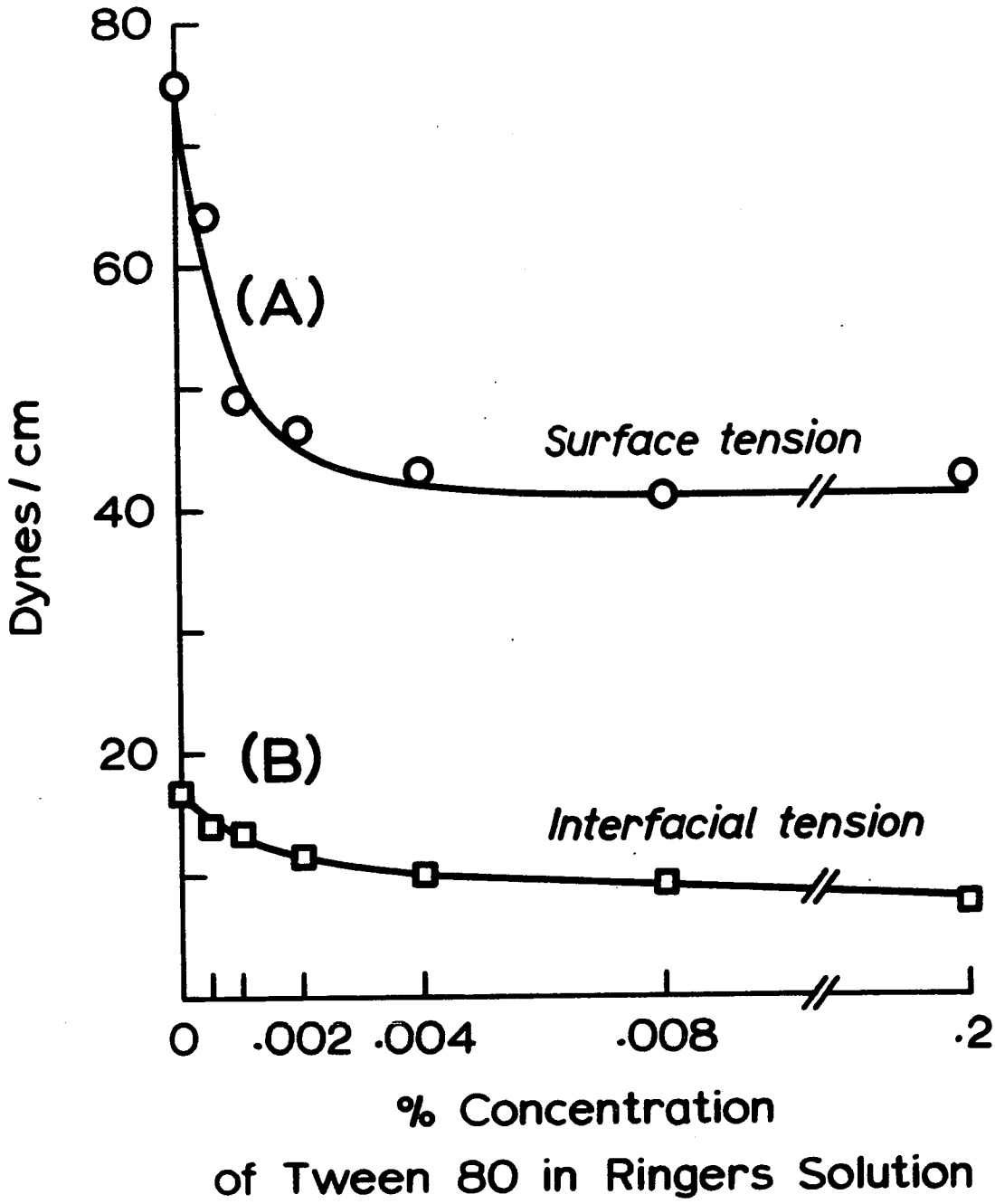
80
60
40
20
Dynes / cm
(A)
Surface tension
(B)
Interfacial tension
0
.002
.004
.008
.2
% Concentration
of Tween 80 in Ringers Solution

tension between an oil (or say red cell membrane) and the buffered Ringer solution (see Figure 36). Therefore, interfacial tension between Oleic acid, a lipid, and the buffered Ringer solution having different percentages of Tween 80 was measured. The variation is presented in Figure 36B.

(ii) Hematocrit Measurement

In order to know the effect of low concentrations of Tween 80 on the volume of red cells, we have done hematocrit measurements.

Ten ml. of fresh blood were taken from a vein and were gently placed in a test tube containing heparin (nearly 1 mg/ml of blood). This blood was diluted 50% by buffered Ringer solution and was divided into four equal samples of 5 ml. each. In three of these samples 0.004%, 0.008% and 0.2% by volume of Tween 80 was added. The fourth sample was kept as it was. All of these samples were gently stirred constantly by electromagnetic stirrers, and their hematocrit was separately determined at intervals of one-half hour for two hours. For each sample the hematocrit determined each time was the mean of three observations. This value (about 21%) was the same for all the four blood samples and did not change with time. We have concluded that Tween 80 in low concentration does not change the volume of red cells.

4. Method

(i) Procedure

Fresh blood from a finger-prick was collected in a one cc plastic syringe containing some buffered Ringer solution (pH = 7.4 and tonicity 306 mOsm) mixed with 0.004% by volume of Tween 80. This cell suspension was further diluted to make the hematocrit low by the same Ringer solution. The cavity of a microscope slide was filled with this suspension and red blood cells, some hanging on edge and some flat on the surface of a coverslip, were obtained and were photographed by a Leitz microscope. Similarly red cells suspended in buffered Ringer only were also photographed. These negative photographs were printed to a final magnification of 7300. Some of these prints are shown in Figure 37.

(ii) Description

As can be seen from Figure 37 the red cells suspended in buffered Ringer solution with Tween 80 have acquired a different shape than the ones which are suspended in buffered Ringer solution alone. These cells on edge have parallel membranes at the dimple region, and look like 'dog bones'. The flat view of these cells show a 'moon crater' at the dimple region rather than their gently rounded biconcavity. In other words, the red blood cells in buffered Ringer solution with Tween 80 change their shape from biconcave discs to the shape of a car wheel. The rim region of these cells look like the wheel tire with two parallel

Figure 37.

Microphotographs of normal red cells with (0.004% by volume) and without Tween 80 in buffered Ringer solution.

(a) Red cells on edge. The first two rows show the red cells without Tween 80, and the last two rows show the red cells treated with Tween 80.

(b) Flat red cells. The first two rows show the red cells without Tween 80, and the last two rows show the red cells treated with Tween 80.

The red cells treated with Tween 80 change their shape with a decrease of least thickness by 43.4% of the normal value (see red cells on edge). The 'crater' can be seen at the dimple region of the red cells treated with Tween 80 (see flat red cells).

(a)

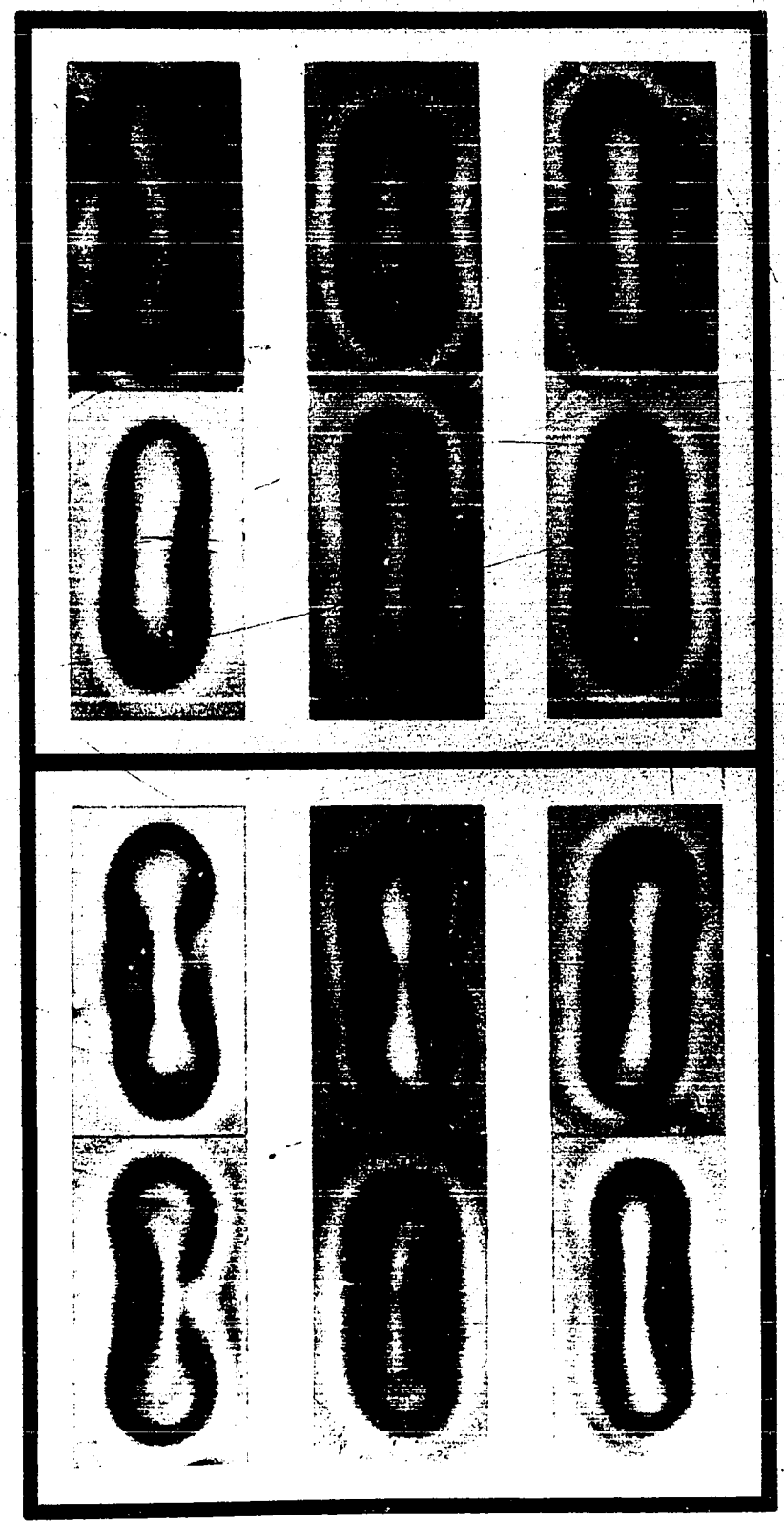

(b)

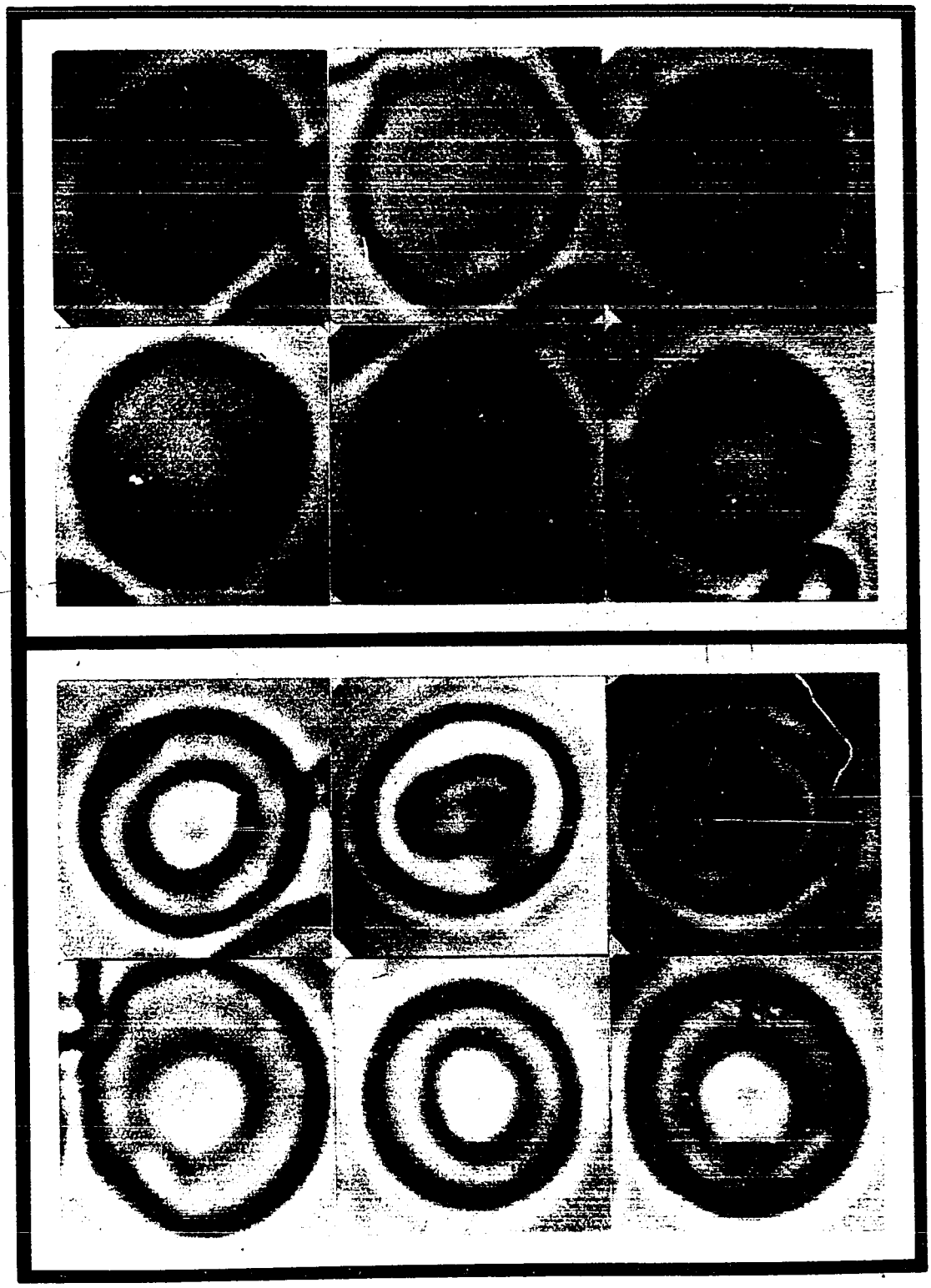

membranes at the dimple region. The interfacial tension of the membranes of the red cell will decrease by suspending them in a fluid of low surface tension. We, therefore, associate this change in shape of the red cells with decrease of the interfacial tension of their membranes.

(iii) Measurements

To validate the change in the shape of the red cells due to their suspension in buffered Ringer solution with Tween 80, we made measurements of least thickness and major diameter of these cells and also of the red cells suspended in buffered Ringer solution alone. The 'crater' diameter was also measured for the red cells suspended in buffered Ringer solution with Tween 80. These measurements were done on red cells both on edge and flat. The data are presented in Table 4.

5. Results

The mean values of the least thickness, and the major diameter for red cells with and without Tween 80 are presented in Table 4.

(i) The decrease in the least thickness due to suspension of the red cells in Ringer solution of low surface tension in comparison to the normal cells is 0.573 microns, which is a 43.4% decrease. The two mean values of the least thickness are highly significantly different ($p < 0.001$).

(ii) In comparison to the normal red cells the

TABLE 4

Comparison of the mean parameters of the normal human red cells (without Tween 80) and the red cells treated with Tween 80.

Red cell parameter on edge E, flat F	Sample population	Mean (μ)	S.D. (μ)	P Value
With Tween 80	138	0.767	± 0.150	
Least Thickness				P<0.01
Without Tween 80	130	1.339	± 0.180	
With Tween 80	138	8.233	± 0.537	
Major Diameter (E)				P = 0.001
Without Tween 80	130	8.014	± 0.554	
With Tween 80	138	8.101	± 0.537	
Major Diameter (F)				P<0.005
Without Tween 80	130	7.883	± 0.452	
(F)	130	7.883	± 0.452	
Major Diameter of normal cells (Without Tween 80)				P = 0.05
(E)	130	8.014	± 0.554	
(F)	138	8.101	± 0.567	
Major Diameter				P = 0.05
(E)	138	8.233	± 0.537	

major diameter of the red cells with Tween 80 is greater by 0.219 microns for the cells on edge, and is greater by 0.218μ for the flat cells. This shows that the increase in the major diameter due to suspension of the red cells in buffered Ringer solution with Tween 80 is about 2.9% only. Statistically the difference between the two mean values of the major diameters in both cases are significantly different.

(iii) In both cases, there seems to be some selection of the red cells hanging on edge in comparison to the cells which are flat. The mean values of the major diameters of the cells on edge and flat, for normal red cells, and also for the red cells suspended in Ringer solution of low surface tension, are probably significantly different ($p = 0.05$). Canham and Burton (1968) using buffered Ringer solution have found no significant difference between the major diameters of the red cells hanging on edge and flat. Therefore, the slight selection in the major diameters are cited above may be attributed to the low surface tension of the suspending medium.

(iv) The mean diameter of the 'crater' for the red cells suspended in Ringer solution of low surface tension for the cells which are flat and on edge are 3.867 ± 0.618 (SD) microns and 2.575 ± 0.524 (SD) microns respectively. The difference in the mean diameters of the crater for the red cells on edge and flat is because of the fact that the crater diameter for the red cells on edge represents the bottom diameter of the crater, while this

diameter for the flat cells is the diameter of the top of the crater. However, because of the sharpness of the two nearly parallel membranes at the dimple region of the red cells on edge, it was not difficult to focus them nicely in the microscope. Therefore, the bottom diameter of the 'crater' is more accurate than the top one.

(v) The mean volume of a red cell suspended in buffered Ringer solution with Tween 80 was calculated from mean values of the least thickness, the major diameter and the bottom diameter of the crater. Assuming that the changed shape of a red cell in Ringer solution of low surface tension is a toroid with parallel membranes at the (circular) crater, the mean volume calculated for the red cells with Tween 80 (data from Table 4) is $103.5\mu^3$. This value coincides very well with the recently published mean volumes of normal red cells for the seven subjects (Canham and Burton, 1968). The mean volume of the red cell for all seven subjects has been reported to be $107.5 \pm 16.8\mu^3$. This confirms our results of hematocrit measurement.

6. Discussion

The positive transmural pressure across the membrane of a red cell may be taken as 2.32 mm of H_2O. Rand (1964b) has shown that this pressure does not change even on swelling the red cell in hypotonic solution. As has been stated before the membrane of the red cells become stabilized (i.e. more resistant to osmotic hemolysis) by

exposing them to low concentrations of non-specific surface-active agents (Seeman, 1966 a,b). Furthermore, we have found that the hematocrit of the red cell suspensions in buffered Ringer solution with low concentrations of Tween 80 does not change. The calculations for the volume from the mean parameters of the red cells treated with Tween 80 also support this conclusion. Under these conditions, therefore, it is assumed that the transmural pressure across the membrane of the red cells would not change by treating them with low concentrations of Tween 80.

The direction of the resultant force due to interfacial tension at the dimple region of the membrane of a red cell is outward, while it is acting inwardly at the extreme point on its rim (Figure 4). Therefore, if the interfacial tension of the red cell membrane is increased by washing and suspending it in buffered Ringer solution which has greater surface tension (74.8 dynes/cm) than the surface tension of the blood plasma (52.8 dynes/cm), the equilibrium of the red cell membrane will change, and the cell would acquire a new equilibrium with increased sphericity. In fact, this is what seems to happen when the red cells washed repeatedly in normal saline buffered to pH 7.4 become spherical (Chaplin et al. 1952). These spherical cells were instantaneously reconverted by these workers to biconcave discs when added to a buffered saline containing RP 3300 in very low concentrations. This further implies that the decrease in surface tension of the buffered

saline due to the presence of RP 3300 has affected the equilibrium of the cell membranes to acquire their normal shapes again. We also have found that repeatedly washed red cells in normal saline first crenate and then become spherical on the coverslip. If these washed cells are suspended in saline containing one part of Tween 80 in 25,000 parts, they become biconcave again (see Figure 38). On the other hand if the interfacial tension of the membrane of a red cell is reduced by suspending it in buffered Ringer solution with 0.004% Tween 80, so that its surface tension is 42.4 dynes/cm (lower than the surface tension of the blood plasma), the force due to interfacial tension of the membrane would also be expected to decrease. Consequently the membrane of the red cell would acquire a new equilibrium, and the two membranes of the red cell at the dimple region will come closer to each other (see Figure 4). Our experimental results on the red cells treated with Tween 80 have shown that the least thickness of these cells decreases by 43.4% of the normal value (see Table 4), with the two membranes at the dimple region becoming nearly parallel to each other (see Figure 37). The rim region of these treated cells look like a toroid or like a tire of a motor car wheel.

Had there been no attraction between the opposite membranes at the dimple region of a red cell, it would have been very difficult to explain the decrease in its least thickness by reducing interfacial tension of the cell membrane. The change in shape of the red cell, where its

Figure 38.

Washed red cells suspended in normal saline, crenate on the surface of the coverslip (a), and become spherical after some time (b). If these cells are suspended in normal saline with 0.004% by volume of Tween 80, they resume a biconcave disc shape (c).

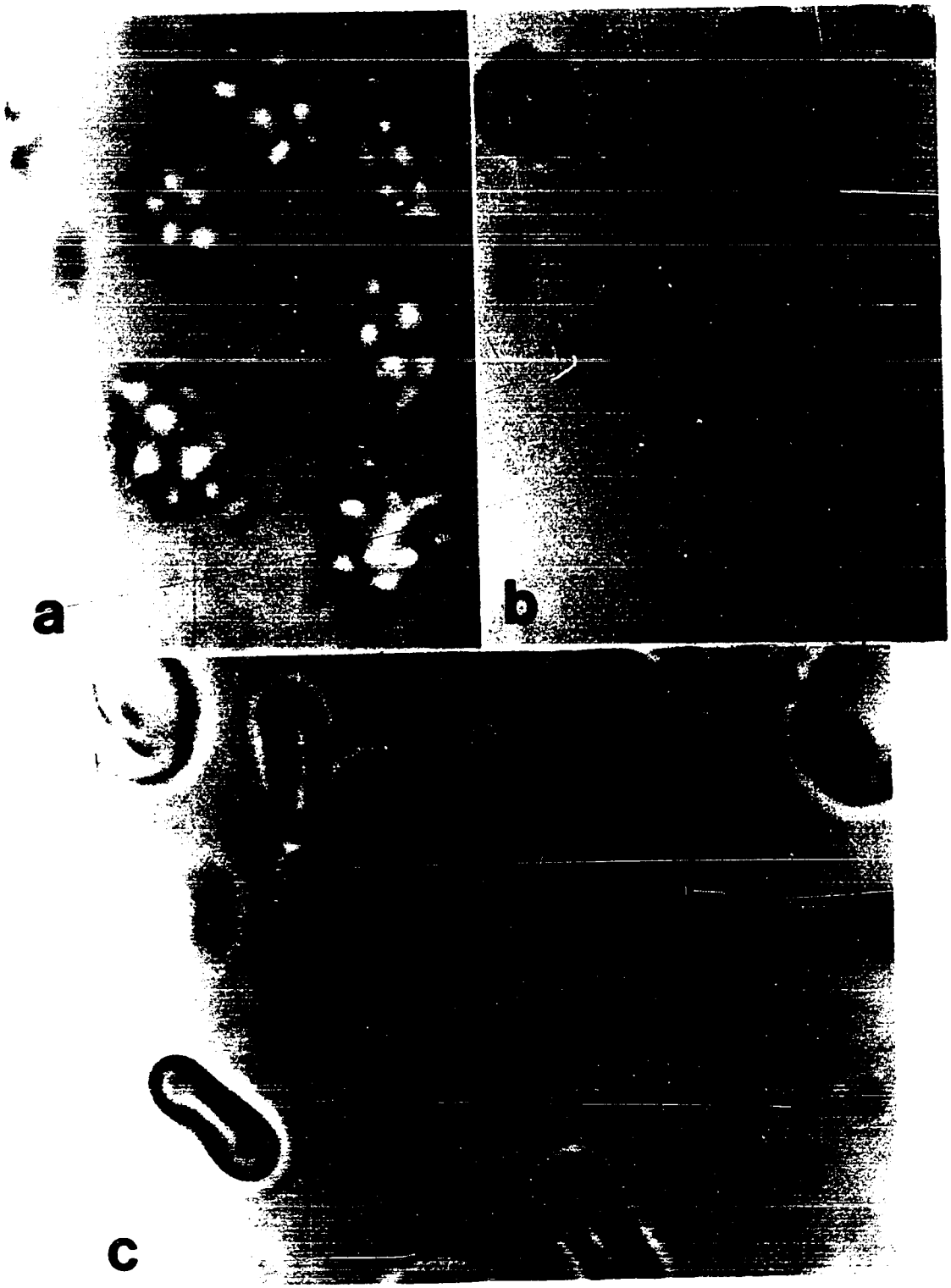
a
b
c

least thickness is decreased by reducing the interfacial tension of its membrane, suggests the presence of an attractive force between the opposite parts of the cell membrane and mainly at its dimple region. This, therefore, supports our proposition of the normally acting attractive force p^1 between the opposite parts of the membrane of the red cell.

The new equilibrium of the membrane of a red cell treated with Tween 80 can also be explained on the basis of Figure 22. Swelling of a red cell increases the distance between the two opposite membranes at its dimple region (least thickness). The curves in Figure 22 represent the variation of p^1, the proposed attractive force between the two membranes at the dimple of the red cell, with increase in the least thickness as the cells swell. Since a decrease of the interfacial tension of the membrane of a red cell decreases its least thickness, it provides us a way to extend our curves of Figure 22 backwards towards the origin of the curves. The interfacial tension of the membrane of a red cell treated with Tween 80 decreases, also the radii of curvature of the two membranes at the dimple region of this cell increase considerably (the two membranes becoming nearly parallel to each other). We, therefore, can neglect the force due to interfacial tension at the dimple region of the red cell treated with Tween 80, and, therefore, the proposed attractive force p^1 at the dimple region of these cells can be approximately taken equal to ΔP (2.32 mm H_2O), the transmural pressure across the cell membrane.

The model experiments (Figures 16 and 17) represent the variation of the force of attraction with distance of separation between the two similarly charged plates, having nylon fiber bridges in between. With reference to these curves, if curves of Figure 22 are extrapolated towards their origin, the point representing the value of p^1 (2.32 mm H_2O) and the least thickness (0.767μ) for the center of the dimple region of the red cells (shown by squares with dot) seems to fall on the extended part of these curves. If the bending moment of the red cell membrane is also considered with the other forces (i.e. ΔP, T and P^1), the curves of Figure 22 will shift upwards on the ordinate axis (we do not know how much), and then the point for treated red cells with Tween 80 (shown by squares with dot, which will not shift) may even fall on the extrapolated broken line.

In conclusion, therefore, the suspension of the red cells in buffered Ringer solution of lower surface tension than that of the plasma provides strong circumstantial evidence supporting the importance of the part played by the interfacial tension of the red cell membrane in the maintenance of its biconcave discoidal shape. Also the decrease in the distance between the two opposite membranes at the dimple region of the red cells treated with Tween 80 supports our proposition of the presence of the normally acting attractive force p^1 between the opposite parts of the cell membrane.

7. Summary

The normal biconcave shape of the red blood cells can be changed by suspending them in solutions (7.4 pH and 306 mOsm) of either higher or lower surface tension. The non-specific surface-active agent, Tween 80, has been used to lower the surface tension of the buffered Ringer solution. The surface tension of the buffered Ringer solution is found to be 74.5 dynes/cm. An amount of 0.004% by volume of Tween 80 reduces the surface tension of the buffered Ringer solution to 42.4 dynes/cm, which is lower than the measured surface tension 52.5 dynes/cm of the blood plasma.

Red cells suspended in buffered Ringer solution of low surface tension change their shape. The volume of these cells does not change, but the least thickness is decreased by 43.4% of the normal value. Each of these red cells on edge looks like a 'dog bone', having two nearly parallel membranes at the dimple region. The flat view of one of these cells is like the wheel of a motor car, with the rim region of the cell like its tire. The central region of the flat red cell looks like a 'moon crater'. This change in the shape of red cells in buffered Ringer solution of low surface tension is consistent with our views of the equilibrium between the forces active on the membrane of the red cells. However, this assumes that decrease in the surface tension of the suspending medium will also decrease the interfacial tension between the red cell membrane and its suspension.

VII. GENERAL DISCUSSION

As explained in Section III, the forces acting on the membrane of the red cell and its physical properties are as follows:

The transmural pressure (ΔP) across the red cell membrane, which has been suggested to be positive inside, and is equal to 2.32 mm of H_2O, i.e. 227.36 dynes/cm^2 (Rand and Burton 1964).

The interfacial tension of the membrane of the red cell is about 0.014 dynes/cm. This force tends to resist an increase in area as in the case of the surface tension in a soap bubble.

The modulus of resistance to bending of the red cell membrane expressed in terms of interfacial tensions is equal to 0.013 dynes/cm. This low value of bending moment allows the red cell membrane to deform with relatively little expenditure of energy.

Young's modulus of the red cell membrane is of the order of 10^7 dynes/cm^2, which is less than that of collagen and more than that of elastin. The energy required to overcome the resistance to increase in the area of the membrane is thus considerably higher than that needed to bend it.

The coefficient of viscosity of the red cell membrane is of the order of 10^7 poise. The red cell membrane, therefore, is viscoelastic and creeps under a stretch. The electron microscopic evidence suggest that this membrane is of uniform thickness, measuring only a few hundred angstrom units.

In general then, the red cell membrane we have considered is a uniformly thin, isotropic, homogenous, and viscoelastic medium wherein tension would always equalize. Under these conditions we have applied 'Laplace's Law' for liquid interfaces to explain the equilibrium of the red cell membrane. While doing so, we have neglected bending energy of the red cell membrane, which, although very small, may not be insignificant in comparison to its surface tensional forces. Such a priority accorded to the surface tensional forces in the red cell membrane inevitably leads us to the analogy of 'Soap-film Physics'. This may sound an oversimplified statement of this case, but the viscoelastic nature and other previously described properties of the red cell membrane compel us to do so.

Since, under normal conditions, a soap film never assumes the biconcave discoidal shape, the familiar equation $\Delta P = T(\frac{1}{R_1} + \frac{1}{R_2})$ could not be invoked to explain the equilibrium of a red cell membrane. However, if a force acting normally on the membrane of a red cell exists, and creates an attraction between its flat surfaces, the above equation can be modified accordingly.

We, therefore, have proposed the existence of normally acting attractive force p^1 (per unit area) between the opposite parts of the membrane of a red cell. Under these conditions, and with reference to the membrane of an intact red cell, the 'Laplace equation' can be modified as follows:

$$\Delta P = T \left(\frac{1}{R_1} + \frac{1}{R_2}\right) + p^1$$

Further, the shape of a red cell membrane in equilibrium demands that the proposed attractive force p^1 must vary from point to point on the membrane, and that such a variation determines the radii of curvature of the membrane at these points. This force p^1 has been calculated to be maximum at the dimple region, and minimum, and considerably smaller than the maximum p^1, at the cell periphery.

It is well known that biological membranes tend to cohere but do not tend to adhere (Weiss, 1960; Moscona, 1962). The attraction between the similar membranes is evident from the phenomenon of rouleaux formation of the red cells. The red cells form rouleaux only in the presence of some long chain molecules, such as fibrinogen, in the suspending medium (Merrill, E.W. et al., 1963). It is proposed that the force of attraction p^1, between the opposite membrane surfaces of the same red cell is due to the presence of long chain molecules, in the form of tactoids within the cell, and mainly at its dimple region. This seems more plausible, since by micromanipulation an inter-

cellular attachment between the two adjacent cell surfaces in rouleaux has been shown. This attachment breaks in a step-wise fashion when the cells are separated, leaving the impression that the cells had been attached by bits of sticky material at discrete points on their contacting surfaces (Grendahl, Olson, and Evans 1965). Polarization microscopy of the red cell interior reveals birefringent properties in the dimple region. This, and swelling of the single red cell in a step-wise fashion in hypotonic solution of decreasing tonicity, support the proposal of the presence of long chain molecules which link the two opposite membranes of cell at its dimple region. Further to this, recently published electron micrographs of the ghosts of red cells unequivocally demonstrate the presence of filamentous material attached to the inner surface of the red cell membrane. This filamentous material appears more prominent after incubation of the ghost cells in a medium containing ATP (Marchesi and Palade, 1967). These authors recognize the interior of the red cell ghosts by the presence of this material. The quantity of this material may well be greater in the intact red cell than in the ghost, as in the process of hemolysis some of it may leak out along with the hemoglogin. This filamentous material in the interior of the red cell ghost could conceivably be the remnants of a tactoid organization inside the normal cell. This material has been identified as a protein having elastic properties like muscle proteins (Marchesi and Steers, 1968).

Similarly, recent experiments performed on the red blood cells suspended in buffered Ringer solution of low surface tension provide a strong circumstantial evidence supporting the importance of the part played by the interfacial tension of the red cell membrane in the maintenance of its biconcave discoidal shape. The decrease in the distance between the two opposite membranes at the dimple region of the red cells treated with Tween 80 also supports our proposition of the presence of normally acting attractive force p^1 between the opposite parts of the cell membrane.

In this laboratory another line of reasoning has been pursued by others to account for the shape of the red cell. If a red cell has a specified area and volume, the normal shape of a red cell may represent the minimum bending energy of its membrane (Canham and Snyder, 1968). In this theory of the shape of a red cell, energy due to tension in the membrane, and the attraction between opposite parts of its membrane at the dimple region have not been included. Under appropriate hypotonic conditions a red cell acquires a planar shape, i.e. its two opposite membranes become flat and parallel to each other, having infinite radii of curvature. This is a stable configuration of a red cell which, in our view, cannot be accounted for by the above theory, (unless the pressure difference inside to outside is zero) since no bending moment could be associated with the planar surfaces where the dimple region existed.

If transmural pressure across the red cell membrane is positive inside, there will be a tendency to bulge the membrane outward giving the cell a biconvex shape, unless some opposing force such as the proposed p^1 were coexistent.

Recently there has been a strong plea that the energy due to tension is as significant as energy due to bending of the red cell membrane (Rand, 1967). This implies that both of the above mentioned energies of the membrane, along with the normally acting force of attraction p^1, must be considered to account for the shape of the red cell. In other words, the two theses outlined above need not be mutually exclusive; they could supplement rather than supplant each other.

For deformable surfaces, such as the membrane of a red cell, no general theory which simultaneously considers surface tensional and bending energies has so far been worked out. For even very simple geometric shapes, such a unified theory is mathematically very difficult.

We, therefore, may write:

Total energy of the red cell membrane

$= E_T + E_A + E_B$ = minimum for its stable normal shape.

Where:

E_T = Total energy due to tension in the membrane, which may be taken as constant, as the surface area of the cell membrane does not change on the swelling of the cell.

E_A = Total energy due to attraction between the opposite parts of the cell membrane.

E_B = Total energy due to bending of the cell membrane. Therefore, the actual shape of the red cell may represent the minimum of $(E_A + E_B)$, which may be minimum of E_A, and also minimum of E_B, at the same time.

VIII. SUMMARY AND CONCLUSIONS

In general, the red cell membrane may be considered a uniformly thin (measuring a few hundred angstrom units), isotropic, homogeneous, and viscoelastic medium, wherein tension would equalize.

Considering only surface tensional forces of the red cell membrane, (if it is compared with the soap film) its equilibrium as a biconcave disc cannot be accounted for with the help of 'Laplace's Law' for liquid interfaces.

Inasmuch as no soap film ordinarily can assume the shape of a red cell, a normally acting inward force of attraction, p^1 (dynes/cm^2), must exist between the opposite surfaces of a red cell membrane. This force p^1 must vary from point to point on the red cell membrane, and this variation will determine the radii of curvature of the membrane of these points.

The radii of curvature at different singular points of the red cells have been determined from the profiles of their enlarged positive photographic prints. The force p^1 has then been calculated at these points. The magnitude of p^1 is a maximum at the center of the dimple region of the cell; 2.82 mm of water. This force is a minimum

at the cell periphery: 0.66 mm of water. This is considerably smaller than the maximum p^1.

The red cells form rouleaux (i.e. their membranes attract each other) only in the presence of some long chain molecules, such as fibrinogen, in the suspending medium. The origin of the attractive force p^1 is proposed to be due to the presence of long chain molecules, in the form of tactoids, in the interior of the red cell, mainly at its dimple region. These tactoids could form bridges linking the opposite flat surfaces of the cell membrane together.

In the fourth section, the properties of an absolute electrometer (a parallel plate capacitor), with nylon fiber bridges between its charged plates are considered and measured. These nylon fiber bridges may be compared to the tactoid bridges hypothesized to exist within the red cell. This system is considered an electrical analogue of the red cell.

The nylon fiber bridges between the charged plates of the electrometer greatly modify the classical laws of electrostatics. The force of attraction between the charged plates increases to a maximum as the distance between them is increased. On further increasing this distance the chains break and the force of attraction falls, following the classical laws of electrostatics. The magnitude of the maximum force and the corresponding distance of separation of the plates depend upon the length of the nylon fibers used, their quantity per unit volume, the voltage and the charge between the plates.

Also, in this section, the variation of p^1 at the dimple region of a single red cell has been described. As the cell is swelled in a step-wise fashion by decreasing the tonicity of the suspending medium,the force increases and then decreases, similar to the variation of force of attraction between the charged plates of the absolute electrometer. In the initial stages of the swelling of the red cell the tactoids resist the swelling and cause an increase in the curvature (or decrease in the radii of curvature) of the cell membrane at the dimple region. Thus, the initial stages of swelling of a red cell cause an increase in p^1. After experiencing maximum stress, corresponding to maximum p^1, these tactoids break. The cell, then, is free to swell in an unrestricted manner.

The polarization microscopic techniques employed to indicate the presence of molecular chains in the interior of the red cell have been described. Single red cells, hanging on edge, were photographed at different angles of orientation between crossed polarization axes. Analysis of the relative intensity data of the red cell interior shows that the interior of the dimple region of a red cell is birefringent, and therefore anisotropic. On the other hand, the rim region of the cell is isotropic. The variation of relative intensity of the red cell dimple interior region is a function of $(\sin^2 \theta \cos^2 \theta)$*. Theoretically this must be if the red cell interior is birefringent. This is strong

* θ = angle of cell orientation.

support for the proposition of the presence of molecular chains, or tactoids at the dimple region of the red cell. Such chains do not exist at the rim region. In osmotically swollen red cells these molecular chains seem to be disrupted.

Finally, the red cells were suspended in buffered Ringer solution of low surface tension. The decrease in interfacial tension of the membrane of red cells changed their shapes. These individual red cells on edge look like a 'dog bone' with distance of separation decreased by 43.4% between the two membranes at the dimple region. The flat view of these cells look like a wheel of a motor car with its tire as the rim region of the cell. This change in the shape of the red cell and decrease in its least thickness support the importance of interfacial tension in maintenance of the shape of the red cell and the existence of the proposed attractive force p^1 between the opposite parts of the cell membrane.

In conclusion, therefore, an integrated theory (as has been described in Section VII) which would incorporate the minimum of the total energy of the membrane of the red cell into one system would be the proper and complete answer to this perplexing biophysical problem.

REFERENCES

1. Abercrombie, M. (1964). Behavior of normal and malignant tissue cells in vitro. Canadian Cancer Conference. 4: 101-118.

2. Abramson, H.A., Furchgott, R.F. and Ponder, E. (1939). The electrophoretic mobility of rabbit erythrocytes and ghosts. J.Gen.Physiol. 22:545-553.

3. Baker, J.R. (1948). The cell theory. Quart. J. Micr. Sci. 89:103-140.

4. Bateman, J.B., Hsu, S.S., Knudsen, J.P. and Yudovitch, K.L. (1953). Hemoglobin spacing in erythrocytes. Arch. Biochem. 45:411-422.

5. Bell, D.J. and Grant, J.K. (eds.)(1963). The structure and function of the membranes and surfaces of cells. Biochem. Soc. Sympos. 22 Cambridge, England. University Press.

6. Brooks, D.E., Millar, J.S., Seaman, G.V.F. and Vassar, P.S. (1967). Some physico-chemical factors relevant to cellular interactions. J. Cell. Physiol. 69: 155-168.

7. Burton, A.C. (1966). Role of geometry, of size and shape, in the microcirculation. Fed. Proc. 25:1753-1760.

8. Canham, P.B. and Burton, A.C. (1968). Distribution of size and shape in populations of normal human red cells. Circ. Res. 22:405-422.

9. Canham, P.B. and Snyder, R.A. (1968). The shape of human red cell as representing a minimum energy of bending.

Presented at the 12th annual meeting of the Biophysical Society. (Biophys. J. Soc. Abstr. Vol. 8. p. A-114.

10. Chaplin, H. Jr., Crawford, H., Cutbush, M. and Mollison, P.L. (1952). The effects of a phenothiazine derivative (RP 3300) on red cell preservation. J. Clin. Path. 5, 91-101.

11. Cook, G.M.W., Heard, D.H. and Seaman, G.V.E. (1961). Sialic acids and the electrokinetic charge of the human erythrocyte. Nature. 191:44-47.

12. Crosby, W.H. (1959). Normal functions of the spleen relative to red blood cells. A review. Blood. 14:399-408.

13. Danon, D. (1967). Structural changes associated with red cell aging. XVIII John G. Gibson II Lecture; College of Physicians and Surgeons, Columbia University.

14. Danon, D., Howe, C. and Lee, L.T. (1965). Interaction of polylysine with soluble components of human erythrocyte membranes. Biochim. Biophys. Acta. 101:201-213.

15. Davies, J.T. and Rideal, E.K. (1961). The physics of the surfaces. in Interfacial Phenomena .Academic Press N.Y. pp. 1-55.

16. Dourmashkin, R.R., Dougherty, R.M. and Harris, R.J.C. (1962). Electron microscope observations on rous sarcoma virus and cell membranes. Nature. 194:1116-1119.

17. Drabkin, D.L. (1945). Hemoglobin, glucose, oxygen and water in the erythrocytes. A concept of biological magnitudes, based on molecular dimensions. Science. 101:445-451.

18. Elul, R. (1967). Fixed charge in the cell membrane. J. Physiol. 189:351-365.

19. Fishman, A.P. (1962). Symposium on the plasma membrane. Circulation. 26:983-1232.

20. Forer, A. (1965). Local reduction of spindle fiber birefringence in living Nephrotoma Suturalis (LOEW) speromatocytes induced by ultraviolet microbeam irradiation. J. Cell. Biol. 25:95-117.

21. Forer, A. (1966). Characterization of the mitotic traction system and evidence that birefringent spindle fibers neither produce nor transmit force for chromosome movement. Chromosoma. 19:44-98.

22. Fricke, H., Parker, E. and Ponder, E. (1939). Relative quantity of the fixed framework of the hemolyzed rabbit red cell. J. Cell. Comp. Physiol. 13:69-76.

23. Friedenberg, R., Blatt, A., Gallucci, V., Daniells, J.F., and Shames, I. (1966). Electrostatics of membrane systems - I. A non-statistical approach to cellular membrane systems. J. Theoret. Biol. 11:465-477.

24. Furchgott, R.F. (1940). Disc sphere transformation in mammalian red cells. J. Exp. Biol. 17:30-44.

25. Ginzburg, B.Z., Friedlander, T. and Pouchovsky, E. (1967). Specific binding of sodium and potassium ions in erythrocyte membrane. Nature. 216:1185-1188.

26. Glaeser, R.M. (1963). The electric charge and surface properties of intact cells. Ph.D. Thesis. University of California.

27. Glaeser, R.M. and Mel, H.C. (1964). The electrophoretic behavior of osmium tetroxide-fixed potassium permanganate-fixed rat erythrocytes. Biochim. Biophys. Acta. 79:606-617.

28. Goldacre, R.J. (1954). Crystalline bacterial arrys and specific long-range forces. Nature. 174:732-734.

29. Gough, A. (1924). The nature of the red blood corpuscle. Biochem. J. 18:202-214.

30. Grendahl, M.J., Olson, C.R. and Evans, R.L. (1965). Intercellular forces and separation energy of red cells sludged by contrast medium. Proc. Soc. Exp. Biol. Med. 118:1124-1127.

31. Harris, J.W. (1965). The Red Cell. 3rd ed. Harvard University Press, Mass.

32. Harry, W., Wing, R. and Seilby, F.W. (1965). Counter-current distribution of red blood cells of different ages and from different species. Biochim. Biophys. Acta. 109:293-301.

33. Hartridge, H. (1919). Shape of red blood corpuscles. J. Physiol. 53:Plxxi.

34. Heard, D.H. and Seaman, G.V.F. (1960). The influence of pH and ionic strength on the electrokinetic stability of the human erythrocyte membrane. J. Gen. Physiol. 43:635-654.

35. Hiller, J. and Hoffman, J.F. (1953). On the ultrastructure of the plasma membrane as revealed by the electronmicroscope. J. Cell. Comp. Physiol. 42:203-247.

36. Hoffman, J.F. (1956). On the producibility in the observed ultrastructure of the normal mammalian red cell plasma membrane. J. Cell. Comp. Physiol. 47:261-271.

37. Hoffman, J.F. (1958). Physiological characteristics of the human red blood cell ghosts. J. Gen. Physiol. 42:9-28.

38. Hughes, A.F.W. and Swann, M.M. (1948). Anaphase movements in living cells. J. Exp. Biol. 25:45-70.

39. Hunter, R.J. (1960). Constancy of the surface charge density of the human erythrocytes at different ionic strengths. Arch. Biochem. Biophys. 88:308-312.

40. Husson, F. and Luzzati, V. (1963). Structure of red cell ghosts and the effect of saponin treatment. Nature. 179:822.

41. Inoué, S. (1964). Organization and function of the mitotic spindle. in Allen, R. and Kamiya, N. ed. Primitive Motile Systems in Cell Biology. New York: Academic. pp. 549-598.

42. Inoué, S. and Dan, K. (1951). Birefringence of the dividing cell. J. Morph. 89:423-455.

43. Jay, A.W.L. (1968). Direct measurement of potential difference across the red cell membrane. Presented at the 12th annual meeting of the Biophysical Society. (Biophys. J. Soc. Abstr. Vol. 8).

44. Katchalsky, A. (1963). Mechanochemistry of cell movement. Symposium on non-muscular contractions in biological system. 7th annual meeting of the Biophysical Society.

45. Katchalsky, A., Keden, O., Klibansky, C. and deVries, A. (1960). Rheological considerations of the hemolysing red blood cell. in Copley, A.L. and Stainsby, G. ed. The flow properties of blood and other biological systems. New York: Pergamon Press. pp. 155-171.

46. Kavanau, J.L. (1965). Structure and function in biological membranes. Vol. I and II. San Francisco: Holden-Day.

47. Kavanau, J.L. (1966). Membrane structure and function. Fed. Proc. 25:1096-1107.

48. Korn, E.D. (1966). Structure of biological membranes. Science. 153:1491-1498.

49. Krogh, A. (1929). The anatomy and physiology of capillaries. Revised and enlarged edition. New Haven Yale University Press.

50. Kugelmass, I.N. (1959). Biochemistry of blood in health and disease. Springfield. Charles C. Thomas.

51. Latta, H. (1952). The surface of the mammalian erythrocyte. Blood. 7:508-521.

52. Lucy, J.A. (1964). Globular lipid micelles and cell membranes. J. Theor. Biol. 7:360-373.

53. Lucy, J.A. and Glauert, A.M. (1964). Structure and assembly of micromolecular lipid complex composed of globular micelles. J. Mol. Biol. 8:727-748.

54. Marchesi, V.T. and Palade, G.E. (1967). The localization of Mg-Na-K-activated adenosine triphosphate on red cell ghost membranes. J. Cell. Biol. 35: 385-404.

55. Marchesi, V.T. and Steers, E. Jr. (1968). Selective solubilization of a protein component of the red cell membrane. Science. 159:203-204.

56. Marikovsky, Y., Danon, D. and Katchalsky, A. (1966). Agglutination by polylysine of young and old red blood cells. Biochim. Biophys. Acta. 124:154-159.

57. Mazia, D. (1961). Mitotis and the physiology of cell division. in Brachet, J. and Mirsky, A.E. ed. The Cell. New York: Academic. Vol. 4:77-412.

58. Merrill, E.W., Cokelet, G.C., Britten, A. and Wells, R.E. (1963). Non-Newtonian rheology of human blood effect of fibrinogen reduced by 'subtraction'. Circ. Res. 13:48-55.

59. Mitchell, C.D. and Hanahan, D.J. (1966). Solubilization of certain proteins from the human erythrocyte stroma. Biochemistry. 5:51-57.

60. Moscona, A.A. (1962). Cellular interaction in experimental histogenesis. Int. Rev. Exp. Path. 1:371-427.

61. Nakao, M., Nakao, T. and Yamazoe, S. (1960). Adenosine triphosphate and maintenance of shape of the human red cells. Nature. 187:945.

62. Nakao, M., Nakao, T. and Yamazoe, S. (1961). Adenosine triphosphate and shape of the erythrocytes. J. Biochem. 49:487-498.

63. Nevo, A. (1960). On the estimation of the thickness of the red cell membrane from ultracentrifuge studies. Exp. Cell. Res. 21:286-291.

64. Novozhilov, V.V. (1959). The theory of thin shells. (Trans. by Lowe, P.G.). Groninger, The Netherlands. P. Noordhoff, Ltd.

65. Ponder, E. (1925). On sedimentation and rouleaux formation. Quart. J. Expt. Physiol. 15:235-252.

66. Ponder, E. (1930). Measurement of diameter of erythrocytes. V. The relation of diameter to thickness. Quart. J. Exp. Physiol. 20:29-39.

67. Ponder, E. (1940). The red cell as an osmometer. Sympos. Quant. Biol. 8:133-143.

68. Ponder, E. (1944). Red cell dimensions: measurement. in Glaeser, O. ed. Medical Physics. Chicago, Ill. The Yearbook Publishers Inc. 1:1203-1214.

69. Ponder, E. (1948). Hemolysis and related phenomena. New York: Grune and Stratton.

70. Ponder, E. (1955). Red cell structure and its breakdown. Protoplasmatologia. 10. no. 2. Wien. Springer-verleg.

71. Prankerd, T.A.J. (1961). The red cell. 1st ed. Blackwell Scientific Publications. Oxford.

72. Prothero, J.W. and Burton, A.C. (1961). The physics of blood flow in capillaries. I. The nature of the motion. Biophys. J. 1:565-580.

73. Prothero, J.W. and Burton, A.C. (1962a). The physics of blood flow in capillaries. II. The capillary resistance to flow. Biophys. J. 2:199-212.

74. Prothero, J.W. and Burton, A.C. (1962b). The physics of blood flow in capillaries. III. The force required to deform erythrocytes in acid-citrate-dextrose. Biophys. J. 2:213-222.

75. Rand, R.P. (1964a). Mechanical properties of the red cell membrane. II. Viscoelastic breakdown of the membrane. Biophys. J. 4:303-316.

76. Rand, R.P. (1964b). Mechanical properties of the red cell. Ph. D. Thesis. University of Western Ontario. London, Canada.

77. Rand, R.P. (1967). Some biophysical considerations of the red cell membrane. Fed. Proc. 26:1780-1784.

78. Rand, R.P. and Burton, A.C. (1963). Area and volume changes in hemolysis of single erythrocytes. J. Cell. Comp. Physiol. 61:245-253.

79. Rand, R.P. and Burton, A.C. (1964). Mechanical properties of the red cell membrane. I. Membrane stiffness and intracellular pressure. Biophys. J. 4:115-135.

80. Rand, R.P.,Burton, A.C, and Canham, P.B. (1965). Reversible changes in shape of red cells in electrical fields. Nature. 205:977-978.

81. Robertson, J.D. (1959). The ultra structure of cell membranes and their derivations. Biochem. Soc. Sympos. 16:3-43.

82. Robertson, J.D. (1960). The molecular structure and contact relationships of cell membranes. Progr. Biophys. 10:343-418.

83. Robertson, J.D. (1967). Origin of the unit membrane concept. Protoplasma. 63:218-245.

84. Seaman, G.V.F. and Uhlenbruck, G. (1963). The surface structure of erythrocytes from some animal sources. Arch. Biochem. Biophys. 100:493-502.

85. Seeman, P. (1966). II. Erythrocyte membrane stabilization by local anesthetics and tranquilizers. Biochemical Pharmacology. 15:1753-1766.

86. Seeman, P. (1966). III. A method for distinguishing specific from nonspecific hemolysins. Biochemical Pharmacology. 15:1767-1774.

87. Seeman, P. and Weinstein, J. (1966). I. Erythrocyte membrane stabilization by tranquilizers and antihistamines. Biochemical Pharmacology. 15:1737-1752.

88. Sjostrand, F.S. (1963). A new repeat structural element of mitochondrial and certain cytoplasmic membranes. Nature. 199:1262-1264.

89. Stone, D. Joyce and Ada, G.L. (1952). Electrophoric studies of virous red cell interaction: Relationship between agglutinability and electrophoretic mobility. Brit. J. Exp. Path. 33:428-439.

90. Timoshenko, S. (1959). Theory of plates and shells. New York: McGraw-Hill.

91. Waugh, D.F. and Schmitt, F.O. (1940). Investigations of the thickness and ultrastructure of cellular membranes by the analytical leptoscope. Sympos. Quant. Biol. 8:233-241.

92. Weiss, L. (1960). The adhesion of cells. Int. Rev. of Cytol. 9:187-225.

93. Weiss, L. (1965). Studies on cell deformability. I. Effect of surface charge. J. Cell. Biol. 26:735-739.

94. Weiss, L. (1967). Studies on cell deformability. IV. A possible role of calcium in cell contact phenomenon. J. Cell. Biol. 35:347-356.

95. Weiss, P. (1958). Cell contact. Int. Rev. of Cytol. 7:155-171.

96. Williams, T.F., Fordham, C.C. and Hollander, W. (1959). A study of the osmotic behavior of human erythrocytes. J. Clin. Invest. 38:1587-1597.

APPENDIX I

TABLE 1

Force vs. distance between the charged plates of the absolute electrometer, when the medium between the plates was specialized by 5 mg. of 1.0 mm long nylon fibers. (The voltage between the plates was 540 volts).

Distance of separation between the plates (mm.)	Force of attraction between the plates F. (mg.) $\pm$ SEM
1.6	103.2 $\pm$ 4.15
2.3	85.9 $\pm$ 3.14
3.0	53.6 $\pm$ 3.74
3.7	43.4 $\pm$ 4.78
4.4	30.8 $\pm$ 4.74
5.1	20.9 $\pm$ 1.35
5.8	15.6 $\pm$ 0.30
6.5	15.4 $\pm$ 1.51
7.2	10.2 $\pm$ 0.20

TABLE 2

Force vs. distance between the charged plates of the absolute electrometer, when the medium between the plates was specialized by 10 mg. of 1.0mm. long nylon fibers. (The voltage between the plates was 540 volts).

Distance of separation between the plates (mm.)	Force of attraction between the plates F. (mg.) ± S.E.M.
1.6	62.5 ± 2.93
2.3	73.5 ± 1.50
3.0	57.0 ± 1.70
3.7	38.3 ± 1.75
4.4	25.9 ± 1.67
5.1	20.2 ± 0.64
5.8	16.6 ± 0.63
6.5	12.8 ± 0.95
7.2	10.2 ± 0.10

TABLE 3

Force vs. distance between the charged plates of the absolute electrometer, when the medium between the plates was specialized by 15 mg. of 1.0 mm long nylon fibers. (The voltage between the plates was 540 volts).

Distance of separation between the plates (mm.)	Force of attraction between the plates F. (mg.) ± SEM
1.6	38.4 ± 3.06
2.3	55.1 ± 2.14
3.0	64.6 ± 1.42
3.7	41.8 ± 0.64
4.4	29.6 ± 0.59
5.1	21.2 ± 0.31
5.8	16.9 ± 0.43
6.5	12.8 ± 0.27
7.2	10.5 ± 0.22

TABLE 4

Force vs. distance between the charged plates of the absolute electrometer, when the medium between the plates was specialized by 20 mg. of 1.0 mm long nylon fibers. (The voltage between the plates was 540 volts).

Distance of separation between the plates (mm.)	Force of attraction between the plates F. (mg.) ± SEM
1.6	12.2 ± 0.80
2.3	29.9 ± 1.24
3.0	47.0 ± 1.34
3.7	38.1 ± 0.81
4.4	30.4 ± 0.80
5.1	22.7 ± 1.00
5.8	16.4 ± 0.56
6.5	12.4 ± 0.43
7.2	10.4 ± 0.20

TABLE 5(a)

Force vs. distance between the charged plates of the absolute electrometer, when the medium between the plates was specialized by 25 mg. of 1.0 mm long nylon fibers. (The voltage between the plates was 540 volts).

Distance of separation between the plates (mm.)	Force of attraction between the plates F. (mg.) ± SEM
1.6	4.5 ± 0.55
2.3	18.5 ± 1.01
3.0	27.5 ± 0.79
3.7	32.9 ± 0.78
4.4	27.0 ± 0.63
5.1	21.9 ± 0.40
5.8	19.0 ± 0.24
6.5	14.7 ± 0.17
7.2	10.6 ± 0.08

TABLE 5(b)

Force vs. distance between the charged plates of the absolute electrometer, when the medium between the plates was specialized by 5 mg. of 0.5 mm long nylon fibers. (The voltage between the plates was 540 volts).

Distance of separation between the plates (mm.)	Force of attraction between the plates F. (mg.) ± SEM
1.6	122.1 ± 3.35
2.3	94.8 ± 2.09
3.0	57.0 ± 4.73
3.7	35.9 ± 1.11
4.4	27.5 ± 0.44
5.1	20.0 ± 0.47
5.8	13.7 ± 0.60
6.5	13.0 ± 0.66
7.2	10.8 ± 0.31

TABLE 5(c)

Force vs. distance between the charged plates of the absolute electrometer, when the medium between the plates was specialized by 10 mg. of 0.5 mm long nylon fibers. (The voltage between the plates was 540 volts).

Distance of separation between the plates (mm.)	Force of attraction between the plates F. (mg.) ± SEM
1.6	82.8 ± 9.92
1.9	116.9 ± 4.80
2.3	95.5 ± 3.17
3.0	57.6 ± 1.77
3.7	36.5 ± 1.28
4.4	27.3 ± 1.28
5.1	19.6 ± 1.03
5.8	14.3 ± 1.16
6.5	13.3 ± 0.58
7.2	11.0 ± 0.33

TABLE 5(d)

Force vs. distance between the charged plates of the absolute electrometer, when the medium between the plates was specialized by 15 mg. of 0.5 mm long nylon fibers. (The voltage between the plates was 540 volts).

Distance of separation between the plates (mm.)	Force of attraction between the plates F. (mg.) ± SEM
1.6	66.0 ± 2.34
2.3	100.2 ± 4.03
3.0	72.3 ± 2.81
3.7	45.0 ± 1.77
4.4	31.3 ± 1.64
5.1	22.9 ± 1.27
5.8	18.6 ± 0.86
6.5	13.9 ± 0.67
7.2	10.6 ± 0.41

TABLE 5(e)

Force vs. distance between the charged plates of the absolute electrometer, when the medium between the plates was specialized by 20 mg. of 0.5 mm long nylon fibers. (The voltage between the plates was 540 volts).

Distance of separation between the plates (mm.)	Force of attraction between the plates F. (mg.) $\pm$ SEM
1.6	43.1 $\pm$ 2.23
2.3	65.1 $\pm$ 3.29
2.6	85.8 $\pm$ 3.71
3.0	67.8 $\pm$ 2.96
3.7	50.5 $\pm$ 2.47
4.4	34.6 $\pm$ 2.06
5.1	24.8 $\pm$ 1.54
5.8	17.7 $\pm$ 0.81
6.5	14.3 $\pm$ 0.31
7.2	11.0 $\pm$ 0.22

TABLE 5(f)

Force vs. distance between the charged plates of the absolute electrometer, when the medium between the plates was specialized by 25 mg. of 0.5 mm long nylon fibers. (The voltage between the plates was 540 volts).

Distance of separation between the plates (mm.)	Force of attraction between the plates F. (mg.) ± SEM
1.6	21.0 ± 1.11
2.3	55.1 ± 1.92
3.0	73.6 ± 3.79
3.7	50.1 ± 2.46
4.4	33.6 ± 1.49
5.1	23.6 ± 1.22
5.8	17.6 ± 0.92
6.5	13.5 ± 0.58
7.2	10.1 ± 0.33

TABLE 6

Force vs. distance between the charged plates (before and after vibrating) of the absolute electrometer, when the medium between the plates was specialized by 20 mg. of 0.5 mm long nylon fibers. (The voltage between the plates was 540 volts).

Distance of separation between the plates	Force of attraction between the plates (before vibrating)	Force of attraction between the plates (after vibrating)
(mm.)	(mg.)	(mg.)
1.6	43.1	21.7
2.3	65.1	51.0
2.6	58.8	81.7
3.0	67.8	66.8
3.7	50.5	49.9
4.4	34.6	36.9
5.1	24.8	24.6
5.8	17.7	21.2
6.5	14.3	14.8
7.2	11.0	11.0

TABLE 7(a)

For 'empty' plates

(Data are derived from curve 'A' of Figure 16).

Force of attraction between the plates	Distance of separation between the plates	r^2	$F.r^2 \propto F_Q$
F. (mg.)	r.(mm.)	(mm^2)	
209.0	1.6	2.6	535.0
90.5	2.3	5.3	491.8
58.0	3.0	9.0	522.0
38.0	3.7	13.7	520.2
27.0	4.4	19.4	522.7
20.0	5.1	26.0	520.2
15.5	5.8	33.6	521.4
12.5	6.5	42.2	528.1
10.0	7.2	51.8	518.4

TABLE 7(b)

For 5 mg. fibers of 1.0 mm length

(Data are derived from curve 'B' of Figure 16).

Force of attraction between the plates	Distance of separation between the plates	r^2	$F.r^2 \propto F_Q$
F. (mg.)	r. (mm.)	(mm^2)	
103.0	1.6	2.6	263.7
86.0	2.3	5.3	454.9
58.0	3.0	9.0	522.0
38.0	3.7	13.7	520.2
27.0	4.4	19.4	522.7
20.0	5.1	26.0	520.2
15.5	5.8	33.6	521.4
12.5	6.5	42.2	528.1
10.0	7.2	51.8	518.4

TABLE 7(c)

For 10 mg. fibers of 1.0 mm length

(Data are derived from the curve 'C' of Figure 16).

Force of attraction between the plates F. (mg.)	Distance of separation between the plates r.(mm.)	r^2 (mm^2)	$F.r^2 \propto F_Q$
62.0	1.6	2.6	158.7
73.0	2.3	5.3	386.2
58.0	3.0	9.0	522.0
38.0	3.7	13.7	520.2
27.0	4.4	19.4	522.7
20.0	5.1	26.0	520.2
15.5	5.8	33.6	521.4
12.5	6.5	42.2	528.1
10.0	7.2	51.8	518.4

TABLE 7(d)

For 15 mg. fibers of 1.0 mm length

(Data are derived from curve 'D' of Figure 16).

Force of attraction between plates	Distance of separation between the plates	r^2	$F.r^2 \propto F_Q$
F. (mg.)	r. (mm)	(mm^2)	
37.0	1.6	2.6	94.7
55.0	2.3	5.3	291.0
58.0	3.0	9.0	522.0
38.0	3.7	13.7	520.2
27.0	4.4	19.4	522.7
20.0	5.1	26.0	520.2
15.5	5.8	33.6	521.4
12.5	6.5	42.2	528.1
10.0	7.2	51.8	518.4

TABLE 7(e)

For 20 mg. fibers of 1.0 mm length

(Data are derived from curve 'E' of Figure 16).

Force of attraction between the plates F. (mg.)	Distance of separation between the plates r.(mm)	r^2 (mm^2)	F. $r^2 \propto F_Q$
12.0	1.6	2.6	30.7
30.0	2.3	5.3	158.7
47.0	3.0	9.0	423.0
38.0	3.7	13.7	520.2
27.0	4.4	19.4	522.7
20.0	5.1	26.0	520.2
15.5	5.8	33.6	521.4
12.5	6.5	42.2	528.1
10.0	7.2	51.8	518.4

TABLE 7(f)

For 25 mg. fibers of 1.0 mm length

(Data are derived from curve 'F' of Figure 16).

Force of attraction between the plates	Distance of separation between the plates	r^2	$F.r^2 \propto F_Q$
F. (mg.)	r.(mm)	(mm^2)	
4.0	1.6	2.6	10.2
18.0	2.3	5.3	95.2
27.0	3.0	9.0	243.0
33.0	3.7	13.7	451.8
27.0	4.4	19.4	522.7
20.0	5.1	26.0	520.2
15.5	5.8	33.6	521.4
12.5	6.5	42.2	528.1
10.0	7.2	51.8	518.4

TABLE 8(a)

For 'empty'plates

(Data are derived from curve A of Figure 17).

Force of attraction between the plates	Distance of separation between the plates	r^2	$F.r^2 \propto F_Q$
F. (mg.)	r.(mm)	(mm^2)	
209.0	1.6	2.6	535.0
90.5	2.3	5.3	491.8
58.0	3.0	9.0	522.0
38.0	3.7	13.7	520.2
27.0	4.4	19.4	522.7
20.0	5.1	26.0	520.2
15.5	5.8	33.6	521.4
12.5	6.5	42.2	528.1
10.0	7.2	51.8	518.4

TABLE 8(b)

For 5 mg. fibers of 0.5 mm length

(Data are derived from curve 'B' of Figure 17).

Force of attraction between the plates	Distance of separation between the plates	r^2	$F.r^2 \propto F_Q$
F. (mg.)	r. (mm)	(mm^2)	
121.5	1.6	2.6	311.0
106.5	1.9	3.6	384.5
99.0	2.3	5.3	524.7
58.0	3.0	9.0	522.0
38.0	3.7	13.7	520.2
27.0	4.4	19.4	522.7
20.0	5.1	26.0	520.2
15.5	5.8	33.6	521.4
12.5	6.5	42.2	528.1
10.0	7.2	51.8	518.4

TABLE 8(c)

For 10 mg. fibers of 0.5 mm length

(Data are derived from curve 'C' of Figure 17).

Force of attraction between the plates	Distance of separation between the plates	r^2	$F. r^2 \propto F_Q$
F.(mg.)	r.(mm.)	(mm^2)	
82.0	1.6	2.6	209.9
116.5	1.9	3.6	420.6
98.0	2.3	5.3	518.4
58.0	3.0	9.0	522.0
38.0	3.7	13.7	520.2
27.0	4.4	19.4	522.7
20.0	5.1	26.0	520.2
15.5	5.8	33.6	521.4
12.5	6.5	42.2	528.1
10.0	7.2	51.8	518.4

TABLE 8(d)

For 15 mg. fibers of 0.5 mm length

(Data are derived from curve 'D' of Figure 17).

Force of attraction between the plates	Distance of separation between the plates	r^2	$F. r^2 \propto F_Q$
F. (mg.)	r. (mm)	(mm^2)	
66.0	1.6	2.6	169.0
90.5	1.9	3.6	326.7
98.0	2.3	5.3	518.4
58.0	3.0	9.0	522.0
38.0	3.7	13.7	520.2
27.0	4.4	19.4	522.7
20.0	5.1	26.0	520.2
15.5	5.8	33.6	521.4
12.5	6.5	42.2	528.1
10.0	7.2	51.8	518.4

TABLE 8(e)

For 20 mg. fibers of 0.5 mm length

(Data are derived from curve 'E' of Figure 17).

Force of attraction between the plates F. (mg.)	Distance of separation between the plates r.(mm)	r^2 (mm^2)	F. $r^2 \propto F_Q$
43.0	1.6	2.6	110.0
64.0	1.9	3.6	231.0
80.5	2.3	5.3	425.8
58.0	3.0	9.0	522.0
38.0	3.7	13.7	520.2
27.0	4.4	19.4	522.7
20.0	5.1	26.0	520.2
15.5	5.8	33.6	521.4
12.5	6.5	42.2	528.1
10.0	7.2	51.8	518.4

TABLE 8(f)

For 25 mg. fibers of 0.5 mm length

(Data are derived from curve 'F' of Figure 17).

Force of attraction between the plates F. (mg.)	Distance of separation between the plates r. (mm)	r^2 (mm^2)	F. $r^2 \propto F_Q$
21.0	1.6	2.6	53.8
42.0	1.9	3.6	151.6
55.0	2.3	5.3	290.9
66.0	2.6	6.8	406.1
58.0	3.0	9.0	522.0
38.0	3.7	13.7	520.2
27.0	4.4	19.4	522.7
20.0	5.1	26.0	520.2
15.5	5.8	33.6	521.4
12.5	6.5	42.2	528.1
10.0	7.2	51.8	518.4

TABLE 9

Data for the four swelling red cell series

The distance (μ) is the separation between the dimple centers of the red cell membrane. The data has been plotted in Figure 22.

Series (A)		Series (B)		Series (C)		Series (D)	
p^1 ± SEM (mm. of water)	Distance (μ)	p^1 ± SEM (mm. of water)	Distance (μ)	p^1 ± SEM (mm. of water)	Distance (μ)	p^1 ± SEM (mm. of water)	Distance (μ)
2.93 ± 0.03	1.30	2.89 ± 0.03	1.50	2.76 ± 0.04	1.82	2.81 ± 0.03	1.60
3.03 ± 0.03	1.30	2.96 ± 0.03	1.55	2.82 ± 0.03	1.95	2.80 ± 0.03	1.65
2.96 ± 0.04	1.80	3.00 ± 0.04	1.65	2.82 ± 0.04	2.21	2.90 ± 0.04	1.80
2.82 ± 0.03	2.20	2.91 ± 0.04	1.95	2.75 ± 0.03	2.34	2.90 ± 0.04	2.00
2.81 ± 0.04	2.25	2.60 ± 0.04	2.60	2.32	3.64	2.32	3.50
2.80 ± 0.05	2.30	2.53 ± 0.04	3.00	2.21 ± 0.03	3.90	2.21 ± 0.04	4.00
2.71 ± 0.05	2.40	2.32	3.60	1.94 ± 0.04	5.20	2.12 ± 0.04	4.50
2.32	3.20	2.05 ± 0.04	4.68	1.55 ± 0.03	6.76	1.90 ± 0.03	5.00
2.00 ± 0.04	3.80	1.50 ± 0.03	6.50			1.47 ± 0.03	7.00
1.80 ± 0.04	4.60						
1.30 ± 0.03	5.60						

N.B. The SEM shown above in the values of p^1 is that due only to the error in the measurement of R, assuming a fixed value for T and ΔP. However, Rand and Burton (1964) have reported T = 0.013 ± 0.003(SEM) dynes/cm, and ΔP = 2.32 ± 0.75(SEM) mm H_2O. So that the true error in p^1 may be much greater than that shown in this table.

Appendix II

TABLE 10

The data presented below are the average value of $(I-\bar{B})$ obtained from 4 red cell series at the same cell orientation to the polarizer axis.

Cell orientation to the polarizer axis	Relative intensity $(I-\bar{B})$ at the dimple interior region, for each of the eight groups of four series together.							
Series No.	1	2	3	4	5	6	7	8
0^{o}	-0.23	+0.01	-0.08	-0.38	-0.05	-0,13	-0.50	-0.29
15^{o}	+0.08	+0.18	-0.09	-0.30	-0.24	-0.09	-0.21	-0.07
30^{o}	+0.04	+0.19	0.00	+0.18	+0.17	+0.06	-0.13	-0.13
45^{o}	+0.13	+0.27	+0.28	+0.34	+0.17	+0.26	+0.05	+0.16
60^{o}	-0.04	+0.22	+0.26	-0.06	+0.12	+0.11	-0.05	+0.05
75^{o}	-0.13	+0.27	-0.15	-0.27	-0.12	-0.15	-0.40	-0.08
90^{o}	-0.13	+0.13	-0.08	-0.22	-0.25	-0.27	-0.49	-0.18

TABLE 11

The data presented below are average of 32 red cell series. Values of $(I-\bar{B})$ obtained at the same cell orientation to the polarizer axis. The data have been plotted in Figure 27.

Red cell orientation to the polarizer axis	$(I-\bar{B})$, the relative intensity at the dimple interior region of the red cell in arbitrary units with SEM
0^{o}	$- 0.20 \pm 0.05$
15^{o}	$- 0.09 \pm 0.05$
30^{o}	$+ 0.05 \pm 0.04$
45^{o}	$+ 0.21 \pm 0.04$
60^{o}	$+ 0.08 \pm 0.04$
75^{o}	$- 0.13 \pm 0.05$
90^{o}	$- 0.19 \pm 0.05$

TABLE 12

The data presented below are average of 32 red cell series values of $(I-\bar{B})$ obtained at the same cell orientation to the polarizer axis. The data have been plotted in Figure 28.

Red cell orientation to the polarizer axis	$(I-\bar{B})$, the relative intensity at the rim interior region of the red cell in arbitrary units with SEM
0°	-0.63 ± 0.07
15°	-0.54 ± 0.07
30°	-0.57 ± 0.06
45°	-0.49 ± 0.06
60°	-0.46 ± 0.05
75°	-0.60 ± 0.06
90°	-0.66 ± 0.07

TABLE 13

Data for relative intensities at dimple region of the red cell suspended in 240 mOsm diluted, buffered Ringer solution.

Red Cell Orientation	(MAI-MI) In arbitrary units Mean ± SEM	(MAI-$\bar{B}$) In arbitrary units Mean ± SEM	(MI-$\bar{B}$) In arbitrary units Mean ± SEM
0°	0.14 ± 0.02	-0.46 ± 0.02	-0.60 ± 0.05
15°	0.17 ± 0.02	-0.50 ± 0.04	-0.67 ± 0.05
30°	0.21 ± 0.02	-0.48 ± 0.05	-0.69 ± 0.05
45°	0.27 ± 0.02	-0.40 ± 0.04	-0.67 ± 0.05
60°	0.23 ± 0.03	-0.42 ± 0.03	-0.65 ± 0.04
75°	0.16 ± 0.02	-0.44 ± 0.03	-0.60 ± 0.04
90°	0.13 ± 0.02	-0.49 ± 0.05	-0.61 ± 0.05

TABLE 14

Data for relative intensities at dimple region of the red cell suspended in 163 mOsm diluted, buffered Ringer solution.

Orientation of the red cell with the polarizer axis	(MAI-MI) Mean ± SEM	(MAI-$\bar{B}$) Mean ± SEM	(MI-$\bar{B}$) Mean ± SEM
0°	-0.00 ± 0.01	-0.49 ± 0.04	-0.49 ± 0.05
15°	+0.01 ± 0.01	-0.47 ± 0.05	-0.48 ± 0.05
30°	-0.00 ± 0.02	-0.52 ± 0.05	-0.52 ± 0.05
45°	+0.01 ± 0.01	-0.52 ± 0.05	-0.53 ± 0.05
60°	-0.01 ± 0.02	-0.56 ± 0.05	-0.55 ± 0.05
75°	-0.00 ± 0.03	-0.59 ± 0.06	-0.59 ± 0.04
90°	-0.00 ± 0.02	-0.57 ± 0.04	-0.57 ± 0.04

TABLE 15

Data for relative intensities at dimple region of the red cells suspended in 194 mOsm diluted, buffered Ringer solution.

Orientation of the red cell with the polarizer axis	(MAI-MI) Mean ± SEM	(MAI-$\bar{B}$) Mean ± SEM	(MI-$\bar{B}$) Mean ± SEM
0^{o}	+0.02 ± 0.02	-0.32 ± 0.05	-0.34 ± 0.05
15^{o}	+0.01 ± 0.02	-0.37 ± 0.05	-0.38 ± 0.05
30^{o}	+0.02 ± 0.03	-0.31 ± 0.07	-0.33 ± 0.06
45^{o}	+0.03 ± 0.04	-0.21 ± 0.07	-0.24 ± 0.06
60^{o}	+0.04 ± 0.04	-0.29 ± 0.06	-0.33 ± 0.06
75^{o}	+0.01 ± 0.02	-0.31 ± 0.05	-0.32 ± 0.05
90^{o}	+0.02 ± 0.02	-0.35 ± 0.06	-0.37 ± 0.05

TABLE 16.

Data for relative intensity of the red cell membrane at dimple region versus cell orientation with the polarizer axis.

Orientation of the red cell membrane with the polarizer axis	Relative intensity ($M-\bar{B}$) in arbitrary units with SEM
0^{o}	-0.98 ± 0.08
15^{o}	-0.96 ± 0.07
30^{o}	-0.96 ± 0.09
45^{o}	-0.86 ± 0.08
60^{o}	-0.87 ± 0.09
75^{o}	-0.91 ± 0.08
90^{o}	-0.93 ± 0.08

Appendix III

Intrinsic and Form Birefringence

On the basis of different types of anisotropy in matter, birefringence can be divided into two main categories.

(a) Crystalline (intrinsic) birefringence is due to regular anisotropic arrangement of chemical bonds, ions or molecules in the system, such as occurs in crystalline objects. This type of birefringence is independent of the refractive index of the medium in which the object is immersed.

(b) Form birefringence is due to small particles non-spherical in shape, having at least one dimension smaller than the wave length of the light which are preferentially oriented in a medium of different refractive index. These dispersed bodies may be filaments (rodlets), or sheets (platelets), or in any other form which will give rise to form birefringence, even if the immersion medium and dispersed bodies be in themselves isotropic. Such birefringence will vanish if the dispersed bodies and the immersion medium have the same refractive indices.